Journal of Radioanalytical and Nuclear Chemistry (2026) 335:3823–3857
https://doi.org/10.1007/s10967-026-10892-2

Prompt gamma rays from the inelastic scattering of fission neutrons on samarium and dysprosium

Eric Mauerhofer[1] · Niklas Ophoven[1] · Zeljko Ilic[1,2] · Christian Stieghorst[3] · Zsolt Révay[3] · Iaroslav Meleshenkovskii[1] · Tsitohaina H. Randriamalala[1]

Received: 25 November 2025 / Accepted: 3 April 2026 / Published online: 16 April 2026

Abstract
Prompt gamma rays produced by inelastic scattering of fission neutrons on samarium and dysprosium were measured with the instrument FaNGaS (Fast Neutron-induced Gamma-ray Spectrometry) at Heinz Maier-Leibnitz Zentrum (MLZ). Relative intensities and production cross sections for 288 gamma lines (140 for samarium, 148 for dysprosium) were calculated considering interferences from radiative capture lines. Consistency with data obtained from irradiation with reactor fast neutrons was evaluated. Our results contribute to the expansion and the improvement of databases related to the interaction of fission neutrons with nuclei. The detection limits of samarium and dysprosium are estimated as 0.6 and 1.6 mg for a measuring time of 12 h.

Keywords Inelastic scattering · Samarium · Dysprosium · Fission neutrons · Cross section · Gamma ray

Introduction

The aim of the FaNGaS (Fast Neutron induced Gamma-ray Spectrometry) instrument operated at MLZ (Heinz-Maier-Leibnitz Zentrum) [1–3] is the determination of the elemental composition of large and thick objects of various origins (e.g. geology, mineralogy, archaeology, cultural heritage, industry, mining and recycling) by means of Prompt Gamma Analysis based on Inelastic Neutron Scattering (PGAINS) using the fission neutron beam delivered by the beam tube 10 (SR10) of FRM II (Forschungs-Neutronenquelle Heinz Maier-Leibnitz). This technique is based on the measurement of isotope-specific prompt gamma rays induced by the inelastic scattering of fission neutrons i.e. $(n,n'\gamma)$ reactions. For some isotopes, the gamma rays from other reactions such as $(n,p\gamma)$, $(n,\alpha\gamma)$ or (n,γ) can be detected as well. PGAINS is suitable for the investigation of critical raw materials, such as neodymium and dysprosium in permanent magnets with a view of their sorting for recycling [4]. The FaNGaS spectrometer consists of the well-shielded electromechanically-cooled n-type high purity germanium of 50% relative efficiency. The fission neutrons are produced from an uranium (93% ^{235}U) converter plugged into the heavy water moderator of FRM II. A photography of the FaNGaS spectrometer at experimental position may be found in [3]. Besides, the FaNGas instrument has already shown, thanks to the penetrating fast neutron beam, its capability to perform in-situ detection and localization of hydrate plugs inside pipelines [5]. Also, the ultimate goal of FaNGaS is to compile a modern comprehensive data catalogue of $(n,n'\gamma)$ reactions [2, 3, 6–13], which is required for various applications in nuclear science and technology such as chemical analysis with neutron interrogation systems, the design of fast neutron reactors and radiation protection.

In this work, we present the results from the measurements of prompt gamma rays induced by inelastic scattering of fission neutrons on samarium(III) chloride heptahydrate ($SmCl_3 \cdot 7H_2O$) and a dysprosium(III) chloride hexahydrate ($DyCl_3 \cdot 6H_2O$) samples. The relative intensities of the prompt gamma rays were compared with the values obtained from the irradiation of samarium(III) oxide (Sm_2O_3) and dysprosium(III) oxide (Dy_2O_3) samples of natural abundance

✉ Eric Mauerhofer
e.mauerhofer@fz-juelich.de

[1] Jülich Centre for Neutron Science, Forschungszentrum Jülich GmbH, 52425 Jülich, Germany

[2] Lehrstuhl Für Experimentalphysik IVc, RWTH Aachen University, 52056 Aachen, Germany

[3] Heinz Maier-Leibnitz Zentrum (MLZ), Technische Universität München, Lichtenbergstraße 1, 85748 Garching, Germany

[14] or isotopically enriched (^{144}Sm [14], ^{147}Sm [15], ^{148}Sm [14], ^{150}Sm [14], ^{152}Sm [14, 16], ^{154}Sm [14, 17], ^{162}Dy [14, 18], ^{163}Dy [19], ^{164}Dy [14, 20]) with reactor fast neutrons at different facilities, namely IRT-M reactor of Nuclear Research Institute in Baghdad for [14], IRT reactor of the Physics Institute of the Latvian SSR Academy of Sciences in Riga for [16, 19] and IR-8 reactor of Russian Research Center Kurchatov Institute for [15, 18, 20]. Additionally, we provide the elemental detection limit for the two considered elements.

Experimental

Powder samples of $SmCl_3 \cdot 7H_2O$ (mass: 1.88 g, Sm: 0.74 g) and $DyCl_3 \cdot 6H_2O$ (mass: 1.86 g, Sm: 0.80 g) contained in PTFE (Polytetrafluorethylene) bag were irradiated with a beam of fission neutrons and the resulting prompt gamma radiation was measured with the FaNGaS instrument [3]. The samples with thicknesses of about 4 mm ($SmCl_3 \cdot 7H_2O$) and 5 mm ($DyCl_3 \cdot 6H_2O$) were placed with an angle of 45° with respect to the beam direction. The neutron energy spectrum at sample position is depicted in [9] and the corresponding neutron flux is given in the supplement material of [11]. The detector was positioned perpendicularly to the beam axis with a distance of 67 cm from the sample position. The irradiation time was 3.6 h for $SmCl_3 \cdot 7H_2O$ and 3.1 h for $DyCl_3 \cdot 6H_2O$. The counting time (live) was 2.8 h and 2.5 h, respectively. The collected spectra for $SmCl_3 \cdot 7H_2O$ are displayed in Figs. 1 and 2 and for $DyCl_3 \cdot 6H_2O$ in Figs. 3 and 4. They were analyzed with the HYPERMET-PC software [21]. The assignment of isotopes to the gamma lines was done with the help of the NuDat 3.0 [22] and PGNAA databases [23, 24] as well as the nuclear data given in [25–35]. Due to the scattering of fast neutrons by the samples towards the spectrometer the count rate of background lines was increased on average by a factor of 1.64 ± 0.28 for $SmCl_3 \cdot 7H_2O$ and 1.54 ± 0.28 for $DyCl_3 \cdot 6H_2O$. These factors have been applied for correction interferences from background gamma rays. The contributions of the single and double escape lines have also been corrected by means of the method described in our previous work on cerium and chlorine [8] where the energy deposition of high-energy gammas in the HPGe detector of FaNGaS was simulated with the MCNP code to evaluate the ratios between net counts of single or double escape peaks and full energy peaks. The composition of the samples was checked by the relative method using as comparator the polyvinylchloride sample measured previously [8]. From the chlorine lines free of interferences at 1184, 1764, 2646, 3002, 3086 and 3103 keV for $SmCl_3 \cdot 7H_2O$ and at 1764, 2646, 3002, 3086, 3103 and 3163 keV for $DyCl_3 \cdot 6H_2O$, an average chlorine mass of (0.53 ± 0.01) g for $SmCl_3 \cdot 7H_2O$ and of (0.533 ± 0.008) g for $DyCl_3 \cdot 6H_2O$ were determined. The values agree well with those derived from the stoichiometry of the samples, 0.52 g and 0.53 g, respectively, and, thus confirm the number of water molecules i.e. the degree of hydration.

Data analysis

The calculation and the treatment of the intensities and the production cross sections of the prompt gamma lines were performed using the method described in [11]. The gamma-ray self-absorption factors $f_{E\gamma}$ were calculated by considering the effective thicknesses of the samples to be 0.6 cm and 0.7 cm, with the densities of 2.38 g cm^{-3} and 2.56 g cm^{-3} for $SmCl_3 \cdot 7H_2O$ and $DyCl_3 \cdot 6H_2O$, respectively. The mass attenuation coefficients were derived from the NIST (National Institute of Standards and Technology) photon cross sections database XCOM [36, 37], including coherent scattering. The dependence of $f_{E\gamma}$ on the gamma-ray energy E_γ can be expressed by:

$$f_{E\gamma} = a_0 + a_1 \cdot \left(1 - e^{-a_2 \cdot E_\gamma}\right) + a_3 \cdot \left(1 - e^{-a_4 \cdot E_\gamma}\right) \quad (1)$$

with $a_0 = -1.5019 \pm 0.1139$, $a_1 = 0.1131 \pm 0.0107$, $a_2 = 0.0020 \pm 0.0002$, $a_3 = 2.3635 \pm 0.1069$ and $a_4 = 0.0178 \pm 0.0006$ for $SmCl_3 \cdot 7H_2O$, and with $a_0 = -1.3188 \pm 0.0482$, $a_1 = 0.1247 \pm 0.0084$, $a_2 = 0.0017 \pm 0.0002$, $a_3 = 2.1617 \pm 0.0421$ and $a_4 = 0.0141 \pm 0.0003$ for the $DyCl_3 \cdot 6H_2O$ and E_γ in keV.

Many gamma lines associated with neutron capture in samarium and dysprosium isotopes were found to interfere with the lines produced by inelastic neutron scattering (see Tables 11 and 17). To evaluate their contribution, the effective cross sections $<\sigma>$ of the (n,γ)-reactions were determined by folding the neutron capture cross sections of the ENDF/B-VIII.0 library [38] with the neutron spectrum using the NJOY Nuclear Data Processing System (Version 2016) [39, 40]. The effective cross sections obtained for the thermal (10^{-10}–$1.4 \cdot 10^{-7}$ MeV), epithermal ($1.4 \cdot 10^{-7}$–0.06 MeV) and fast (0.06–20 MeV) neutrons are given in Table 1, along with the derived cross sections of (n,n') reactions. By considering the uncertainties, the thermal $<\sigma_{th}>$ and the fast neutrons $<\sigma_{fast}>$ cross sections are in good agreement with the values given the JANIS database [41]. The spectrum-averaged cross sections $<\sigma_{int}>$ were calculated using the thermal cross sections of JANIS due to the large uncertainty on value of the thermal neutron flux.

The net counts $\boldsymbol{P_{E\gamma}}$ of the gamma lines from neutron capture that potentially interfere with the $(n,n'\gamma)$-lines were evaluated by means of the following relation:

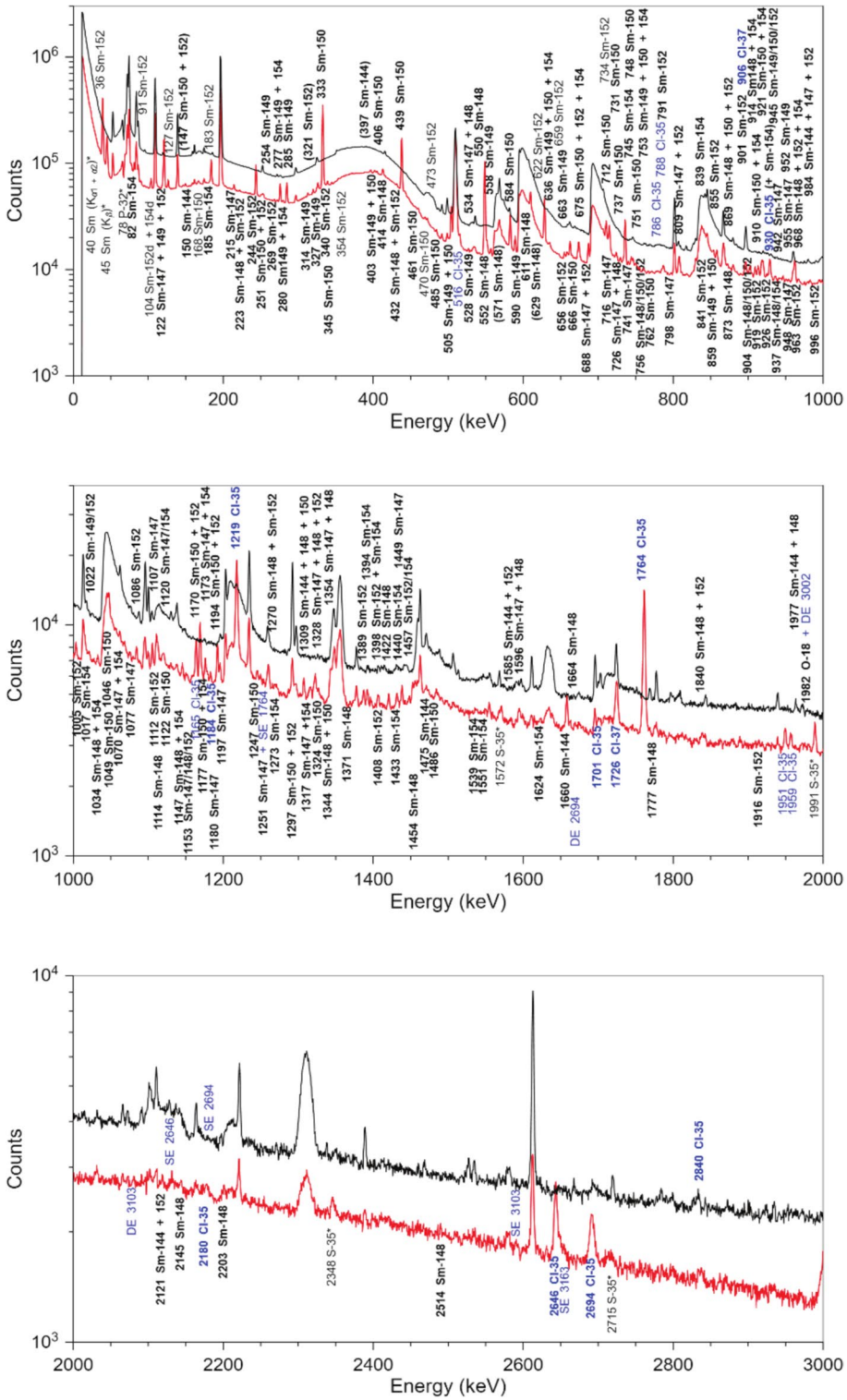

Fig. 1 Gamma-ray spectra in the energy range 0–3000 keV recorded during 10,209 s live time for the $SmCl_3 \cdot 7H_2O$ (red) sample and 51,506 s for the beam background (black). Prompt gamma rays produced by inelastic scattering in Sm and *O* are written in black and bold. Neutron capture gamma rays are written in black for Sm and in blue for Cl. Lines from $(n,n'\gamma)$ reaction in Cl are written in blue and bold. Lines of *S*-35 and *P*-32 from $(n,p\gamma)$ and $(n,\alpha\gamma)$ reactions in Cl and are written in black with asterisks. X-rays are also written in black with asterisks and denoted with *K*. Abbreviations SE and DE indicate single and double escape peaks, respectively, and the abbreviation d stands for delayed

$$P_{E\gamma} = \frac{m}{M} N_A h \varepsilon_{E\gamma} I_\gamma f_{E\gamma} t_c \sum_i < \sigma_i > \Phi_i f_{n,i} f_{mod,i} \quad (2)$$

where m (g) is the mass of the irradiated element, M (g mol^{-1}) the molar mass of the element, N_A the Avogadro number, h the abundance of the considered isotope, $\varepsilon_{E\gamma}$ the full-energy-peak (FEP) efficiency, I_γ the intensity of the line for thermal neutron capture, $f_{E\gamma}$ the gamma-ray self-absorption factor, t_c (s) the counting (live) time, $<\sigma_i>$ (cm^2) the effective cross section for neutron capture reaction, Φ_i (cm^{-2} s^{-1}) the neutron flux, $f_{n,i}$ the neutron self-shielding factor and $f_{mod,i}$ a factor for neutron moderation. The index

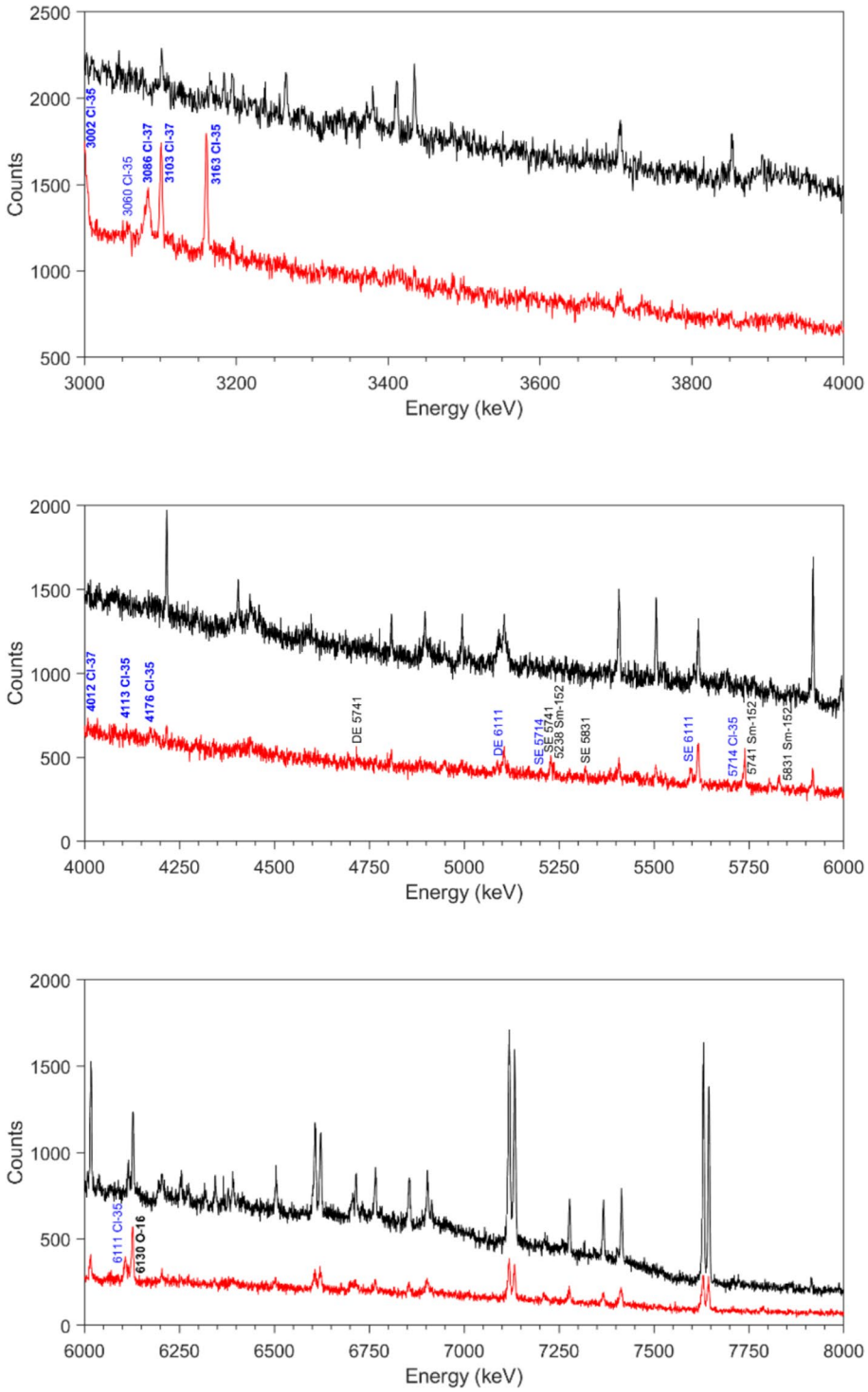

Fig. 2 Gamma-ray spectra in the energy range 3000–8000 keV recorded during 10,209 s live time for the $SmCl_3{\cdot}7H_2O$ (red) sample and 51,506 s for the beam background (black). Prompt gamma rays produced by neutron capture in Sm are written in black and for Cl in blue. Lines from $(n,n'\gamma)$ reaction in Cl are written in blue and bold. SE and DE indicate single and double escape peaks, respectively

i in relation (2) corresponds to the aforementioned neutron energy regions, i.e. thermal ($i=1$), epithermal ($i=2$) and fast ($i=3$). Numerical simulations with the Monte Carlo N-Particle (MCNP, version 6.1) code [42, 43] were carried out to estimate the neutron self-shielding f_n and moderation f_{mod} factors. The latter is due to the presence of water (approximately 30 wt%) in the samples. The neutron self-shielding factors were calculated as the ratio of the neutron flux within the sample (F4 tally) to the incident neutron flux (F2 tally). The moderation factors were calculated as the ratio of the thermal, epithermal and fast neutron flux within the sample obtained from simulations with the part of the incident neutron-energy distribution of interest (i.e. thermal, epithermal and fast) to the simulation with the whole

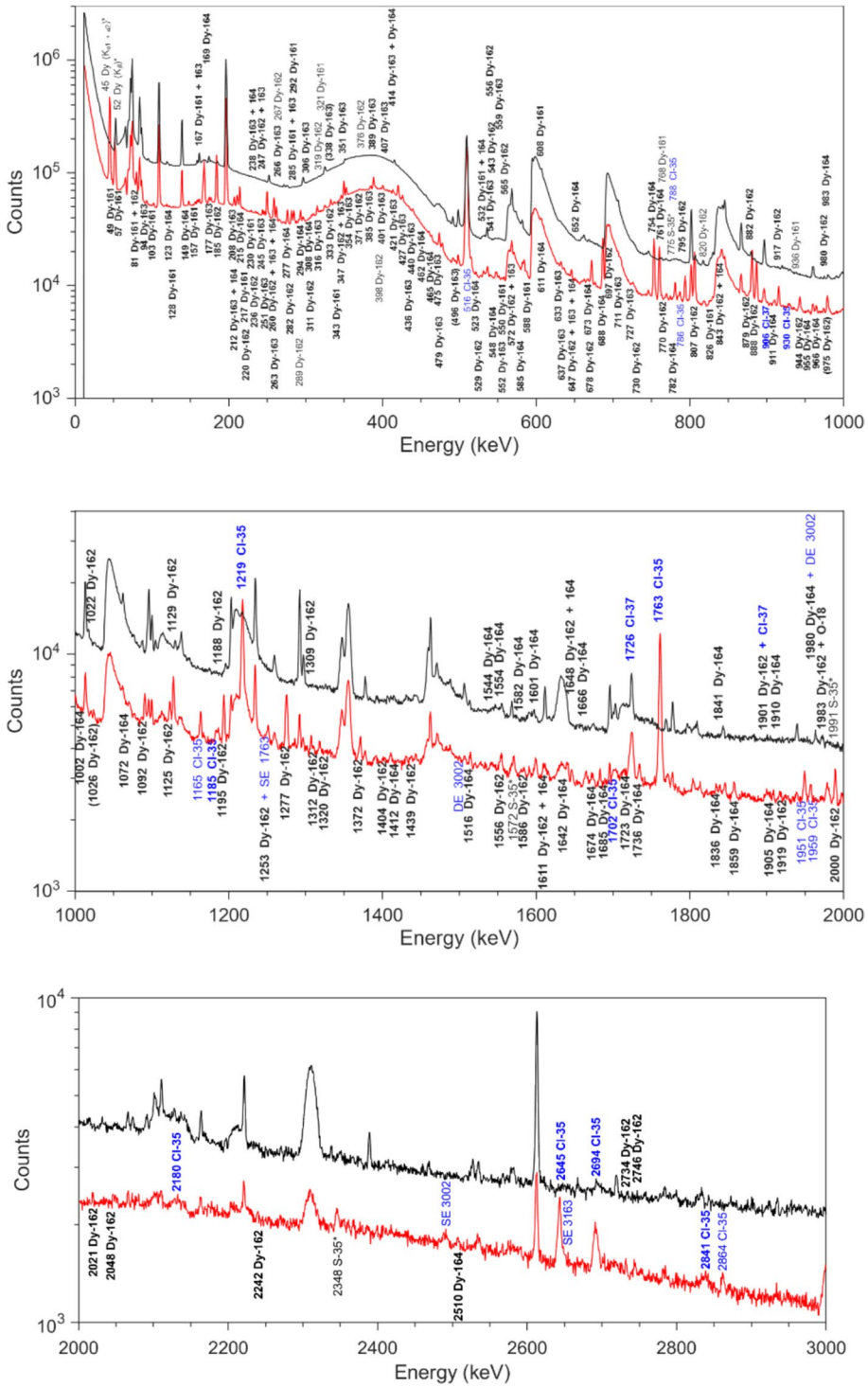

Fig. 3 Gamma-ray spectra in the energy range 0–3000 keV recorded during 8980 s live time for the $DyCl_3{\cdot}6H_2O$ (red) sample and 51,506 s for the beam background (black). Prompt gamma rays produced by inelastic scattering in Sm are written in black and bold. Neutron capture gamma rays are written in black for Dy and in blue for Cl. Lines from $(n,n'\gamma)$ reaction in Cl are written in blue and bold. Lines written in brackets are mainly issued by (n,γ) reactions in Dy. Lines of S-35 and P-32 from (n,pγ) and $(n,\alpha\gamma)$ reactions in Cl and are written in black with asterisks. X-rays are also written in black with asterisks and denoted with *K*. Abbreviations SE and DE indicate single and double escape peaks, respectively

incident neutron-energy distribution. For $SmCl_3{\cdot}7H_2O$ sample, the values of $f_n = 0.083$ and $f_{mod} = 6.30 \pm 2.82$ for thermal, $f_n = 1.053$ and $f_{mod} = 1.62 \pm 0.29$ for epithermal and $f_n = 1.017$ for fast neutrons were determined. For the case of $DyCl_3{\cdot}6H_2O$, the values of $f_n = 0.444$ and $f_{mod} = 7.33 \pm 3.21$ for thermal, $f_n = 1.020$ and $f_{mod} = 1.73 \pm 0.32$ for epithermal and $f_n = 1.008$ for fast neutrons were obtained.

The (n,γ) reaction was mainly induced by the fast neutrons for ^{144}Sm (91%) and by the epithermal neutrons for ^{147}Sm (94%), ^{148}Sm (70%), ^{149}Sm (80%),^{150}Sm (90%) ^{152}Sm (99%), ^{154}Sm (82%), ^{156}Dy (83%), ^{158}Dy (74%), ^{160}Dy (93%), ^{161}Dy (94%), ^{162}Dy (98%) ^{163}Dy (96%) and ^{164}Dy (75%). The contribution of thermal neutrons has been neglected for all isotopes, excepted ^{149}Sm (15%) and ^{164}Dy

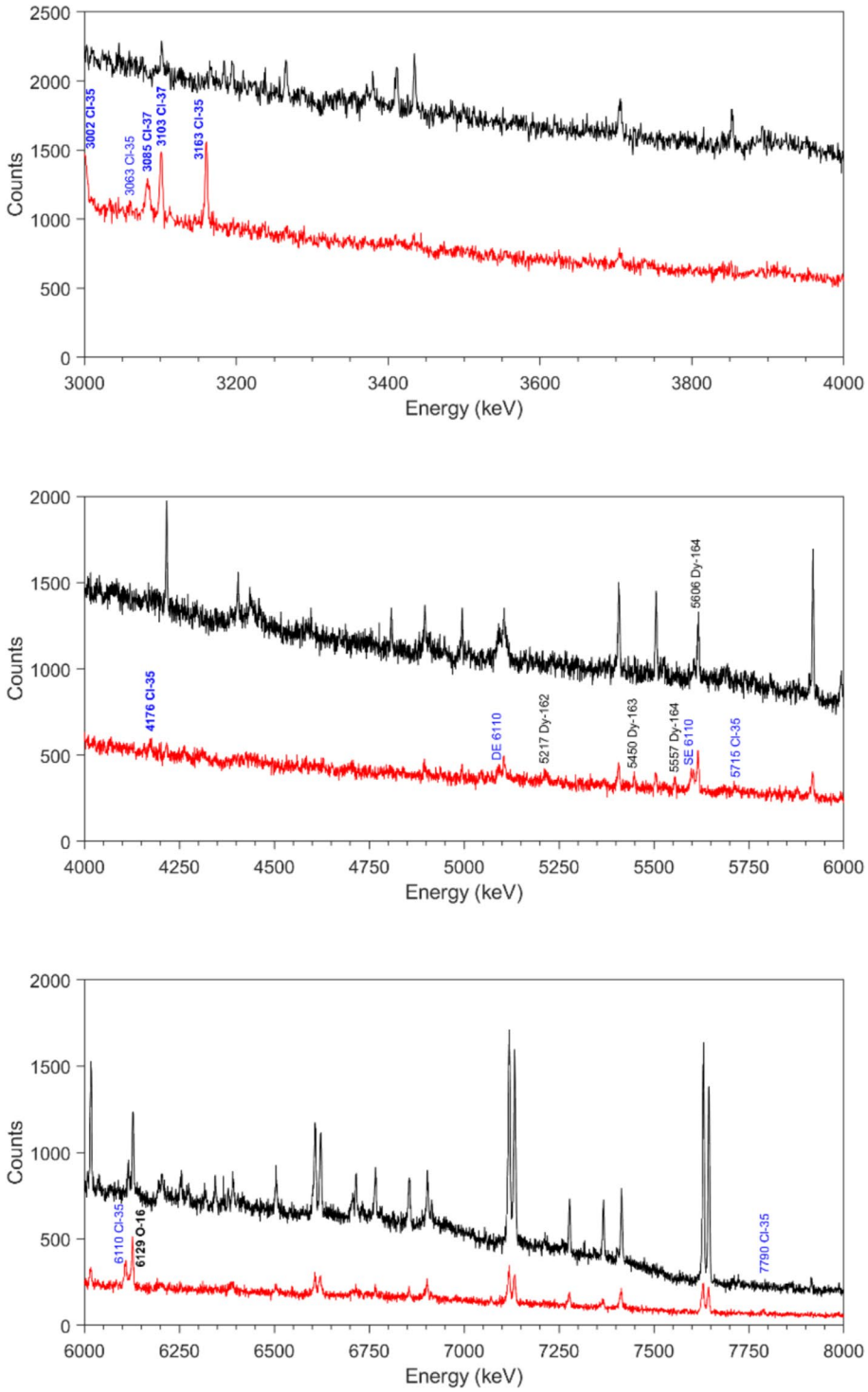

Fig. 4 Gamma-ray spectra in the energy range 3000–8000 keV recorded during 8980 s live time for the $DyCl_3{\cdot}6H_2O$ (red) sample and 51,506 s for the beam background (black). Prompt gamma rays produced by neutron capture in Dyn are written in black and for Cl in blue. Lines from $(n,n'\gamma)$ reaction in Cl are written in blue and bold. SE and DE indicate single and double escape peaks, respectively

(15%). The contribution of fast neutrons was 29% for ^{148}Sm, 17% for ^{154}Sm and ^{156}Dy and 26% for ^{158}Dy. The rates of the (n,n´)-reaction for samarium and dysprosium isotopes, with the exception of ^{144}Sm, ^{148}Sm, ^{154}Sm and ^{164}Dy, were of the same order of magnitude as their respective (n,γ)-reaction rates. In the case of ^{144}Sm and ^{154}Sm, the rate of the (n,n´) reaction was about 15 times higher than that of the (n,γ) reaction and, 10 times higher for ^{148}Sm and ^{164}Dy.

The correlation between the intensities ($\boldsymbol{I_R}$) of $(n,n'\gamma)$-lines measured in this work and the intensities ($\boldsymbol{I_{RD}}$) given in [14–20] was analyzed with the following semi-empirical function:

Table 1 Effective cross sections $<\sigma>$ for (n,γ) reactions produced from the irradiation of the $SmCl_3{\cdot}7H_2O$ and $DyCl_3{\cdot}6H_2O$ samples and interfering with $(n,n'\gamma)$ lines of interest calculated as described in our previous work [9]. Neutron self-shielding factors f_n for all three neutron-energy ranges considered were determined by means of Monte Carlo simulations with the MCNP6 [42, 43]

Neutron-energy Range Flux	10^{-10} – $1.4{\cdot}10^{-7}$ MeV (thermal) $(3.16\pm1.28)\ 10^3$ cm^{-2} s^{-1}			$1.4{\cdot}10^{-7}$ – 0.06 MeV (epithermal) $(2.94\pm0.77)\ 10^6$ cm^{-2} s^{-1}	0.06 – 20 MeV (fast) $(1.13\pm0.04)\ 10^8$ cm^{-2} s^{-1}			10^{-10} – 20 MeV (integral) $(1.16\pm0.04)\ 10^8$ cm^{-2} s^{-1}
Cross sections	$<\sigma_{th}>$ (b)	$<\sigma_{th}>$ (b)[a]	$<\sigma_{th}>$ (b)[b]	$<\sigma_{epi}>$ (b)	$<\sigma_{fast}>$ (mb)	$<\sigma_{fast}>$ (mb)[a]	$<\sigma_{(n,n')}>$ (b)	$<\sigma_{int}>$ (mb)[a]
$^{35}Cl(n,\gamma)^{36}Cl$	38(18)	43.61(1)	43.6(4)	0.37(1)	0.72(19)	0.77(31)	0.24(2)	0.72(25)
$^{144}Sm(n,\gamma)^{145}Sm$	1.42(69)	1.63(1)	1.64(10)	0.12(2)	56(6)	61(9)	0.97(9)	58(6)
$^{147}Sm(n,\gamma)^{148}Sm$	50(24)	57.20(27)	57(3)	36(5)	95(13)	146(28)	2.01(21)	1014(276)
$^{148}Sm(n,\gamma)^{149}Sm$	2(1)	2.40(1)	2.4(6)	2.97(41)	54(7)	72(11)	1.85(18)	129(24)
$^{149}Sm(n,\gamma)^{150}Sm$	61,550(28,524)	68,250(557)	40,140(600)	68(9)	160(23)	223(23)	2.24(24)	3771(901)
$^{150}Sm(n,\gamma)^{151}Sm$	87(42)	101(3)	100(4)	17(2)	81(11)	93(5)	2.13(22)	517(127)
$^{152}Sm(n,\gamma)^{153}Sm$	180(87)	206.8(2)	206(6)	128(16)	60(8)	75(10)	2.26(23)	3337(958)
$^{154}Sm(n,\gamma)^{155}Sm$	7(3)	8.38(7)	8.3(5)	2.98(41)	28(4)	36(4)	2.35(24)	104(23)
$^{156}Dy(n,\gamma)^{157}Dy$	29(14)	33.45(19)	33(3)	37(5)	340(40)	400(20)	2.24(23)	1281(286)
$^{158}Dy(n,\gamma)^{159}Dy$	37(18)	42.49(10)	43(6)	13(2)	200(30)	230(30)	2.34(24)	530(107)
$^{160}Dy(n,\gamma)^{161}Dy$	49(28)	57(2)	55(3)	44(6)	150(20)	170(10)	2.44(25)	1274(336)
$^{161}Dy(n,\gamma)^{162}Dy$	517(251)	592(5)	600(25)	38(5)	88(13)	128(6)	2.80(31)	1074(289)
$^{162}Dy(n,\gamma)^{163}Dy$	170(80)	196(2)	194(10)	89(11)	61(8)	70(9)	2.59(27)	2340(665)
$^{163}Dy(n,\gamma)^{164}Dy$	109(53)	128(5)	134(7)	29(4)	44(7)	66(4)	2.83(31)	788(222)
$^{164}Dy(n,\gamma)^{165}Dy$	2281(1109)	2619(2)	2650(278)	4.12(60)	23(3)	28(5)	2.63(28)	200(43)

a: mean value of cross sections from various data libraries provided in JANIS [41]. b: values from [24]

$$I_R = a \cdot \left(I_{RD}\right)^b \tag{3}$$

where a and b are the coefficients returned by the fit to the measured data. Furthermore, the degree of agreement between the data is estimated from the intensity residual distribution in units of the standard deviation [σ], defined as:

$$R = \frac{I_R - I_{RD}}{\sqrt{\left(s_{I_R}\right)^2 + \left(s_{I_{RD}}\right)^2}} \tag{4}$$

where s is the absolute uncertainty of the intensity.

Gamma rays of samarium

One hundred and fourteen prompt gamma rays induced by inelastic scattering of fission neutrons with samarium were identified. These gamma rays are depicted in Figs. 1 and 2 and the corresponding data are given in Tables 2, 3, 4, 5, 6, 7, 8 and 9. From the observed lines, 2 were assigned to ^{144}Sm, 13 to ^{147}Sm, 14 to ^{148}Sm, 9 to ^{149}Sm, 20 to ^{150}Sm, 18 to ^{152}Sm and 12 to ^{154}Sm. The other 52 lines belong to the multi-isotope lines, and they were found to be fed by two or three samarium isotopes with significant contributions. With

Table 2 Prompt gamma rays of ^{144}Sm induced by inelastic scattering of fission neutrons

This work				From [14]		
E_γ (keV)	$P_{E\gamma}(90°)/(\varepsilon_{E\gamma}{\cdot}f_{E\gamma})$ $\times10^{-8}$ (count)	I_R(relative) (%)	$<\sigma_{E\gamma}(90°)>$ (mb)	E_γ (keV)	I_{RD}(relative) (%)	R
149.99 ± 0.06[a]	0.31 ± 0.07	5.16 ± 1.48	294 ± 86	149.8 ± 0.4	6.2 ± 0.8	−0.62
		43 ± 10		**150.05 ± 0.10[b]**	**58 ± 10[b]**	**−1.06**
1659.70 ± 0.11	0.72 ± 0.04	12.1 ± 2.0	690 ± 45	1659.8 ± 0.2	6.6 ± 0.9	2.51
		100		**1659.77 ± 0.10[b]**	**100**	

E_γ is the gamma-ray energy, $P_{E\gamma}(90°)/(\varepsilon_{E\gamma}{\cdot}f_{E\gamma})$ the net counts in the gamma-ray peak divided by the full-energy-peak efficiency and the gamma-ray self-absorption factor, I_R the relative intensity of the gamma ray and $<\sigma_{E\gamma}(90°)>$ the fission-neutron spectrum-averaged partial cross section for gamma-ray production at an angle of 90° between neutron beam and detector. R is the residual calculated by Eq. (4)

[a]Corrected for (n,γ) interference from Sm. [b]from isotopic measurement [14]

Table 3 Prompt gamma rays of ^{147}Sm induced by inelastic scattering of fission neutrons

This work				From [14, 15]		
E_γ (keV)	$P_{E\gamma}(90°)/(\varepsilon_{E\gamma}.f_{E\gamma})$ $\times 10^{-8}$ (count)	I_R(relative) (%)	$<\sigma_{E\gamma}(90°)>$ (mb)	E_γ (keV)	I_{RD}(relative) (%)	R
215.02 ± 0.05	0.63 ± 0.03	10.5 ± 1.7	123 ± 7	215.11 ± 0.10	10.2 ± 1.2	0.15
		26 ± 7		**215.23 ± 0.10[d]**	**19 ± 2[d]**	**0.96**
715.86 ± 0.07[a]	2.45 ± 0.61	41 ± 12	479 ± 120	716.5 ± 0.3	23 ± 3	1.45
		100		**716.15 ± 0.15[d]**	**100**	
741.31 ± 0.10[a]	0.22 ± 0.03	3.71 ± 0.80	43 ± 6	–	–	–
		8.98 ± 2.55		**741.5 ± 0.2[d]**	**8.9 ± 0.8[d]**	**0.03**
798.25 ± 0.13	0.13 ± 0.02	2.12 ± 0.48	25 ± 4	–	–	–
		5.31 ± 1.55		**798.58 ± 0.15[d]**	**3.9 ± 0.8[d]**	**0.81**
942.21 ± 0.18	0.15 ± 0.03	2.50 ± 0.58	29 ± 6	–	–	–
		6.12 ± 1.95		**942.18 ± 0.15[d]**	**8.3 ± 1.8[d]**	**–0.82**
947.71 ± 0.11[a]	0.27 ± 0.07	4.55 ± 1.37	53 ± 14	–	–	–
		11 ± 4		**947.9 ± 0.1[d]**	**14 ± 2[d]**	**–0.67**
955.32 ± 0.25	0.10 ± 0.02	1.64 ± 0.46	19 ± 4	–	–	–
		4.08 ± 1.30		**955.78 ± 0.15[d]**	**4.2 ± 0.6[d]**	**–0.36**
1076.67 ± 0.19[b]	0.11 ± 0.03	1.92 ± 0.52	22 ± 6	–	–	–
		4.49 ± 1.65		**1077.0 ± 0.1[d]**	**7.0 ± 1.4[d]**	**–1.16**
1106.59 ± 0.09[a,b]	0.40 ± 0.03	6.68 ± 1.16	78 ± 6	–	–	–
		16 ± 4		**1107.3 ± 0.1[d]**	**20 ± 3[d]**	**–0.80**
1180.10 ± 0.18	0.20 ± 0.03	3.27 ± 0.66	38 ± 6	–	–	–
		8.16 ± 2.37		**1180.5 ± 0.2[d]**	**8.8 ± 1.7[d]**	**–0.22**
1196.94 ± 0.09[a,b]	0.26 ± 0.02	4.30 ± 0.72	50 ± 4	–	–	–
		10.6 ± 2.8		**1197.2 ± 0.2[d]**	**10 ± 3[d]**	**0.15**
1250.99 ± 0.23[c]	0.05 ± 0.01	0.83 ± 0.22	10 ± 2	–	–	–
		2.04 ± 0.65		**1252.0 ± 0.5[d]**	**2.2 ± 0.6[d]**	**– 0.18**
1449.23 ± 0.21	0.17 ± 0.03	2.89 ± 0.66	34 ± 6	–	–	–
		6.94 ± 2.12		**1449.2 ± 0.2[d]**	**5.8 ± 0.8[d]**	**0.50**

E_γ is the gamma-ray energy, $P_{E\gamma}(90°)/(\varepsilon_{E\gamma}.f_{E\gamma})$ the net counts in the gamma-ray peak divided by the full-energy-peak efficiency and the gamma-ray self-absorption factor, I_R the relative intensity of the gamma ray and $<\sigma_{E\gamma}(90°)>$ the fission-neutron spectrum-averaged partial cross section for gamma-ray production at an angle of 90° between neutron beam and detector. R is the residual calculated by Eq. (4)

[a]Corrected for (n,γ) interference from Sm. [b]corrected for background interference. [c]corrected for contribution of the single escape peak of the 1763.5-keV line of ^{35}Cl (69% of net counts). [d]from isotopic measurement [15]

respect to [23] and [24], several pure neutron capture lines have also been identified, as given in Table 10. Their intensities were determined using Eq. (2). Additionally, the delayed gamma line at 104.2 keV ($I\gamma = 74.5\%$ [22]) of the activation product ^{155}Sm ($T_{1/2} = 22.2$ m) was observed. This line contains also the contribution of the 103.2-keV ($I\gamma = 29.1\%$ [22]) line of ^{153}Sm ($T_{1/2} = 46.3$ h). Each single line from the $(n,n'\gamma)$ reaction was carefully checked for possible interferences. The counts produced by the neutron capture were calculated according to Eq. (2) and are given in Table 11. For 70 $(n,n'\gamma)$-lines, the contribution of the neutron capture to the net counts ranges from 1 to 100%. The gamma lines with a contribution above 90% were assumed to be pure capture γ -rays. According to Table 10, the intensities of the lines from the ^{152}Sm$(n,\gamma)^{153}$Sm reaction show a systematic discrepancy from the values derived from the thermal neutron data [23, 24]. This can be attributed to the high resonance capture cross sections. To correct this deviation, an average intensity ratio of 0.30 ± 0.06 was applied as a scaling factor for the counts produced by the capture reaction only in ^{152}Sm.

The intensities of the $(n,n'\gamma)$-lines were calculated relative to the 550-keV line of ^{148}Sm (100%). They are given together with the values determined in [14] from the measurement of a Sm_2O_3 sample with natural abundance in columns 3 and 6 of Tables 2, 3, 4, 5, 6, 7, and 8. Additionally, for comparison to the intensities obtained from irradiation of isotopically- enriched Sm_2O_3 samples (^{144}Sm (92.4%), ^{148}Sm (95.4%), ^{150}Sm (95.0%), ^{152}Sm (99.0%), and ^{154}Sm (98.6%) [14], ^{147}Sm (99.5%) [15], ^{152}Sm (97.4%) [16], ^{154}Sm (97.9%) [17]) the intensities of the lines for each isotope

Table 4 Prompt gamma rays of ^{148}Sm induced by inelastic scattering of fission neutrons

This work				From [14]		
E_γ (keV)	$P_{E\gamma}(90°)/(\varepsilon_{E\gamma}\cdot f_{E\gamma})$ $\times 10^{-8}$ (count)	I_R(relative) (%)	$<\sigma_{E\gamma}(90°)>$ (mb)	E_γ (keV)	I_{RD}(relative) (%)	R
413.67 ± 0.05[a]	0.45 ± 0.07	7.45 ± 1.60	116 ± 18	414.2	8.5 ± 1.0	−0.56
				414.23 ± 0.10[f]	**4.2 ± 0.3[f]**	**1.99**
549.60 ± 0.04[a]	5.98 ± 0.94	100	1558 ± 251	550.23 ± 0.10	100	
		100		**550.23 ± 0.10[f]**	**100**	
552.44 ± 0.08[a]	0.91 ± 0.06	15.3 ± 2.6	143 ± 10	**–**	**–**	–
610.66 ± 0.04[a]	0.66 ± 0.13	11.1 ± 2.8	172 ± 34	611.9	22 ± 3	–2.67
				611.06 ± 0.10[f]	**16.4 ± 0.9[f]**	**–1.80**
873.40 ± 0.11[b]	0.27 ± 0.03	4.45 ± 0.87	69 ± 8	–	–	–
				874.0 ± 0.2[f]	**1.7 ± 0.2[f]**	**3.08**
1114.09 ± 0.14[c]	0.23 ± 0.05	3.84 ± 1.10	60 ± 13	1114	37 ± 4[d]	–3.59
				1113.70 ± 0.10[f]	**2.6 ± 0.2[f]**	**1.11**
1370.51 ± 0.27[b]	0.10 ± 0.03	1.75 ± 0.57	27 ± 8	–	–	–
				1371.1 ± 0.4[f]	**0.38 ± 0.10[f]**	**2.37**
1421.97 ± 0.15	0.22 ± 0.02	3.69 ± 0.70	58 ± 6	1422.9 ± 1.2	1.8 ± 0.8	2.34
				1422.0 ± 0.2[f]	**1.40 ± 0.15[f]**	**3.20**
1454.02 ± 0.13[b]	0.51 ± 0.03	8.48 ± 1.44	132 ± 9	–		–
				1454.5 ± 0.2[f]	**3.5 ± 0.3[f]**	**3.38**
1664.19 ± 0.21[b]	0.15 ± 0.02	2.57 ± 0.56	40 ± 5	–	–	–
				1663.6 ± 0.4[f]	**1.12 ± 0.15[f]**	**2.50**
1776.61 ± 0.31	0.15 ± 0.03	2.45 ± 0.68	38 ± 8	–	–	–
2145.18 ± 0.49	0.12 ± 0.03	1.96 ± 0.60	31 ± 8	–	–	–
2203.06 ± 0.33[b]	0.09 ± 0.02	1.54 ± 0.42	24 ± 5	–	–	–
				2204.1 ± 0.1[f]	**0.24 ± 0.10[f]**	**3.01**
2514.29 ± 0.41[b]	0.05 ± 0.02	0.91 ± 0.30	14 ± 6	–	–	–
				2512.1 ± 0.9[f]	**0.22 ± 0.10[f]**	**2.18**

E_γ is the gamma-ray energy, $P_{E\gamma}(90°)/(\varepsilon_{E\gamma}\cdot f_{E\gamma})$ the net counts in the gamma-ray peak divided by the full-energy-peak efficiency and the gamma-ray self-absorption factor, I_R the relative intensity of the gamma ray and $<\sigma_{E\gamma}(90°)>$ the fission-neutron spectrum-averaged partial cross section for gamma-ray production at an angle of 90° between neutron beam and detector. R is the residual calculated by Eq. (4)

[a] Corrected for (n,γ) interference from Sm. [b] confirmed by Demidov´s isotopic measurements. [c] corrected for background interference. [d]1112 and 1114 keV (unresolved doublet by Demidov). [e]corrected for (n,g) interference from Cl. [f]from isotopic measurement [14]

were calculated relative to the following lines: 1560 keV for ^{144}Sm, 716 keV for ^{147}Sm, 550 keV for ^{148}Sm, 334 keV for ^{150}Sm, 963 keV for ^{152}Sm and 839 keV for ^{154}Sm. The calculated values are given in bold in columns 3 and 6 of Tables 2, 3, 4, 6, 7 and 8. The corrections for radiative neutron capture in [14] were done using the data given in [44]. We identified 58 of 73 lines given in [14] from the measurement of the samarium sample with natural abundance and the 53 lines listed in [14] from the measurement of the isotopically-enriched samples (2 for ^{144}Sm, 9 for ^{148}Sm, 17 for ^{150}Sm, 15 for ^{152}Sm and 10 for ^{154}Sm). All the lines observed for ^{152}Sm and ^{154}Sm came from isotopic measurements documented by [16] and [17]. For ^{147}Sm, we observed the 13 lines listed in [15]. 13 of 73 lines in [14] have been listed as tentative assignments. The lines at 215.1, 222.8, 461.5, 716.5, 969.4 and 1408.9 keV were observed in our measurement which were attributed to $(n,n'\gamma)$ transitions in Sm according to the data given in [22, 25, 27–31]. However, except for the 461.5-, 969.4- and 1408.9 keV lines, these gamma rays have not been observed in the isotopic measurement of Demidov et al. [14]. The net counts of the 1251.0-keV line from ^{147}Sm includes a significant contribution of (69 ± 3) % from the single escape peak of the 1763.5-keV line produced by the ^{35}Cl$(n,n'\gamma)^{35}$Cl reaction. The lines at the energies of 158.7, 197.4, 228.5, 297.7, 361.6, 535.8, 563.2 930.0, 1096.5 and 1204 keV in [14] have not been observed. The absence of the unassigned lines at 228.5 and 361.6 keV and plausible data provided in [22] suggests that these lines do not belong to Sm. These two lines were not observed in Demidov´s isotopic measurements [14] either. The line at 930.0 keV could not be identified uniquely due to interference from the ^{35}Cl$(n,n'\gamma)^{35}$Cl reaction. The assignment

Table 5 Prompt gamma rays of ^{149}Sm induced by inelastic scattering of fission neutrons

This work				From [14]		
E_γ (keV)	$P_{E\gamma}(90°)/(\varepsilon_{E\gamma} f_{E\gamma})$ $\times 10^{-8}$ (count)	I_R(relative) (%)	$<\sigma_{E\gamma}(90°)>$ (mb)	E_γ (keV)	I_{RD}(relative) (%)	R
254.31 ± 0.10[a,b]	0.18 ± 0.03	3.02 ± 0.66	38 ± 6	254.6 ± 0.6	3.8 ± 0.8	−0.76
285.43 ± 0.03[b]	2.38 ± 0.08	40 ± 6	504 ± 25	285.84 ± 0.10	26 ± 3	1.96
313.61 ± 0.10[b]	0.22 ± 0.03	3.67 ± 0.81	46 ± 6	314.4 ± 0.4	3.7 ± 0.4	−0.03
326.95 ± 0.05	1.16 ± 0.05	19.3 ± 3.2	245 ± 14	327.8 ± 0.4	10.9 ± 1.5	2.41
527.70 ± 0.17	0.27 ± 0.05	4.46 ± 1.12	56 ± 10	528.7 ± 0.8	1.9 ± 0.3	2.21
557.63 ± 0.08	0.37 ± 0.04	6.12 ± 1.20	78 ± 9	–	–	–
590.21 ± 0.05[b]	0.85 ± 0.04	14.2 ± 2.3	180 ± 10	591.0 ± 0.3	3.5 ± 0.5	4.54
663.43 ± 0.05[a,b]	0.90 ± 0.05	15.0 ± 2.5	190 ± 12	664.05 ± 0.10	10.8 ± 1.2	1.53
951.93 ± 0.20[b]	0.10 ± 0.02	1.60 ± 0.45	20 ± 4	–	–	–

E_γ is the gamma-ray energy, $P_{E\gamma}(90°)/(\varepsilon_{E\gamma} f_{E\gamma})$ the net counts in the gamma-ray peak divided by the full-energy-peak efficiency and the gamma-ray self-absorption factor, I_R the relative intensity of the gamma ray and $<\sigma_{E\gamma}(90°)>$ the fission-neutron spectrum-averaged partial cross section for gamma-ray production at an angle of 90° between neutron beam and detector. R is the residual calculated by Eq. (4)

[a] Corrected for background interference. [b]corrected for (n,γ) interference from Sm

of the 930.0-keV to ^{154}Sm by the isotopic measurements [14, 17] was confirmed by this work due to the observation of the 745.5-keV line, coupled with the first by the excitation level $E^* = 1012.4$ keV [22, 31]. For the lines at 158.7, 197.4, 535.8, 563.2, 1096.5 and 1204 keV, strong interferences of the background lines were identified with respect to [1, 2] and [14]. Possible transitions are provided in [22]. Correct assignment was assumed for the lines at 297.7 keV (^{150}Sm), 563.2 keV (^{152}Sm) and 1096.5 keV (^{154}Sm) as they have been recognized in the isotopic measurements [14, 16]. Nevertheless, those lines should be reviewed carefully owing to background interferences. The line at 535.8 keV being assigned to the ^{149}Sm$(n,n'\gamma)^{149}$Sm reaction in [14] is plausible since the line at 557.6 keV belonging to the same level ($E^* = 558.4$ keV [124, 174]) was clearly observed in this work. The lines at 127.3 and 166.5 keV, listed but not assigned by Demidov et al. have been observed and found to belong to the (n,γ) reactions in ^{152}Sm and ^{150}Sm with absolute intensities of 7.4 and 9.9% [23], respectively.

Compared to the elemental measurement in [14], we identify 80 new lines. All corresponding transitions are specified in [22]. Among of these lines, 11 were assigned to ^{147}Sm, 8 to ^{148}Sm, 2 to ^{149}Sm, 12 to ^{150}Sm, 10 to ^{152}Sm, 5 to ^{154}Sm and 32 to more than one contributing isotope. A total of 40 of those lines have been confirmed by isotopic measurements [14–17]. The absence of the remaining 40 lines in Demidov's measurement can be explained by the difference in the neutron-energy spectra and hence in the excitation level of the nuclei. However, the absence of the lines identified at 761.8 (^{150}Sm), 869.4 ($^{148+150+152}$Sm), 951.9 (^{149}Sm) and 983.6 keV ($^{144+48+152}$ Sm), also in the isotopic measurements, might be reasoned in possible background interferences with respect to [14]. The identification of the lines at 747.6 (^{150}Sm), 838.9 (^{154}Sm), 919.0 (^{152}Sm), 1111.9 (^{152}Sm), 1196.9 (^{147}Sm) and 1170.4 keV ($^{150+152}$Sm) resulted from the resolution of doublets at the energies of 745.8, 840.5, 920.1, 1114, 1194 and 1172 keV in [14]. For this last measurement, further potential doublets at the energies of 405.4, 550.2, 664.0, 857.6, 903.5, 1047.4 and 1392.6 keV were resolved in the present work on the basis of the relative intensities. The broad line at 550.2 keV in [14] associated to ^{148}Sm was resolved as a doublet of 549.6 and 552.4 keV lines, both from ^{148}Sm. This doublet (if present in [14]) might slightly influence the relative intensities obtained in this work, as the measured net counts of the 552.4-keV line was about 15% of that of the 549.6-keV line. The relationship between the relative intensities I_R obtained in this work and the values I_{RD} from [14–17] is shown in Fig. 5. The values of the fit parameters according to Eq. (3) are $a = 2.26 \pm 0.14$ and $b = 0.80 \pm 0.02$. The average intensity ratio I_R/I_{RD} is 1.83 ± 1.44, which clearly indicates a strong discrepancy between the two set of data, probably due to inaccurate correction for neutron capture interferences.

The γ-lines observed at 147.3 ($^{150+152}$Sm), 320.6 (^{152}Sm), 397.3 (^{144}Sm), 571.2 (^{148}Sm) and 629.3 keV (^{148}Sm) were found to have significant interferences with the (n,γ) reactions in Sm, with contributions of (114 ± 28)%, (95 ± 26)%, (99 ± 37)%, (117 ± 27)% and (98 ± 23)%, respectively. Hence, although those lines might in principle also be fed by $(n,n'\gamma)$ transitions listed in [22], all of them were assumed to be pure (n,γ) lines. The lines at 320.6 (unassigned), 397.3 (^{144}Sm) and 629.3 (^{148}Sm) were also identified by [14]. The first line (at 320.6-keV), also found in [14], is probably the 321.1-keV ($I\gamma = 2.9\%$ [23]) neutron capture line from the ^{152}Sm$(n,\gamma)^{153}$Sm reaction. The two last ones have been assigned to inelastic

Table 6 Prompt gamma rays of ^{150}Sm induced by inelastic scattering of fission neutrons

This work				From [14]		
E_γ (keV)	$P_{E\gamma}(90°)/(\varepsilon_{E\gamma}\cdot f_{E\gamma})$ $\times 10^{-8}$ (count)	I_R(relative) (%)	$<\sigma_{E\gamma}(90°)>$ (mb)	E_γ (keV)	I_{RD}(relative) (%)	R
333.37 ± 0.05[a]	20.34 ± 2.02	340 ± 63	8077 ± 851	333.92 ± 0.07	151 ± 15	2.92
		100		**333.92 ± 0.07[d]**	**100**	
		100		**333.92 ± 0.07[e]**	**100**	
345.34 ± 0.10[a,b]	0.21 ± 0.03	3.44 ± 0.75	82 ± 12	–	–	–
		1.03 ± 0.18		**346.00 ± 0.10[e]**	**0.80 ± 0.08[e]**	**1.17**
405.83 ± 0.06[a]	0.59 ± 0.05	9.83 ± 1.73	233 ± 21	405.4	4.2 ± 0.6	3.08
		2.90 ± 0.38		**405.4[d]**	**2.78 ± 0.48[d]**	**0.20**
				404.46 ± 0.08[e]	**7.7 ± 0.4[e]**	**−8.70**
438.68 ± 0.04[a]	8.46 ± 0.98	142 ± 28	3358 ± 407	439.4	66 ± 8	2.63
		41 ± 6		**439.4[d]**	**44 ± 7[d]**	**−0.32**
				439.40 ± 0.04[e]	**15.8 ± 0.9[e]**	**4.15**
461.01 ± 0.11[a]	0.38 ± 0.05	6.31 ± 1.27	150 ± 20	461.5 ± 0.6	3.5 ± 0.5	2.06
		1.87 ± 0.30		**461.5 ± 0.6[d]**	**2.32 ± 0.40[d]**	**−0.90**
				462.7 ± 0.4[e]	**0.20 ± 0.04[e]**	**5.51**
485.40 ± 0.08[a]	0.11 ± 0.02	1.92 ± 0.47	46 ± 8	–	–	–
583.58 ± 0.04[a,c]	1.55 ± 0.16	26 ± 5	615 ± 67	584.3	6.3 ± 0.7	3.97
		7.62 ± 1.09		**584.3[d]**	**4.17 ± 0.62[d]**	**2.75**
				584.30 ± 0.10[e]	**1.70 ± 0.12[e]**	**5.40**
666.05 ± 0.14[a,b,c]	0.03 ± 0.01	0.58 ± 0.15	14 ± 5	–	–	–
		0.15 ± 0.05		**668.0 ± 0.6[e]**	**0.30 ± 0.06[d]**	**−1.92**
711.70 ± 0.06[a]	1.26 ± 0.13	21 ± 4	501 ± 55	712.5 ± 0.6	8.4 ± 1.2	3.06
		6.19 ± 0.89		**712.5 ± 0.6[d]**	**5.56 ± 0.97[d]**	**0.48**
				712.23 ± 0.08[e]	**7.4 ± 0.5[e]**	**−1.18**
730.99 ± 0.07[a,b]	0.12 ± 0.02	1.95 ± 0.44	46 ± 8	–	–	–
		0.59 ± 0.11		**731.4 ± 0.2[e]**	**0.40 ± 0.07[e]**	**1.45**
736.92 ± 0.05[a]	2.31 ± 0.24	39 ± 7	918 ± 101	737.45 ± 0.08	11.4 ± 1.2	3.69
		11 ± 2		**737.45 ± 0.08[d]**	**7.55 ± 1.09[d]**	**1.51**
				737.45 ± 0.08[e]	**7. 5 ± 0.5[e]**	**1.70**
747.61 ± 0.08[a,b,c]	0.14 ± 0.01	2.34 ± 0.39	56 ± 4	–	–	–
		0.69 ± 0.08		**748.8 ± 0.2[e]**	**0.42 ± 0.05[e]**	**2.86**
751.02 ± 0.11[a]	0.35 ± 0.03	5.89 ± 1.04	140 ± 13	–	–	–
761.76 ± 0.15[a,b,c]	0.11 ± 0.02	1.78 ± 0.39	42 ± 8	–	–	–
		0.54 ± 0.11		**761.4 ± 0.3[e]**	**0.21 ± 0.03[e]**	**2.89**
1046.04 ± 0.09[a,b]	0.48 ± 0.06	8.11 ± 1.57	192 ± 25	1047.4 ± 0.8	1.4 ± 0.4	4.14
		2.36 ± 0.38		**1047.4 ± 0.8[d]**	**0.93 ± 0.28[d]**	**3.03**
				1047.2 ± 0.2[e]	**1.47 ± 0.17[e]**	**2.14**
1048.71 ± 0.09[a]	0.72 ± 0.03	12.1 ± 2.0	287 ± 16	–	–	–
1122.23 ± 0.14[a,b]	0.11 ± 0.02	1.84 ± 0.41	44 ± 8	–	–	–
		0.54 ± 0.11		**1123.2 ± 0.5[e]**	**0.11 ± 0.03[e]**	**3.77**
1246.57 ± 0.17[a,b]	0.13 ± 0.02	2.13 ± 0.52	50 ± 8	–	–	–
		0.64 ± 0.12		**1247.7 ± 0.6[e]**	**0.10 ± 0.03[e]**	**4.36**
1323.85 ± 0.20[a,b]	0.37 ± 0.04	6.26 ± 1.24	148 ± 17	–	–	–
		1.82 ± 0.27		**1124.5 ± 0.2[e]**	**0.96 ± 0.11[e]**	**2.95**
1486.18 ± 0.25[a,b,c]	0.15 ± 0.02	2.46 ± 0.51	58 ± 8	–	–	–
		0.74 ± 0.12		**1486.5 ± 0.6[e]**	**0.17 ± 0.04[e]**	**4.51**

E_γ is the gamma-ray energy, $P_{E\gamma}(90°)/(\varepsilon_{E\gamma}\cdot f_{E\gamma})$ the net counts in the gamma-ray peak divided by the full-energy-peak efficiency and the gamma-ray self-absorption factor, I_R the relative intensity of the gamma ray and $<\sigma_{E\gamma}(90°)>$ the fission-neutron spectrum-averaged partial cross section for gamma-ray production at an angle of 90° between neutron beam and detector. R is the residual calculated by Eq. (4)

[a]Corrected for (n,γ) interference from Sm. [b]confirmed by Demidov´s isotopic measurement. [c]corrected for background interference. [d]from elemental measurement [14]. [e]from isotope measurement [14]

Table 7 Prompt gamma rays of ^{152}Sm induced by inelastic scattering of fission neutrons

This work				From [14] [16]		
E_γ (keV)	$P_{E\gamma}(90°)/(\varepsilon_{E\gamma} f_{E\gamma}) \times 10^{-8}$ (count)	I_R(relative) (%)	$<\sigma_{E\gamma}(90°)>$ (mb)	E_γ (keV)	I_{RD}(relative) (%)	R
244.37 ± 0.03	4.49 ± 0.14	75 ± 12	492 ± 23	244.66 ± 0.10	46 ± 5	2.24
		335 ± 16		**244.66 ± 0.10[e]**	**287 ± 47[e]**	**0.97**
				244.66 ± 0.03[f]	**348 ± 55[f]**	**−0.23**
				244.6 ± 0.1[g]	**267 ± 42[g]**	**1.51**
268.81 ± 0.12[a]	0.03 ± 0.01	0.45 ± 0.14	2.97 ± 0.99	–	–	–
		2.24 ± 0.75		**269.4 ± 0.2[g]**	**1.23 ± 0.45[g]**	**1.15**
339.80 ± 0.05[a]	0.61 ± 0.15	10.3 ± 3.0	67 ± 17	340.6 ± 0.3	4.8 ± 0.7	1.77
		45 ± 11		**340.6 ± 0.3[e]**	**53 ± 10[e]**	**−0.54**
				340.33 ± 0.04[f]	**58 ± 5[f]**	**−1.07**
				340.3 ± 0.1[g]	**41 ± 6[g]**	**0.32**
655.96 ± 0.07	0.33 ± 0.02	5.56 ± 0.96	36 ± 2	656.5 ± 0.4	3.7 ± 0.4	1.79
		25 ± 2		**656.5 ± 0.4[e]**	**23 ± 4[e]**	**0.44**
				656.52 ± 0.09[f]	**26 ± 3[f]**	**−0.28**
				656.5 ± 0.1[g]	**21 ± 3[g]**	**1.11**
791.36 ± 0.25[a]	0.10 ± 0.03[h]	1.62 ± 0.50	11 ± 3	–	–	–
		7.46 ± 2.25		**791.7 ± 0.2[g]**	**5.68 ± 2.18[g,h]**	**0.24**
841.12 ± 0.16	0.78 ± 0.10	13.0 ± 2.6	88 ± 12	840.5	10 ± 2[b]	−0.20
		58 ± 8		**840.5[e]**	**62 ± 14[e,b]**	**−0.25**
				841.6 ± 0.2[f]	**51 ± 7[f]**	**0.66**
				841.4 ± 1[g]	**55 ± 8[g]**	**0.26**
854.85 ± 0.08[a]	0.35 ± 0.03	5.82 ± 1.02	38 ± 3	–	–	–
		26 ± 2		**854.9 ± 0.2[f]**	**21 ± 3[f]**	**1.39**
				855.2 ± 0.1[g]	**16 ± 3[g]**	**2.77**
900.89 ± 0.19[d]	0.20 ± 0.03	3.39 ± 0.71	22 ± 3	–	–	–
		15 ± 2		**901.1 ± 0.2[f]**	**14 ± 2[f]**	**0.35**
				901.4 ± 0.1[g]	**11 ± 2[g]**	**1.41**
918.99 ± 0.08[c,d]	0.88 ± 0.05	14.7 ± 2.5	96 ± 6	–	–	–
		66 ± 4		**919.30 ± 0.10[f]**	**65 ± 8[f]**	**0.11**
				919.2 ± 0.1[g]	**62 ± 9[g]**	**0.41**
926.00 ± 0.14[c,d]	0.22 ± 0.03	3.67 ± 0.78	24 ± 3	–	–	–
		16 ± 2		**926.6 ± 0.3[f]**	**15 ± 2[f]**	**0.35**
				926.4 ± 0.1[g]	**15 ± 2[g]**	**0.35**
963.31 ± 0.07	1.34 ± 0.05	22 ± 4	147 ± 7	963.30 ± 0.10	16 ± 2	1.57
		100		**963.30 ± 0.10[f]**	**100**	–
		100		**963.5 ± 0.1[g]**	**100**	–
995.84 ± 0.17[a,c,d]	0.10 ± 0.02	1.62 ± 0.39	11 ± 2	–	–	–
		7.46 ± 1.52		**995.2 ± 0.4[f]**	**3.08 ± 0.67[f]**	**2.64**
				995.5 ± 0.2[g]	**3.90 ± 0.63[g]**	**2.16**
1004.76 ± 0.11	0.29 ± 0.03	4.92 ± 0.89	32 ± 3	1005.5 ± 1.6	1.7 ± 0.3	3.43
		22 ± 2		**1005.5 ± 1.6[e]**	**11 ± 2[e]**	**3.89**
				1005.1 ± 0.2[f]	**17 ± 2[f]**	**1.77**
				1005.1 ± 0.1[f]	**18 ± 2[g]**	**1.41**
1085.70 ± 0.13	0.34 ± 0.03	5.64 ± 1.03	37 ± 3	1085.8 ± 0.3	2.1 ± 0.3	3.31
		25 ± 2		**1085.8 ± 0.3[e]**	**13 ± 2[e]**	**4.24**
				1085.70 ± 0.10[f]	**29 ± 4[f]**	**−0.89**
				1085.7 ± 0.1[f]	**30 ± 4[g]**	**−1.12**
1111.91 ± 0.09[c,d]	0.64 ± 0.04	10.7 ± 1.8	70 ± 5	–	–	–
		48 ± 3		**1112.03 ± 0.06[f]**	**35 ± 4[f]**	**2.60**
				1112.1 ± 0.1[f]	**42 ± 6[g]**	**0.89**

Table 7 (continued)

This work				From [14] [16]		
E_γ (keV)	$P_{E\gamma}(90°)/(\varepsilon_{E\gamma} f_{E\gamma})$ $\times 10^{-8}$ (count)	I_R(relative) (%)	$<\sigma_{E\gamma}(90°)>$ (mb)	E_γ (keV)	I_{RD}(relative) (%)	R
1388.67 ± 0.12[c]	0.39 ± 0.03	6.52 ± 1.15	43 ± 4	–	–	–
		29 ± 2		**1389.0 ± 0.2[f]**	**17 ± 2[f]**	**4.24**
				1389.1 ± 0.1[f]	**16 ± 2[g]**	**4.60**
1408.04 ± 0.15[d]	0.22 ± 0.02	3.69 ± 0.70	24 ± 2	1408.9 ± 1.2	2.3 ± 0.6	1.50
		16 ± 1		**1408.9 ± 1.2[e]**	**14 ± 4[e]**	**0.48**
				1407.9 ± 0.2[f]	**16 ± 2[f]**	**0**
				1408.0 ± 0.1[f]	**15 ± 2[g]**	**0.45**
1915.84 ± 0.36	0.08 ± 0.02	1.39 ± 0.46	9 ± 2	–	–	–

E_γ is the gamma-ray energy, $P_{E\gamma}(90°)/(\varepsilon_{E\gamma} f_{E\gamma})$ the net counts in the gamma-ray peak divided by the full-energy-peak efficiency and the gamma-ray self-absorption factor, I_R the relative intensity of the gamma ray and $<\sigma_{E\gamma}(90°)>$ the fission-neutron spectrum-averaged partial cross section for gamma-ray production at an angle of 90° between neutron beam and detector. R is the residual calculated by Eq. (4)

[a]Corrected for (n,γ) interference from Sm. [b]839 and 841 keV (unresolved doublet by Demidov). [c]confirmed by Demidov´s isotopic measurement. [d]corrected for background interference. [e]from element measurement [14]. [f]from isotope measurement [14]. [g]from isotope measurement [16]. [h]includes the intensity of the 790 keV line of ^{152}Sm [16]

scattering reactions in ^{144}Sm and ^{148}Sm, respectively. In the isotopic measurement of ^{148}Sm, Demidov, in [14], has used the same line as a reference for intensities as in the elemental measurement (550.2-keV line). The intensity of (25 ± 3) % of the 629.3-keV line from the elemental measurement disagrees by a factor of 1.8 higher to that one derived from the isotopic measurement, i.e. (14.2 ± 0.7)% [14]. For the 397.3-keV line of ^{144}Sm, the intensities disagreed by a factor 6 between elemental and isotopic measurements in [14] when using as reference line the 1660-keV line of ^{144}Sm. Note that the latter line is free of any interference. For ^{148}Sm, the average intensity ratio I_R/I_{RD} is 2.35 ± 1.71 and improved to 1.24 ± 0.70 when no correction is applied. In fact, the 550-keV line was also strongly affected by neutron capture mainly in the isotope ^{147}Sm (550.1 keV [23]), but also in ^{149}Sm (548.3 keV [23]), ^{150}Sm (550.9 keV [23]) and ^{154}Sm (551.2 keV [23]). The overall contribution to net counts was (62 ± 15) % (see Table 10). With respect to [44], the capture line at 550 keV is listed with a question mark and an intensity of 1.2%. The intensity is in good agreement with the value derived from [23], i.e. (1.12 ± 0.07) %. Therefore, it is very likely that Demidov et al. [14] did not correct this line as its presence was at that time uncertain. The (n,γ) lines listed at 127.3 and 166.5 keV in [14] were given with relative intensities of (4.6 ± 1.0) % and (2.7 ± 0.8) %, respectively. In this work, intensities of (18.0 ± 2.9) % and (4.7 ± 0.2) % were determined. However, relative intensities of (6.9 ± 0.3) % and (1.8 ± 0.1) % were obtained when the reference line at 549.6 keV was uncorrected. The fact that the intensities from this work compare better to the work of Demidov et al. [14] if no (n,γ) corrections are performed, is a further indication for missing or inaccurate corrections for neutron capture in [14]. The intensities of the lines of ^{147}Sm, ^{152}Sm and ^{154}Sm measured in this work agree well with the values derived from the isotopic measurements [14–16] using the reference lines free of any interferences at 716 keV, 963 keV and 839 keV as the contributions of (n,γ)-lines were in most of the cases negligible. The values of I_R/I_{RD} are 1.04 ± 0.30 for ^{147}Sm, 1.38 ± 0.49 for ^{152}Sm and 1.42 ± 0.53 for ^{154}Sm. If no correction for neutron capture is applied, the values are statistically consistent: 0.93 ± 0.28, 1.28 ± 0.52 and 1.24 ± 0.60. In the case of ^{150}Sm, many lines are strongly affected by the neutron capture lines, and better agreement with the values from the elemental measurement in [14] was obtained by using the reference line at 334 keV of ^{150}Sm instead of the 550 keV-line of ^{148}Sm. However, a large difference was observed for some lines compared to the isotopic measurement in [14]. Note that the 334-keV line is also a strong capture line of the ^{149}Sm$(n,\gamma)^{150}$Sm reaction which intensity given in [44], 83.26% is near the more recent value of 86% [23]. The value of I_R/I_{RD} is 2.57 ± 1.98 was not improved by neglecting the contributions of neutron capture lines, 2.19 ± 1.78. For the lines emitted by several samarium isotopes, the average intensity I_R/I_{RD} is 2.62 ± 2.30 and is improved to 1.15 ± 1.06 without corrections of neutron capture. Considering all data and no correction for neutron capture yields an average intensity ratio of $I_R/I_{RD} = 1.37 \pm 1.05$, which can, besides the large uncertainty, be considered as another hint for missing or inaccurate corrections for neutron capture in the Atlas [14]. In this case, the data show a better correlation with $a = 1.42 \pm 0.10$ and $b = 0.89 \pm 0.03$ in Eq. (3) as shown in Fig. 5. The histograms of the residuals R obtained with and without correction of neutron capture are shown on

Table 8 Prompt gamma rays of ^{154}Sm induced by inelastic scattering of fission neutrons

This work				From [14, 17]		
E_γ (keV)	$P_{E\gamma}(90°)/(\varepsilon_{E\gamma}.f_{E\gamma})$ $\times 10^{-8}$ (count)	I_R(relative) (%)	$<\sigma_{E\gamma}(90°)>$ (mb)	E_γ (keV)	I_{RD}(relative) (%)	R
81.90 ± 0.04[a]	4.33 ± 0.19	72 ± 12	558 ± 31	–	–	–
184.69 ± 0.03	3.85 ± 0.12	65 ± 10	497 ± 23	185.06 ± 0.06	46 ± 5	1.62
		448 ± 49		**185.06 ± 0.06[d]**	**537 ± 60[d]**	**−1.15**
				184.88 ± 0.03[e]	**479 ± 21[e]**	**−0.58**
745.48 ± 0.06[b,c]	0.44 ± 0.03	7.40 ± 1.28	57 ± 4	745.8	6.3 ± 0.8	0.73
		51 ± 6		**745.39 ± 0.08[d]**	**60 ± 4[d]**	**−1.25**
				745.50 ± 0.04[e]	**50 ± 2[e]**	**−0.16**
838.90 ± 0.08[a]	0.86 ± 0.09	14.4 ± 2.7	112 ± 12	–	–	–
		100		**839.83 ± 0.08[d]**	**100**	–
		100		**839.36 ± 0.02[e]**	**100**	–
1016.73 ± 0.14[b]	0.40 ± 0.03	6.71 ± 1.20	52 ± 4	1017.6	4.8 ± 0.8	1.32
		46 ± 6		**1018.00 ± 0.08[d]**	**42 ± 2[d]**	**0.63**
				1017.23 ± 0.10[e]	**30 ± 1[e]**	**2.63**
1272.56 ± 0.48[a]	0.13 ± 0.03	2.10 ± 0.66	16 ± 4	–	–	–
		15 ± 4		**1272.5 ± 0.2[d]**	**11.3 ± 0.8[d]**	**0.90**
				1272.34 ± 0.07[e]	**9.6 ± 0.5[e]**	**1.39**
1393.67 ± 0.12[c]	0.36 ± 0.03	6.00 ± 1.07	39 ± 3	1392.6	6.1 ± 1.0	−0.07
		42 ± 6		**1394.46 ± 0.07[d]**	**43 ± 2[d]**	**−0.16**
				1393.83 ± 0.03[e]	**34 ± 1[e]**	**1.31**
1432.95 ± 0.15[c]	0.23 ± 0.02	3.85 ± 0.73	30 ± 3	1432.2 ± 1.6	2.7 ± 0.6	1.22
		27 ± 4		**1433.0 ± 0.4[d]**	**23 ± 2[d]**	**0.89**
				1433.19 ± 0.05[e]	**23.7 ± 0.9[e]**	**0.80**
1439.76 ± 0.12	0.37 ± 0.03	6.14 ± 1.08	47 ± 4	1440.2 ± 0.6	2.4 ± 0.5	3.14
		43 ± 6		**1440.08 ± 0.10[d]**	**36 ± 2[d]**	**1.10**
				1440.05 ± 0.10[e]	**41.9 ± 1.5[e]**	**0.18**
1538.62 ± 0.38[a]	0.10 ± 0.02	1.65 ± 0.45	13 ± 2	–	–	–
		12 ± 3		**1538.2 ± 0.4[d]**	**6.0 ± 0.8[d]**	**1.93**
				1538.35 ± 0.14[e]	**4.7 ± 0.3[e]**	**2.42**
1551.48 ± 0.32[a]	0.10 ± 0.02	1.74 ± 0.49	13 ± 3	–	–	–
		12 ± 3		**1550.8 ± 0.4[d]**	**7.4 ± 1.3[d]**	**1.40**
				1551.54 ± 0.09[e]	**5.9 ± 0.3[e]**	**2.02**
1624.42 ± 0.35[a,c]	0.07 ± 0.02	1.23 ± 0.39	9 ± 3	–	–	–
		8.1 ± 2.5		**1624.9 ± 0.6[d]**	**3.0 ± 0.7[d]**	**1.96**
				1624.87 ± 0.12[e]	**6.5 ± 0.3[e]**	**0.63**

E_γ is the gamma-ray energy, $P_{E\gamma}(90°)/(\varepsilon_{E\gamma}.f_{E\gamma})$ the net counts in the gamma-ray peak divided by the full-energy-peak efficiency and the gamma-ray self-absorption factor, I_R the relative intensity of the gamma ray and $<\sigma_{E\gamma}(90°)>$ the fission-neutron spectrum-averaged partial cross section for gamma-ray production at an angle of 90° between neutron beam and detector. R is the residual calculated by Eq. (4)

[a]Confirmed by Demidov´s isotopic measurement. [b]corrected for (n,γ) interference from Sm. [c]corrected for background interference. [d]from isotope measurement [14]. [e]from isotope measurement [17]

Fig. 6. The fit with a Gaussian indicates an agreement between the data at the 1.8σ level for both cases. The shift of the Gaussian centroid to 1.37 ± 0.06 reveals a relevant systematic effect for the corrected intensities. When neutron capture interferences were neglected the centroid has shifted to 0.32 ± 0.13. All these results show that the corrections for neutron capture carried out by Demidov et al. [14] using data from [44] were inaccurate or missed. Furthermore, it is not indicated in [14] which cross section data was used for the capture of epithermal neutrons. It is only mentioned that the intensity of gamma rays could differ from the one from the thermal neutron capture. The partial cross sections for gamma-ray production are given in column 4 of Tables 2, 3, 4, 5, 6, 7, 8, and 9.

Table 9 Prompt gamma rays induced by inelastic scattering of fission neutrons in multiple isotopes of samarium

This work				From [14]		
E_γ (keV)	$P_{E\gamma}(90°)/(\varepsilon_{E\gamma} f_{E\gamma})$ $\times 10^{-8}$ (count)	I_R(relative) (%)	$<\sigma_{E\gamma}(90°)>$ (mb)	E_γ (keV)	I_{RD}(relative) (%)	R
$^{144}Sm + ^{148}Sm$						
1977.23 ± 0.31	0.11 ± 0.02	1.86 ± 0.48	22 ± 4	–	–	–
$^{144}Sm + ^{152}Sm$						
1584.75 ± 0.32[b]	0.17 ± 0.03	2.87 ± 0.71	17 ± 3	–	–	–
2120.54 ± 0.46	0.11 ± 0.03	1.87 ± 0.60	11 ± 3	–	–	
$^{144}Sm + ^{154}Sm$						
1475.05 ± 0.22	0.10 ± 0.02	1.66 ± 0.39	11 ± 2	–	–	–
$^{147}Sm + ^{148}Sm$						
533.88 ± 0.20[a]	0.29 ± 0.05	4.83 ± 1.11	32 ± 6	–	–	–
725.57 ± 0.07[b,c]	0.41 ± 0.03	6.85 ± 1.19	46 ± 4	–	–	–
1354.18 ± 0.12[a]	0.88 ± 0.09	14.7 ± 2.8	98 ± 11	1352	8.5 ± 2.0	1.82
1596.26 ± 0.18[b,c]	0.32 ± 0.03	5.42 ± 0.97	36 ± 4	–	–	–
$^{147}Sm + ^{152}Sm$						
687.89 ± 0.05[c]	0.69 ± 0.04	11.6 ± 1.9	48 ± 3	688.3 ± 0.4	6.1 ± 1.2	2.43
809.08 ± 0.06[a]	1.02 ± 0.06	17.1 ± 2.9	72 ± 5	810.5	11.3 ± 1.2	1.86
$^{147}Sm + ^{154}Sm$						
1069.78 ± 0.23	0.23 ± 0.04	3.91 ± 0.89	18 ± 3	1069.2	1.6 ± 0.4	2.37
1172.88 ± 0.20	0.20 ± 0.03	3.30 ± 0.68	15 ± 2	1172	19 ± 2[d]	–0.15
1317.46 ± 0.29	0.23 ± 0.04	3.78 ± 0.90	17 ± 3	1318.0 ± 0.6	1.7 ± 0.4	2.11
1120.26 ± 0.18[b]	0.16 ± 0.02	2.65 ± 0.56	12 ± 1	–	–	–
$^{148}Sm + ^{150}Sm$						
1344.48 ± 0.13[b,c]	0.52 ± 0.06	8.71 ± 1.71	82 ± 10	–	–	–
$^{148}Sm + ^{152}Sm$						
222.54 ± 0.13[a]	0.08 ± 0.01	1.37 ± 0.31	6.1 ± 0.8	222.8 ± 0.6	2.1 ± 0.4	−1.44
432.11 ± 0.10[a,b]	0.11 ± 0.02	1.87 ± 0.49	9 ± 2	–	–	–
1269.81 ± 0.52	0.11 ± 0.04	1.88 ± 0.66	9 ± 3	–	–	–
1840.12 ± 0.27	0.20 ± 0.03	3.42 ± 0.69	15 ± 2	1842	2.4 ± 0.5	1.20
$^{148}Sm + ^{154}Sm$						
914.47 ± 0.08[a,c]	0.55 ± 0.04	9.18 ± 1.59	47 ± 4	913.0	5.1 ± 1.0	2.17
937.32 ± 0.10[a]	0.26 ± 0.03	4.36 ± 0.84	22 ± 3	–	–	–
1033.69 ± 0.22[b]	0.17 ± 0.03	2.90 ± 0.70	15 ± 3	–	–	–
1146.76 ± 0.13[b]	0.26 ± 0.04	4.39 ± 0.91	22 ± 3	–	–	–
$^{149}Sm + ^{150}Sm$						
402.74 ± 0.20[b,c]	0.70 ± 0.05	11.8 ± 2.0	97 ± 8	–	–	–
504.90 ± 0.20[c]	1.92 ± 0.08	32 ± 5	266 ± 14	505.6 ± 0.6	3.4 ± 0.8	5.47
859.45 ± 0.20[c]	0.55 ± 0.05	9.25 ± 1.64	76 ± 7	857.6	6.0 ± 1.2	1.97
$^{149}Sm + ^{152}Sm$						
1022.26 ± 0.17[a,b]	0.19 ± 0.02	3.26 ± 0.64	14 ± 1	–	–	–
$^{149}Sm + ^{154}Sm$						
276.65 ± 0.03[a,c]	1.73 ± 0.34	29 ± 7	139 ± 28	277.2	19.4 ± 2.0	1.28
280.44 ± 0.10[b,c]	0.13 ± 0.03	2.13 ± 0.66	10 ± 2	–	–	–
$^{150}Sm + ^{152}Sm$						
251.17 ± 0.09[c]	0.16 ± 0.02	2.60 ± 0.52	13 ± 2	251.4 ± 0.6	2.5 ± 0.6	0.13
1170.35 ± 0.08[b,c,]	0.89 ± 0.09	14.9 ± 2.8	76 ± 8	–	–	–
1193.52 ± 0.08[c]	0.61 ± 0.05	10.3 ± 1.9	53 ± 5	1194	5.7 ± 0.8[e]	2.42
1296.84 ± 0.20	0.27 ± 0.03	4.46 ± 0.86	23 ± 3	–	–	–
$^{150}Sm + ^{154}Sm$						

Table 9 (continued)

This work				From [14]		
E_γ (keV)	$P_{E\gamma}(90°)/(\varepsilon_{E\gamma}{\cdot}f_{E\gamma})$ $\times 10^{-8}$ (count)	I_R(relative) (%)	$<\sigma_{E\gamma}(90°)>$ (mb)	E_γ (keV)	I_{RD}(relative) (%)	R
910.48 ± 0.08[a,b,c]	0.30 ± 0.07	5.00 ± 1.40	29 ± 7	–	–	–
921.04 ± 0.08[a]	0.80 ± 0.13	13.4 ± 3.0	78 ± 13	920.1	15 ± 2[f]	1.53
1177.31 ± 0.10[a,b,c] ^{152}Sm + ^{154}Sm	0.32 ± 0.07	5.35 ± 1.44	31 ± 7	–	–	–
1398.33 ± 0.20[b]	0.16 ± 0.03	2.70 ± 0.63	10 ± 2	–	–	–
1457.26 ± 0.15[a,b] ^{144}Sm + ^{147}Sm + ^{152}Sm	0.42 ± 0.03	7.10 ± 1.23	25 ± 2	–	–	–
983.56 ± 0.16[a,b] ^{144}Sm + ^{148}Sm + ^{150}Sm	0.18 ± 0.02	2.93 ± 0.59	12 ± 1	–	–	–
1308.80 ± 0.21[b,c] ^{147}Sm + ^{148}Sm + ^{152}Sm	0.23 ± 0.03	3.80 ± 0.80	31 ± 4	–	–	–
1152.59 ± 0.27[a,b]	0.15 ± 0.04	2.56 ± 0.72	8 ± 2	–	–	–
1328.16 ± 0.33[a,c,g] ^{147}Sm + ^{149}Sm + ^{152}Sm	0.22 ± 0.03	3.62 ± 0.79	12 ± 3	–		–
121.56 ± 0.03[a,c] ^{148}Sm + ^{150}Sm + ^{152}Sm	11.97 ± 2.20	200 ± 48	631 ± 118	121.6	198 ± 25	0.04
756.26 ± 0.11	0.21 ± 0.03	3.44 ± 0.69	13 ± 2	–	–	–
869.40 ± 0.10[b,c]	0.66 ± 0.08	11.1 ± 2.2	43 ± 5	–	–	–
903.51 ± 0.08 ^{148}Sm + ^{152}Sm + ^{154}Sm	0.62 ± 0.04	10.3 ± 1.7	40 ± 3	903.5	3.4 ± 0.6	3.76
968.30 ± 0.14[a] ^{149}Sm + ^{150}Sm + ^{152}Sm	0.20 ± 0.05	3.43 ± 0.99	10 ± 2	969.4 ± 0.4	0.51 ± 0.10	2.92
944.60 ± 0.20 ^{149}Sm + ^{150}Sm + ^{154}Sm	0.16 ± 0.02	2.61 ± 0.58	10 ± 1	–	–	–
636.22 ± 0.08[c]	0.24 ± 0.03	4.06 ± 0.76	16 ± 2	637.0 ± 0.6	0.85 ± 0.15	4.14
753.12 ± 0.15[b,c] ^{150}Sm + ^{152}Sm + ^{154}Sm	0.23 ± 0.03	3.89 ± 0.75	15 ± 2	–	–	–
674.97 ± 0.05[c]	1.02 ± 0.09	17.0 ± 3.1	52 ± 5	675.44	9.0 ± 1.0	2.50

E_γ is the gamma-ray energy, $P_{E\gamma}(90°)/(\varepsilon_{E\gamma}{\cdot}f_{E\gamma})$ the net counts in the gamma-ray peak divided by the full-energy-peak efficiency and the gamma-ray self-absorption factor, I_R the relative intensity of the gamma ray and $<\sigma_{E\gamma}(90°)>$ the fission-neutron spectrum-averaged partial cross section for gamma-ray production at an angle of 90° between neutron beam and detector. R is the residual calculated by Eq. (4)

[a]Corrected for background interference. [b]confirmed by Demidov´s isotopic measurements. [c]corrected for (n,γ) interference from Sm. [d]1170 and 1173 keV (unresolved doublet by Demidov). [e]1194 and 1197 keV (unresolved doublet by Demidov). [f] 919 and 921 keV (unresolved doublet by Demidov). [g] Corrected for (n,γ) interference from Cl

Gamma rays of dysprosium

One hundred and forty-eight prompt gamma rays issued from inelastic scattering of fission neutrons with dysprosium were identified. These gamma rays are depicted in Figs. 3 and 4 and their data are given in Tables 12, 13, 14, 15 and 16. From the observed lines, 13 were assigned to ^{161}Dy, 48 to ^{162}Dy, 28 to ^{163}Dy, 44 to ^{164}Dy. The other 15 lines are fed by two dysprosium isotopes with significant contributions. The lines identified as pure neutron capture lines are given in Table 10. Their intensities were calculated using Eq. (2). Like in the case of samarium, the interferences of the radiative neutron capture in the $(n,n'\gamma)$-lines were verified. The net counts produced in (n,γ) lines were calculated according to Eq. (2). For 103 lines, relevant contributions to the net counts were found. For certain lines of the isotopes ^{161}Dy and ^{162}Dy, the calculated counts of neutron capture lines exceed the measured counts by a factor of up to 3. Regarding Table 10, the intensity ratio of neutron capture lines of the isotopes follows no trend, but rather random. Therefore, instead of taking a mean value as in the case of ^{152}Sm, the lowest intensity ratios were used as a scaling factors to calculate neutron capture counts. These factors are 0.46 ± 0.27 for ^{161}Dy and 0.33 ± 0.21 for ^{162}Dy. The uncertainties were neglected in the conservative correction process for the net counts produced by neutron capture. As with the samarium

Table 10 Prompt gamma rays induced by radiative neutron capture on samarium and dysprosium isotopes

This work Neutron capture				From PGAA database [23, 24] Capture of thermal neutrons		
$E\gamma$ (keV)	$P_{E\gamma}/\varepsilon_{E\gamma}{\cdot}f_{\gamma}(\times10^{-8})$ (Count)	$\langle\sigma_{E\gamma}\rangle$ (mb)	$I_{E\gamma}$ (%)	$\sigma_{E\gamma,\mathrm{th}}$ (b)	$I_{E\gamma,\mathrm{th}}$ (%)	$I_{E\gamma}/I_{E\gamma,\mathrm{th}}$
^{150}Sm						
167.8 + 168.4	0.28 ± 0.01	68 ± 30	13.1 ± 6.6	11.7 ± 3.4	11.7 ± 3.4	1.12 ± 0.65
^{152}Sm						
90.8 + 90.9 + 91.5	0.57 ± 0.08	36 ± 17	1.08 ± 0.40	8.1 ± 3.0	3.92 ± 1.45	0.28 ± 0.14
127.3	1.08 ± 0.04	68 ± 30	2.04 ± 0.70	15.3 ± 1.1	7.40 ± 0.53	0.27 ± 0.09
182.5 + 182.9	0.28 ± 0.03	17 ± 8	0.52 ± 0.18	3.53 ± 1.12	1.71 ± 0.54	0.30 ± 0.14
354.8	0.21 ± 0.02	13 ± 6	0.39 ± 0.14	2.36 ± 0.41	1.14 ± 0.20	0.34 ± 0.13
321.1	0.48 ± 0.05	29 ± 13	0.86 ± 0.31	5.98 ± 1.12	2.89 ± 0.54	0.34 ± 0.14
397.9	0.67 ± 0.04	42 ± 19	1.27 ± 0.44	7.85 ± 1.49	3.80 ± 0.72	0.33 ± 0.09
470.8	0.33 ± 0.05	21 ± 10	0.63 ± 0.23	4.34 ± 0.79	2.10 ± 0.38	0.30 ± 0.12
473.6	0.43 ± 0.07	27 ± 13	0.82 ± 0.30	5.20 ± 0.93	2.51 ± 0.45	0.32 ± 0.13
622.7	0.35 ± 0.04	22 ± 10	0.66 ± 0.24	3.29 ± 0.82	1.59 ± 0.40	0.41 ± 0.18
660.0	0.35 ± 0.04	22 ± 10	0.67 ± 0.24	4.82 ± 0.86	2.33 ± 0.41	0.29 ± 0.11
734.9	0.25 ± 0.03	16 ± 7	0.47 ± 0.17	3.81 ± 0.75	1.84 ± 0.36	0.25 ± 0.10
5238.1	0.11 ± 0.01	7 ± 3	0.21 ± 0.07	2.36 ± 0.41	1.14 ± 0.20	0.18 ± 0.07
5741.0	0.53 ± 0.13	34 ± 17	1.02 ± 0.43	10.1 ± 1.9	4.88 ± 0.92	0.21 ± 0.10
5832.4	0.22 ± 0.02	14 ± 6	0.42 ± 0.15	2.28 ± 0.41	1.10 ± 0.20	0.38 ± 0.15
^{161}Dy						
321.8 + 321.9	0.11 ± 0.03	11 ± 6	1.02 ± 0.44	13.3 ± 3.1	2.25 ± 0.52	0.45 ± 0.22
768.8	0.07 ± 0.02	7 ± 4	0.68 ± 0.30	3.07 ± 1.16	0.52 ± 0.20	1.31 ± 0.77
937.2	0.08 ± 0.02	8 ± 4	0.73 ± 0.31	7.40 ± 2.64	1.25 ± 0.45	0.58 ± 0.32
5450.3	0.19 ± 0.02	18 ± 8	1.71 ± 0.62	11.1 ± 2.1	1.87 ± 0.35	0.91 ± 0.37
^{162}Dy						
289.5	0.10 ± 0.04	7 ± 4	0.31 ± 0.18	2.67 ± 0.27	1.36 ± 0.14	0.23 ± 0.13
318.1	0.11 ± 0.04	8 ± 5	0.35 ± 0.20	1.88 ± 0.23	0.96 ± 0.12	0.36 ± 0.21
376.5	0.13 ± 0.05	9 ± 6	0.40 ± 0.23	0.90 ± 0.12	0.46 ± 0.06	0.87 ± 0.51
398.9	0.12 ± 0.04	9 ± 5	0.37 ± 0.20	3.10 ± 0.39	1.58 ± 0.20	0.23 ± 0.13
820.8	0.15 ± 0.03	10 ± 6	0.45 ± 0.21	1.88 ± 0.23	0.96 ± 0.12	0.47 ± 0.23
5125.3a	0.24 ± 0.05	17 ± 9	0.74 ± 0.35	1.49 ± 0.20	0.76 ± 0.10	0.97 ± 0.48
^{164}Dy						
5557.3	0.21 ± 0.04	11 ± 5	5.50 ± 2.37	101 ± 5	3.86 ± 0.19	1.42 ± 0.61
5607.7	0.35 ± 0.03	18 ± 8	8.90 ± 3.52	127 ± 6	4.85 ± 0.23	1.83 ± 0.73

$E\gamma$ is the gamma-ray energy, $P_{E\gamma}/\varepsilon_{E\gamma}{\cdot}f\gamma$ the net count in the gamma-ray peak divided by the full-energy-peak efficiency and the gamma-ray self-absorption factor, $\langle\sigma_{E\gamma}\rangle$ the neutron spectrum-averaged isotopic cross section for gamma ray production, $I_{E\gamma}$ the gamma-ray intensity

analysis, the gamma lines with a contribution above 90% were assumed to be pure neutron capture γ-rays.

The intensities of the lines were calculated relative to the 754.3-keV line of ^{164}Dy (100%). They are given together with the values determined in [14] from the measurement of a Dy_2O_3 sample with natural isotopic abundance in columns 3 and 6 of Table 12, 13, 14, 15, and 16. Additionally, for comparison to the intensities from the measurement of isotopically- enriched Dy_2O_3 samples (^{162}Dy (95.2%) [14] [18], ^{163}Dy (92.5%) [19], ^{164}Dy (97.2%) [14], ^{164}Dy (94.7%) [20]), the intensities of the lines from each isotope were calculated relative to the following lines: 184.8 keV for ^{162}Dy, 250.5 keV for ^{163}Dy and 168.7 keV for ^{164}Dy. The values are given in bold in columns 3 and 6 of Tables 13, 14, and 15. We identified 76 of 92 lines given in [14] for the measurement of the dysprosium sample with natural abundance and the 65 lines listed in [14] for the measurement of the isotopically-enriched samples (32 for ^{162}Dy and 33 for ^{164}Dy). All the lines observed for ^{162}Dy, ^{163}Dy and ^{164}Dy were observed in the isotopic measurements performed in

Table 11 Relevant contributions of neutron capture (n,γ) reactions to gamma lines primarily identified as $(n,n'\gamma)$ lines of samarium

This work (n,n′γ)		PGNAA database (n,γ) [23, 24]		$P_{E\gamma}(n,\gamma)/P_{E\gamma}$ (%)
E_γ (keV)	^{A}Z	E_γ in keV (^{A}Z)	$I_{E\gamma}$ (%)	
121.5[a]	^{148}Sm + ^{150}Sm + ^{152}Sm	119.8 (^{152}Sm)	3.36 ± 1.41	4.15 ± 1.46
149.9	^{144}Sm	148.9 (^{150}Sm), 149.4 (^{152}Sm)	0.050 ± 0.031 (^{150}Sm), 0.029 ± 0.005(^{152}Sm)	3.38 ± 0.81
222.5	^{148}Sm	223.5 (^{149}Sm), 223.2 (^{152}Sm)	0.012 ± 0.003 (^{149}Sm), 0.29 ± 0.05 (^{152}Sm)	37 ± 11
251.2	^{150}Sm + ^{152}Sm	251.6 (^{149}Sm), 250.8 (^{150}Sm)	0.32 ± 0.01 (^{149}Sm), 1.80 ± 0.25 (^{150}Sm)	36 ± 7
254.3[a]	^{149}Sm	255.4 (^{149}Sm), 254.3 (^{150}Sm), 254.8 (^{152}Sm)	0.031 ± 0.005 (^{149}Sm), 0.07 ± 0.02 (^{150}Sm), 0.50 ± 0.09 (^{152}Sm)	32 ± 14
268.8	^{152}Sm	269.2 (^{152}Sm)	0.90 ± 0.30 (^{152}Sm)	12.1 ± 3.2
276.6[a]	^{149}Sm + ^{154}Sm	276.1 (^{150}Sm), 276.7 (^{152}Sm)	1.05 ± 0.43 (^{150}Sm), 2.21 ± 0.56 (^{152}Sm)	17.4 ± 5.6
280.4	^{149}Sm + ^{154}Sm	280.2 (^{150}Sm)	5.60 ± 2.34 (^{150}Sm)	49 ± 13
285.4	^{149}Sm	285.0 (^{149}Sm), 285.9 (^{154}Sm)	0.25 ± 0.09 (^{149}Sm), 1.64 ± 0.14 (^{154}Sm)	3.57 ± 0.54
313.6	^{149}Sm	313.9 (^{150}Sm), 313.6 (^{152}Sm)	0.025 ± 0.007 (^{150}Sm), 0.38 ± 0.10(^{152}Sm)	32 ± 8
333.4	^{150}Sm	334.0 (^{149}Sm), 334.6 (^{150}Sm)	86.4 ± 1.7 (^{149}Sm), 0.13 ± 0.02 (^{150}Sm)	40 ± 10
339.8	^{152}Sm	340.1 (^{150}Sm)	2.50 ± 0.77	8.02 ± 1.97
345.3	^{150}Sm	346.0 (^{149}Sm), 345.0 (^{150}Sm)	0.76 ± 0.02 (^{149}Sm), 0.30 ± 0.08 (^{150}Sm)	38 ± 10
402.7	^{149}Sm + ^{150}Sm	403.0 (^{149}Sm), 400.7 (^{150}Sm)	0.79 ± 0.02 (^{149}Sm), 0.11 ± 0.02 (^{150}Sm)	15.1 ± 3.6
405.8	^{150}Sm	406.5 (^{149}Sm), 404.6 (^{150}Sm), 407.4 (^{152}Sm) (^{152}Sm)	0.63 ± 0.02 (^{149}Sm), 0.84 ± 0.15 (^{150}Sm), 0.19 ± 0.04 (^{152}Sm)	20 ± 4
413.7	^{148}Sm	413.4 (^{147}Sm,) 413.8 (^{152}Sm)	10.8 ± 2.6 (^{147}Sm), 3.6 ± 1.1 (^{152}Sm)	77 ± 14
432.1	^{148}Sm	432.8 (^{147}Sm)	3.28 ± 0.82	72 ± 19
438.7	^{150}Sm	439.4 (^{149}Sm), 439.5 (^{152}Sm)	51.6 ± 2.8 (^{149}Sm), 3.6 ± 1.1 (^{152}Sm)	50 ± 11
461.0	^{150}Sm	461.9 (^{149}Sm), 459.8 (^{150}Sm)	0.15 ± 0.01 (^{149}Sm), 0.22 ± 0.06 (^{150}Sm)	7.03 ± 1.67
485.4	^{150}Sm	486.0 (^{149}Sm)	1.30 ± 0.06	64 ± 16
504.9	^{149}Sm + ^{150}Sm	505.5 (^{149}Sm)	1.32 ± 0.20	9.53 ± 2.29
549.6	^{148}Sm	550.1 (^{147}Sm)	112 ± 7	62 ± 15
552.4	^{148}Sm	552.0 (^{152}Sm)	0.11 ± 0.03	1.77 ± 0.47
583.6[a]	^{150}Sm	584.3 (^{149}Sm), 582.9 (^{152}Sm), 582.1 (^{154}Sm)	8.7 ± 1.2 (^{149}Sm), 0.30 ± 0.07 (^{152}Sm), 2.3 ± 0.4 (^{154}Sm)	48 ± 14
590.2	^{149}Sm	590.8 (^{149}Sm)	0.19 ± 0.01	3.36 ± 0.81
610.7	^{148}Sm	610.7 (^{147}Sm)	26.9 ± 4.7	78 ± 19
636.2	^{154}Sm	636.3 (^{150}Sm)	1.64 ± 1.90	12.6 ± 3.3
663.4[a]	^{149}Sm	663.6 (^{150}Sm), 664.0 (^{154}Sm)	0.22 ± 0.10 (^{150}Sm), 0.56 ± 0.05 (^{154}Sm)	1.29 ± 0.21
666.0[a]	^{150}Sm	667.1 (^{149}Sm)	0.39 ± 0.39	3.13 ± 0.76
674.9	^{150}Sm + ^{152}Sm + ^{154}Sm	675.8 (^{149}Sm), 672.5 (^{150}Sm)	3.1 ± 0.1 (^{149}Sm), 0.27 ± 0.05 (^{150}Sm)	32 ± 8
687.9	^{147}Sm + ^{152}Sm	688.4 (^{149}Sm)	0.056 ± 0.007	1.23 ± 0.30

Table 11 (continued)

This work (n,n′γ)		PGNAA database (n,γ) [23, 24]		$P_{E\gamma}(n,\gamma)/P_{E\gamma}$ (%)
E_γ (keV)	^{A}Z	E_γ in keV (^{A}Z)	$I_{E\gamma}$ (%)	
711.7	^{150}Sm	712.2 (^{149}Sm)	4.82 ± 0.10	37 ± 9
715.9	^{147}Sm	717.7 (^{150}Sm)	2.26 ± 0.60	1.94 ± 0.48
725.6	^{147}Sm + ^{148}Sm	725.1 (^{154}Sm)	1.76 ± 0.15	5.06 ± 1.15
730.9	^{150}Sm	731.20 (^{149}Sm)	0.97 ± 0.07	56 ± 14
736.9	^{150}Sm	737.4 (^{149}Sm), 736.2 (^{150}Sm)	10.8 ± 0.2 (^{149}Sm), 0.50 ± 0.20 (^{150}Sm)	42 ± 16
741.3	^{147}Sm	741.8 (^{154}Sm)	0.30 ± 0.05	1.68 ± 0.44
745.5[a]	^{154}Sm	745.0 (^{154}Sm)	0.68 ± 0.07	1.86 ± 0.62
747.6[a]	^{150}Sm	748.1 (^{149}Sm)	1.22 ± 0.04	57 ± 21
751.0	^{150}Sm	750.3 (^{152}Sm)	0.21 ± 0.07	16.9 ± 13.7
753.1	^{154}Sm	753.0 (^{150}Sm)	0.52 ± 0.33	5.20 ± 1.36
761.8[a]	^{150}Sm	761.4 (^{149}Sm)	0.20 ± 0.03	22 ± 8
791.4	^{152}Sm	792.1 (^{150}Sm)	0.24 ± 0.07	5.12 ± 1.83
854.8	^{152}Sm	853.8 (^{154}Sm)	0.95 ± 0.15	3.28 ± 0.75
859.4	^{149}Sm + ^{150}Sm	859.9 (^{149}Sm)	1.59 ± 0.07	31 ± 7
869.4	^{148}Sm + ^{150}Sm + ^{152}Sm	869.3 (^{149}Sm)	2.15 ± 0.11	33 ± 9
910.5[a]	^{150}Sm + ^{154}Sm	911.0 (^{149}Sm), 909.4 (^{154}Sm)	0.79 ± 0.05 (^{149}Sm), 0.37 ± 0.05 (^{154}Sm)	30 ± 16
914.5[a]	^{148}Sm + ^{154}Sm	914.5 (^{154}Sm)	4.08 ± 0.36	8.42 ± 3.50
921.0[a]	^{150}Sm + ^{154}Sm	921.6 (^{149}Sm)	0.45 ± 0.05	8.00 ± 2.54
937.3	^{148}Sm	935.6 (^{154}Sm)	1.95 ± 0.54	8.51 ± 2.05
947.7	^{147}Sm	948.7 (^{150}Sm)	0.62 ± 0.14	4.68 ± 1.19
951.9	^{149}Sm	951.3 (^{150}Sm)	0.85 ± 0.17	16.0 ± 5.3
968.3	^{148}Sm	968.1 (^{154}Sm)	2.01 ± 0.20	10.8 ± 2.6
995.8[a]	^{152}Sm	997.0(^{149}Sm)	0.27 ± 0.02	30 ± 10
1016.7	^{154}Sm	1016.6 (^{149}Sm)	0.77 ± 0.07	23 ± 6
1046.0	^{150}Sm	1045.7 (^{149}Sm)	0.56 ± 0.79	14.3 ± 4.4
1048.7	^{150}Sm	1049.1 (^{149}Sm)	0.36 ± 0.36	6.77 ± 1.64
1106.6[a]	^{147}Sm	1106.6 (^{154}Sm)	1.68 ± 0.14	4.97 ± 1.52
1122.2	^{150}Sm	1122.5 (^{149}Sm)	0.58 ± 0.04	43 ± 11
1152.6	^{148}Sm	1152.2 (^{154}Sm)	0.13 ± 0.03	1.06 ± 0.33
1170.3	^{150}Sm + ^{152}Sm	1170.6 (^{149}Sm)	4.15 ± 0.19	42 ± 10
1177.3[a]	^{150}Sm + ^{154}Sm	1177.3 (^{149}Sm)	1.03 ± 0.06	33 ± 15
1193.5	^{150}Sm + ^{152}Sm	1193.8 (^{149}Sm)	1.91 ± 0.06	32 ± 8
1196.9[a]	^{147}Sm	1197.3 (^{149}Sm)	0.50 ± 0.03	23 ± 8
1246.6	^{150}Sm	1247.0 (^{149}Sm)	0.92 ± 0.06	53 ± 14
1308.8	^{144}Sm + ^{148}Sm + ^{150}Sm	1308.7 (^{149}Sm), 1309.1 (^{154}Sm)	0.72 ± 0.16 (^{149}Sm,), 0.42 ± 0.05 (^{154}Sm)	34 ± 9
1323.8[a]	^{150}Sm	1321.9 (^{149}Sm)	1.37 ± 0.16	36 ± 9
1328.2	^{148}Sm	1327.4 (^{35}Cl), 1327.8 (^{154}Sm)	1.22 ± 0.19 (^{35}Cl), 0.36 ± 0.05 (^{154}Sm)	3.30 ± 1.49
1344.5	^{148}Sm + ^{150}Sm	1343.9 (^{147}Sm), 1345.8 (^{154}Sm)	4.3 ± 1.0 (^{147}Sm,), 0.74 ± 0.09 (^{154}Sm)	42 ± 10
1486.2[a]	^{150}Sm	1485.6 (^{149}Sm)	0.61 ± 0.09	39 ± 16

E_γ is the gamma-ray energy, ^{A}Z denotes the considered isotopes, $I_{E\gamma}$ is the absolute gamma-ray intensity and $P_{E\gamma}(n,\gamma)/P_{E\gamma}$ is the fraction of calculated neutron capture counts to the net counts in the gamma-ray peak

[a]Corrected for background interference

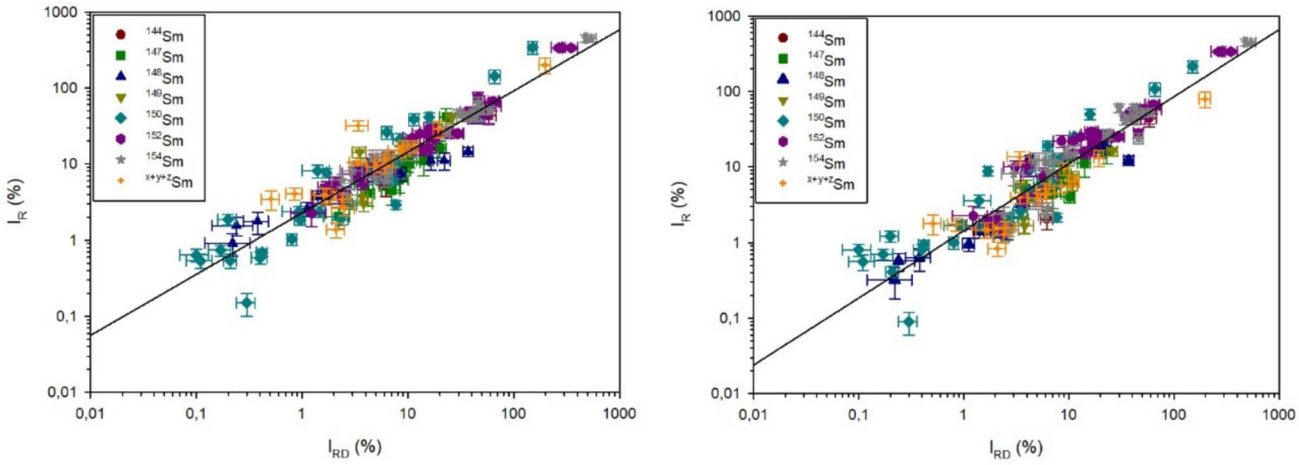

Fig. 5 Correlation between the relative intensities I_R of the prompt gamma rays from inelastic scattering ($n,n'\gamma$) reactions on samarium measured in this work and the relative intensities I_{RD} obtained from measurement with reactor fast neutrons [14–17]. Data points of $^{X+Y+Z}$Sm indicate multi-isotope lines (see Table 9). Left: the gamma lines measured in this work are corrected for neutron capture interferences. Right: the gamma lines measured in this work are not corrected for neutron capture interferences. The fit of the data with Eq. (3) is shown by the solid line with $a = 2.26 \pm 0.14$ and $b = 0.80 \pm 0.02$ (left plot), and $a = 1.42 \pm 0.10$ and $b = 0.89 \pm 0.03$ (right plot)

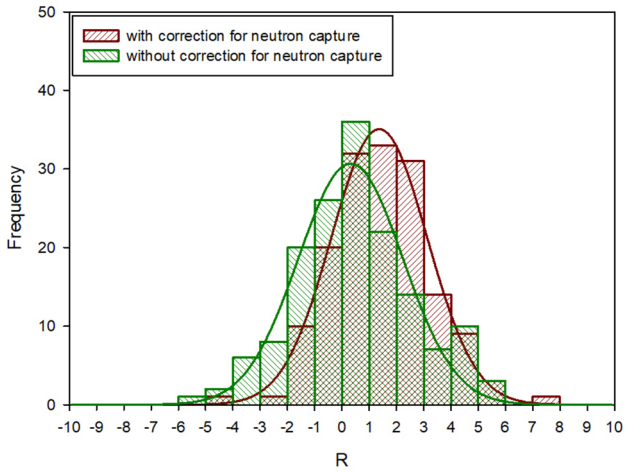

Fig. 6 Histogram of the residuals R in units of standard deviation [σ] calculated with Eq. (4) showing the level of agreement between the relative intensities of prompt gamma rays produced by inelastic scattering on samarium derived in this work (corrected and uncorrected for neutron capture interferences) with the data listed in [14–17]. The data was fitted with a Gaussian, which is shown by the solid lines

[18, 19] and [20]. 26 of 92 lines were listed as tentative assignments in [14], of which 21 lines were observed by this work and assigned as ($n,n'\gamma$) transitions in Dy, according to data given in [22, 32–35]. The origin of the lines at 245.3, 371.3, 548.5, 633.6, 728.5, 842.7, 1251.9, 1585.1, 1735.4 and 1685.8 keV from inelastic scattering reactions in Dy have been confirmed by the isotopic measurements done in [18–20]. The line at 842.7 keV was assigned to ^{162}Dy and ^{164}Dy. However, based on the intensities given in [19, 20], this line is mainly fed by ^{164}Dy (87% for ^{164}Dy and 13% for ^{162}Dy). The most intense line at 1124.6 keV from the same level ($E^* = 1390.5$ keV [35]) was clearly observed in this work. For the line at 1252.6 keV from ^{162}Dy, a significant contribution to the net counts of (31 ± 3) %, from the single escape peak of the 1763.4-keV line resulting from ^{35}Cl($n,n'\gamma$)^{35}Cl was found. The lines from the elemental measurement in [14] at 326.0, 538.5, 569.7, 846.6, 1217.4, 1224.0, 1273.6, 1369.8 and 1705.6 keV were not observed in this work. From the isotopic measurement, the following lines have been observed for ^{162}Dy: 327.0 and 1273.0 keV [14], 1217.8 and 1223.3 keV [18], for ^{164}Dy: 326.3, 538.3, 569.1, 1217.4, 1224.0 keV [14], 325.8, 846.6, 1217.0, 1223.9, 1371.0 and 1705.7 keV [20]. However, the lines at 327.0 and 1273.0 keV were wrongly assigned to ^{162}Dy, as they were not mentioned in [22, 32] and not detected in [18]. The line at 1273 keV could correspond to an unresolved doublet of ^{164}Dy lines at 1271.4 and 1274.9 keV [20]. The line at 538.5 keV could correspond to the ^{164}Dy line at 542.5 keV noticed as multiplet in [20]. The 569.7-keV line was mentioned in [32] as a ^{164}Dy line but was not included in the energy level scheme. This line was not observed in [20]. The 1371-keV line is not included in the energy level scheme of ^{164}Dy [32]. The line at 326.0 keV was not observed in this work due to background interference (^{70}Ge [2]). The line at 1217.4 keV interfered with the 1219.2-keV line of ^{35}Cl($n,n'\gamma$)^{35}Cl. The 1224.0-keV line was not detected, probably due to the low mass of the sample. The lines at 538.5, 569.7, 846.6 and 1705.6 keV were not observed due to background interferences [1, 2]. Note that the aforementioned lines were not assumed to be produced by (n,γ) reaction in

Table 12 Prompt gamma rays of ^{161}Dy induced by inelastic scattering of fission neutrons

This work				From [14]		
E_γ (keV)	$P_{E\gamma}(90°)/(\varepsilon_{E\gamma} f_{E\gamma})$ $\times 10^{-8}$ (count)	I_R(relative) (%)	$<\sigma_{E\gamma}(90°)>$ (mb)	E_γ (keV)	I_{RD}(relative) (%)	R
48.62 ± 0.13	2.83 ± 0.71	138 ± 41	495 ± 125	–	–	–
56.70 ± 0.20	1.29 ± 0.34	63 ± 19	225 ± 60	–	–	–
102.63 ± 0.07	0.59 ± 0.05	29 ± 5	103 ± 9	–	–	–
128.46 ± 0.20	0.09 ± 0.03	4.17 ± 1.55	15 ± 5	–	–	–
157.00 ± 0.08[a]	0.35 ± 0.04	17.0 ± 3.2	61 ± 7	–	–	
217.31 ± 0.10	0.24 ± 0.04	11.6 ± 2.5	42 ± 7	–	–	
230.18 ± 0.13[a]	0.11 ± 0.02	5.57 ± 1.22	20 ± 4	–	–	
292.02 ± 0.11[a,b]	0.21 ± 0.03	10.3 ± 2.1	37 ± 5	–	–	
343.25 ± 0.25[a]	0.10 ± 0.03	5.11 ± 1.51	18 ± 6	344.0 ± 0.4	16 ± 4	−2.55
549.62 ± 0.10	0.20 ± 0.02	9.96 ± 1.88	36 ± 4	–	–	
588.34 ± 0.12	0.16 ± 0.04	7.78 ± 2.20	28 ± 7	589.8 ± 0.2	8.5 ± 1.5	−0.27
607.85 ± 0.11[a,c]	0.22 ± 0.05	10.7 ± 2.9	39 ± 9	606.8 ± 0.5	41 ± 5	5.24
826.46 ± 0.26	0.14 ± 0.05	6.77 ± 2.53	24 ± 9	825.9 ± 0.2	4.3 ± 0.8	0.93

E_γ is the gamma-ray energy, $P_{E\gamma}(90°)/(\varepsilon_{E\gamma} f_{E\gamma})$ the net counts in the gamma-ray peak divided by the full-energy-peak efficiency and the gamma-ray self-absorption factor, I_R the relative intensity of the gamma ray and $<\sigma_{E\gamma}(90°)>$ the fission-neutron spectrum-averaged partial cross section for gamma-ray production at an angle of 90° between neutron beam and detector R is the residual calculated by Eq. (4)

[a]Corrected for (n,γ) interference from Dy. [b]corrected for (n,γ) interference from Cl. [c]corrected for background interference

Dy, as they should have also been observed in this work then.

Compared to the elemental measurement in [14], 68 new γ-lines were identified. All lines were specified in [22, 32–35] and among these, 9 were associated to ^{161}Dy, 22 to ^{162}Dy, 10 to ^{163}Dy, 23 to ^{164}Dy and 4 to more than one contributing isotope. A total of 40 lines was confirmed by the isotopic measurements [14, 18–20]. The identification of new lines is mainly associated with the improved energy resolution and the higher mean energy of the neutron beam of FaNGaS. In particular, the observation of relative new low energy gamma lines (below 120 keV) was the result of the lower energy threshold of the spectrometer. In contrast to [14], the doublets at energies of 267.4, 294.7, 310.0, 548.5, 980.6, 1556.4 and 1585.1 keV were successfully resolved. The new lines at 238.2, 607.9 and 982.6 keV could not be observed by Demidov et al. due to the background interference [14]. The intensity plot is depicted in Fig. 7. The fitted values of the coefficients in Eq. (3) are a = 2.26 ± 0.10 and b = 0.71 ± 0.02. The calculated average intensity ratio I_R/I_{RD} of 1.76 ± 1.64 indicates a large discrepancy, which is probably due to inaccurate corrections for neutron capture interferences like in the case of samarium. The lines observed at 267.4 (^{163}Dy) 337.8 (^{163}Dy), 495.8 keV (^{163}Dy), 975.4 (^{164}Dy), and 1025.8 keV(^{164}Dy) were found to have a large interference with the (n,γ) reactions in Dy, with contributions of (92 ± 34) %, (106 ± 35) %, (161 ± 59) %, (108 ± 41) % and (102 ± 42) %, respectively. The line at 337.8 keV was emitted from a level at 766.2 keV above g.s. [34], from which another line at 414.4 keV was observed. The latter one has a contribution of neutron capture of (76 ± 25) % (see Table 17). Taking the large uncertainty into account, it might be possible that this level is fed only by neutron capture. For the 495.8-keV line ($E^* = 884.3$ keV [34]) another line at 532.3 keV was also observed due to inelastic scattering in ^{163}Dy. The 532.3-keV line interfered with the neutron capture line of ^{162}Dy and has contributed to the net counts by (23.7 ± 7.8) %. The reference line of 754.3 keV of ^{164}Dy has been strongly contaminated by a (n,γ)-line of ^{163}Dy, with a contribution to the net counts of (50 ± 15) %. The contributions of neutron capture in the reference lines at 168.7, 184.8 and 250.5 keV used in the measurements of isotopically-enriched samples [18–20] are somewhat less with (23.6 ± 8.9) %, (31 ± 9) % and (37 ± 12) %, respectively. By omitting the correction from the neutron capture, a similar average intensity with I_R/I_{RD} ratio of 1.55 ± 1.33 was deduced. The correlation coefficients, $a = 1.91 \pm 0.08$ and $b = 0.75 \pm 0.02$ (see Fig. 7) are about the same as with correction. The agreement is reasonable for the intensities of the lines of ^{161}Dy, ^{163}Dy and the lines associated to more than one dysprosium isotope with respective I_R/I_{RD}-values of 0.76 ± 0.61, 0.99 ± 0.56 and 0.99 ± 73. The values of I_R/I_{RD} for ^{162}Dy and ^{164}Dy were 1.82 ± 1.54 and 2.25 ± 2.02, respectively. The values were significantly improved by the correction applied for the neutron capture to 1.56 ± 1.23 and 1.88 ± 1.67, respectively. The histograms of the residuals R obtained with and without correction of neutron capture are shown in Fig. 8. The data agrees at the 2.2σ level in both

Table 13 Prompt gamma rays of ^{162}Dy induced by inelastic scattering of fission neutrons

This work				From [14, 18]		
E_γ (keV)	$P_{E\gamma}(90°)/(\varepsilon_{E\gamma}{\cdot}f_{E\gamma})$ $\times 10^{-8}$ (count)	I_R(relative) (%)	$<\sigma_{E\gamma}(90°)>$ (mb)	E_γ (keV)	I_{RD} (relative) (%)	R
184.83 ± 0.03[a,c]	7.14 ± 0.54	348 ± 60	937 ± 78	185.07 ± 0.10	400 ± 80	−0.52
		100		**185.07 ± 0.10[n]**	**100**	
				185.0 ± 0.2[o]	**100**	
				185.00 ± 0.01[p]	**100**	
219.78 ± 0.10	0.19 ± 0.03	9.09 ± 2.13	24 ± 4	–	–	–
		2.66 ± 0.46		**220.08 ± 0.24[p]**	**0.26 ± 0.04[p]**	**5.20**
235.65 ± 0.10[b,c]	0.09 ± 0.02	4.22 ± 1.06	11 ± 3	–	–	–
		1.26 ± 0.30		**234.1 ± 0.3[o]**	**0.8 ± 0.3[o]**	**1.08**
				235.98 ± 0.08[p]	**1.41 ± 0.09[p]**	**−0.42**
282.44 ± 0.03[c]	0.96 ± 0.08	47 ± 8	126 ± 11	282.9 ± 0.2	45 ± 8	0.18
		13.4 ± 1.5		**282.9 ± 0.2[n]**	**11 ± 3[n]**	**0.72**
				282.8 ± 0.2[o]	**12 ± 1[o]**	**0.78**
				282.88 ± 0.02[p]	**15.5 ± 0.8[p]**	**−1.23**
310.72 ± 0.14[c]	0.04 ± 0.01	1.79 ± 0.54	5 ± 1	310.0 ± 0.3	9.0 ± 0.4[d]	1.88
		0.56 ± 0.15		**311.22 ± 0.05[o]**	**1.20 ± 0.08[o]**	**−3.76**
333.48 ± 0.04[c]	0.56 ± 0.05	27 ± 5	74 ± 7	334.2 ± 0.3	24 ± 4	0.50
		7.84 ± 0.92		**334.2 ± 0.3[n]**	**6.00 ± 1.56[n]**	**1.02**
				334.1 ± 0.2[o]	**4.3 ± 0.5[o]**	**3.38**
				334.07 ± 0.01[p]	**5.97 ± 0.30[p]**	**1.93**
371.16 ± 0.22[c]	0.19 ± 0.04	9.17 ± 2.44	25 ± 5	371.3 ± 0.3	4.1 ± 0.9	1.95
		2.66 ± 0.59		**371.3 ± 0.3[n]**	**1.03 ± 0.30[n]**	**2.46**
				372.7 ± 0.2[o]	**1.9 ± 0.5[o]**	**0.98**
				372.20 ± 0.09[p]	**1.65 ± 0.10[p]**	**1.69**
528.71 ± 0.24[c]	0.07 ± 0.02	3.25 ± 1.05	9 ± 3	–	–	–
		0.98 ± 0.29		**529.29 ± 0.12[p]**	**0.80 ± 0.06[p]**	**0.61**
543.16 ± 0.29	0.13 ± 0.03	6.56 ± 1.69	16 ± 4	–	–	–
		1.82 ± 0.44		**543.54 ± 0.12[p]**	**1.12 ± 0.08[p]**	**1.56**
556.11 ± 0.16[c]	0.07 ± 0.02	3.50 ± 0.96	9 ± 3	–	–	–
		0.98 ± 0.29		**556.33 ± 0.19[p]**	**0.45 ± 0.05[p]**	**1.80**
565.27 ± 0.10[c]	0.19 ± 0.03	9.23 ± 2.12	25 ± 4	565.6 ± 0.2	16 ± 2	−2.32
		2.66 ± 0.47		**565.6 ± 0.2[n]**	**4.00 ± 0.94[n]**	**−1.27**
				565.77 ± 0.22[p]	**0.27 ± 0.05[p]**	**5.06**
677.62 ± 0.09	0.16 ± 0.02	7.65 ± 1.53	21 ± 3	678.0 ± 0.2	11 ± 2	−1.33
		2.24 ± 0.33		**678.0 ± 0.2[n]**	**2.75 ± 0.74[n]**	**−0.63**
				678.05 ± 0.13[p]	**0.42 ± 0.04[p]**	**5.47**
696.58 ± 0.09[c]	0.47 ± 0.06	23 ± 5	62 ± 8	696.9 ± 0.4	28 ± 3	−0.86
		6.59 ± 0.98		**696.9 ± 0.4[n]**	**7.00 ± 1.59[n]**	**−0.22**
				698.4 ± 0.10[o]	**4 ± 2[o]**	**1.16**
				697.29 ± 0.02[p]	**5.3 ± 0.3[p]**	**1.26**
729.63 ± 0.27[b]	0.15 ± 0.03	7.07 ± 1.70	19 ± 4	728.5 ± 0.2	6.2 ± 0.9	0.45
		2.10 ± 0.45		**728.5 ± 0.2[n]**	**1.55 ± 0.38[n]**	**0.93**
				728.40 ± 0.13[q]	**0.82 ± 0.06[q]**	**2.82**
770.44 ± 0.10[a,c]	0.09 ± 0.02	4.57 ± 1.08	12 ± 3	–	–	–
		1.26 ± 0.30		**770.96 ± 0.22[q]**	**0.22 ± 0.04[q]**	**3.50**
794.86 ± 0.05[c]	0.65 ± 0.07	32 ± 6	86 ± 10	795.40 ± 0.10	22 ± 3	1.49
		9.10 ± 1.20		**795.40 ± 0.10[n]**	**5.50 ± 1.33[n]**	**2.00**
				795.5 ± 0.2[o]	**9 ± 2[o]**	**0.04**

Table 13 (continued)

This work				From [14, 18]		
E_γ (keV)	$P_{E\gamma}(90°)/(\varepsilon_{E\gamma}{\cdot}f_{E\gamma})$ $\times 10^{-8}$ (count)	I_R(relative) (%)	$<\sigma_{E\gamma}(90°)>$ (mb)	E_γ (keV)	I_{RD} (relative) (%)	R
				795.31 ± 0.01[p]	**9.6 ± 0.5[p]**	**0.38**
807.13 ± 0.04[a,c]	2.09 ± 0.14	102 ± 17	274 ± 21	807.54 ± 0.10	80 ± 8	1.17
		29 ± 3		**807.54 ± 0.10[n]**	**20 ± 4[n]**	**1.80**
				807.6 ± 0.2[o]	**27 ± 3[o]**	**0.47**
				807.50 ± 0.01[p]	**27.1 ± 0.1[p]**	**0.63**
878.70 ± 0.16[b]	0.13 ± 0.03	6.19 ± 1.61	17 ± 4	–	–	–
		1.82 ± 0.44		**878.54 ± 0.10[p]**	**0.84 ± 0.06[p]**	**2.21**
881.93 ± 0.05[a,c]	2.33 ± 0.19	113 ± 20	305 ± 27	882.34 ± 0.10	72 ± 8	1.90
		33 ± 4		**882.34 ± 0.10[n]**	**18 ± 4[n]**	**2.65**
				882.3 ± 0.2[o]	**28 ± 3[o]**	**1.00**
				882.27 ± 0.01[p]	**26.1 ± 0.1[p]**	**1.72**
887.82 ± 0.05[c]	1.88 ± 0.13	92 ± 16	247 ± 19	888.18 ± 0.10	53 ± 6	2.28
		26 ± 3		**888.18 ± 0.10[n]**	**13 ± 3[n]**	**3.06**
				888.3 ± 0.2[o]	**17 ± 2[o]**	**2.50**
				888.27 ± 0.01[p]	**24.4 ± 1.2[p]**	**0.50**
916.72 ± 0.05[a,c]	0.50 ± 0.05	24 ± 4	65 ± 7	917.10 ± 0.10	22 ± 2	0.45
		7.00 ± 0.88		**917.10 ± 0.10[n]**	**5.50 ± 1.20[n]**	**1.01**
				917.0 ± 0.2[o]	**4.4 ± 0.5[o]**	**2.57**
				917.089 ± 0.01[p]	**5.4 ± 0.3[p]**	**1.72**
944.16 ± 0.06[c]	0.23 ± 0.04	11.4 ± 2.7	31 ± 6	944.4	20 ± 2	–2.56
		3.22 ± 0.61		**944.4[n]**	**5.00 ± 1.12[n]**	**− 1.40**
				944.3 ± 0.3[o]	**3.4 ± 0.5[o]**	**− 0.23**
				944.444 ± 0.02[p]	**3.94 ± 0.20[p]**	**− 1.12**
980.10 ± 0.06[a,c]	0.27 ± 0.04	13.0 ± 2.9	35 ± 5	980.6 ± 0.2	12 ± 2[f]	1.91
		3.78 ± 0.63		**980.6 ± 0.2[n]**	**3.00 ± 0.78[n]**	**0.78**
				980.3 ± 0.5[o]	**2.7 ± 0.4[o]**	**1.45**
				980.352 ± 0.02[p]	**5.11 ± 0.26[p]**	**− 1.95**
1021.83 ± 0.14[a,c]	0.05 ± 0.01	2.21 ± 0.64	5.96 ± 1.21	–	–	–
		0.70 ± 0.15		**1022.07 ± 0.16[p]**	**0.38 ± 0.05[p]**	**2.02**
1091.96 ± 0.07[c]	0.37 ± 0.03	18.2 ± 3.3	49 ± 6	1092.0	11.3 ± 2.2	1.74
		5.18 ± 0.57		**1092.02[n]**	**2.82 ± 0.79[n]**	**2.42**
				1092.1 ± 1.0[o]	**4.0 ± 0.8[o]**	**1.20**
				1092.23 ± 0.02[p]	**4.26 ± 0.22[p]**	**1.51**
1124.63 ± 0.08[a,c]	0.13 ± 0.02	6.17 ± 1.42	17 ± 3	1124.8 ± 0.2	7.8 ± 1.6	− 0.76
		1.82 ± 0.31		**1124.8 ± 0.2[n]**	**1.95 ± 0.56[n]**	**2.42**
				1125.5 ± 0.5[o]	**2.6 ± 0.4[o]**	**1.20**
				1124.95 ± 0.03[p]	**2.36 ± 0.13[p]**	**− 1.61**
1129.24 ± 0.06[a,c,g]	0.61 ± 0.06	30 ± 5	80 ± 8	1129.7 ± 0.2	17 ± 3	2.22
		8.54 ± 1.06		**1129.7 ± 0.2[n]**	**4.25 ± 1.13[n]**	**2.77**
				1129.8 ± 0.5[o]	**5.4 ± 0.7[o]**	**2.47**
				1129.12 ± 0.01[p]	**6.7 ± 0.3[p]**	**1.67**
1187.61 ± 0.12[c]	0.13 ± 0.02	6.12 ± 1.32	17 ± 3	1187.7 ± 0.2	9.7 ± 1.9	− 1.55
		1.82 ± 0.31		**1187.7 ± 0.2[n]**	**2.43 ± 0.68[n]**	**− 0.82**
				1187.6 ± 0.2[o]	**1.8 ± 0.4[o]**	**0.04**
				1187.74 ± 0.04[p]	**2.52 ± 0.13[p]**	**− 2.08**
1195.16 ± 0.11[c]	0.63 ± 0.05	31 ± 5	82 ± 7	1195.20 ± 0.10	20 ± 4	1.72
		8.82 ± 0.97		**1195.20 ± 0.10[n]**	**5.00 ± 1.41[n]**	**2.23**

Table 13 (continued)

This work				From [14, 18]		
E_γ (keV)	$P_{E\gamma}(90°)/(\varepsilon_{E\gamma}{\cdot}f_{E\gamma})$ $\times 10^{-8}$ (count)	I_R(relative) (%)	$<\sigma_{E\gamma}(90°)>$ (mb)	E_γ (keV)	I_{RD} (relative) (%)	R
				1195.0 ± 0.3[o]	**7.9 ± 0.9[o]**	**0.69**
				1195.10 ± 0.01[p]	**9.0 ± 0.4[p]**	**− 0.17**
1252.56 ± 0.19[c,h]	0.21 ± 0.02	10.1 ± 1.8	27 ± 3	1251.9	2 ± 1	3.92
		2.94 ± 0.36		**1251.9[n]**	**0.50 ± 0.27[n]**	**5.42**
				1252.5 ± 0.5[o]	**1.1 ± 0.4[o]**	**3.42**
				1252.79 ± 0.06[p]	**1.44 ± 0.08[p]**	**4.07**
1276.50 ± 0.07[c]	0.95 ± 0.07	46 ± 8	124 ± 10	1276.6 ± 0.2	26 ± 5	2.12
		13.3 ± 1.4		**1276.6 ± 0.2[n]**	**6.50 ± 1.80[n]**	**− 0.82**
				1276.9 ± 0.3[o]	**8 ± 1[o]**	**0.04**
				1276.56 ± 0.02[p]	**11.5 ± 1.9[p]**	**− 2.08**
1308.61 ± 0.17[b,c]	0.19 ± 0.03	9.10 ± 1.96	25 ± 4	–	–	–
		2.66 ± 0.47		**1308.64 ± 0.06[p]**	**1.78 ± 0.10[p]**	**1.83**
1311.53 ± 0.22	0.09 ± 0.02	4.20 ± 1.09	11 ± 3	–	–	–
		1.26 ± 0.29		**1309.3 ± 0.4[o]**	**1.2 ± 0.4[o]**	**0.12**
				1312.3 ± 0.3[p]	**0.28 ± 0.04[p]**	**3.35**
1319.59 ± 0.14[b]	0.16 ± 0.02	7.89 ± 1.52	21 ± 3	–	–	–
		2.24 ± 0.33		**1319.5 ± 0.2[o]**	**1.8 ± 0.5[o]**	**1.14**
				1319.65 ± 0.04[p]	**2.44 ± 0.14[p]**	**− 0.56**
1372.35 ± 0.11[c]	0.36 ± 0.03	17.5 ± 3.2	47 ± 4	1372.7 ± 0.5	9.4 ± 2.4	2.05
		5.04 ± 0.57		**1372.7 ± 0.5[n]**	**2.35 ± 0.76[n]**	**2.83**
				1373.1 ± 0.3[o]	**2.1 ± 0.9[o]**	**2.76**
				1372.80 ± 0.04[p]	**3.50 ± 0.18[p]**	**2.58**
1403.95 ± 0.47	0.07 ± 0.02	3.57 ± 1.07	10 ± 3	–	–	–
		0.98 ± 0.29		**1404.0 ± 0.03[p]**	**0.31 ± 0.04[p]**	**2.29**
1438.84 ± 0.34[i]	0.09 ± 0.02	4.30 ± 1.14	12 ± 3	–	–	–
		1.26 ± 0.30		**1438.6 ± 0.3[p]**	**0.28 ± 0.04[p]**	**3.24**
1556.41 ± 0.16[a]	0.17 ± 0.02	8.38 ± 1.74	23 ± 3	1556.4 ± 0.8	8.6 ± 2.2[j]	1.51
		2.38 ± 0.33		**1556.4 ± 0.8[n]**	**2.15 ± 0.70[n]**	**0.30**
				1556.4 ± 1.0[o]	**1.3 ± 0.5[o]**	**1.80**
				1556.67 ± 0.10[p]	**1.65 ± 0.09[p]**	**2.13**
1585.67 ± 0.19	0.15 ± 0.02	7.52 ± 1.45	20 ± 3	1585.1 ± 1.2	17 ± 3 [k]	− 1.11
		2.10 ± 0.32		**1585.1 ± 1.2[n]**	**4.25 ± 1.13[n]**	**–0.50**
				1585.2 ± 0.4[o]	**0.6 ± 0.3[o]**	**3.42**
				1585.62 ± 0.10[p]	**1.09 ± 0.07[p]**	**3.08**
1901.48 ± 0.33[b,l]	0.07 ± 0.02	3.54 ± 0.93	10 ± 3	–	–	–
		0.98 ± 0.29		**1901.0 ± 1.0[o]**	**0.5 ± 0.2[o]**	**1.36**
				1902.29 ± 0.12[p]	**1.09 ± 0.07[p]**	**− 0.37**
1919.01 ± 0.33[b]	0.09 ± 0.02	4.43 ± 1.22	12 ± 3	–	–	–
		1.26 ± 0.30		**1918.8 ± 0.5[o]**	**0.5 ± 0.2[o]**	**2.11**
				1918.80 ± 0.13[p]	**1.00 ± 0.07[p]**	**0.84**
1982.58 ± 0.33[b,m]	0.07 ± 0.01	3.18 ± 0.82	9 ± 1	–	–	–
		0.98 ± 0.29		**1981.0 ± 1.0[o]**	**0.5 ± 0.2[o]**	**1.36**
				1982.55 ± 0.13[p]	**1.08 ± 0.07[p]**	**− 0.33**
1999.65 ± 0.20[b]	0.15 ± 0.02	7.22 ± 1.55	20 ± 3	–	–	–
		2.10 ± 0.32		**1999.3 ± 0.5[o]**	**0.3 ± 0.2[o]**	**4.77**
				1999.98 ± 0.16[p]	**1.00 ± 0.07[p]**	**3.36**
2020.85 ± 0.21[c]	0.05 ± 0.01	2.45 ± 0.70	7 ± 1	–	–	–
		0.70 ± 0.15		**2022.1 ± 0.3[p]**	**0.38 ± 0.04[p]**	**2.06**

Table 13 (continued)

This work				From [14, 18]		
E_γ (keV)	$P_{E\gamma}(90°)/(\varepsilon_{E\gamma}\cdot f_{E\gamma})$ $\times 10^{-8}$ (count)	I_R(relative) (%)	$<\sigma_{E\gamma}(90°)>$ (mb)	E_γ (keV)	I_{RD} (relative) (%)	R
2048.04 ± 0.27	0.08 ± 0.02	3.69 ± 1.01	10 ± 3	–	–	–
		1.12 ± 0.29		**2045.5 ± 1.0[o]**	**0.50 ± 0.30[p]**	**1.48**
				2047.79 ± 0.19[p]	**0.50 ± 0.05[p]**	**2.10**
2241.54 ± 0.36[c]	0.04 ± 0.01	2.07 ± 0.74	6 ± 1	–	–	–
		0.56 ± 0.15		**2240.4 ± 0.4[p]**	**0.35 ± 0.05[p]**	**1.38**
2734.31 ± 0.26	0.07 ± 0.02	3.35 ± 0.98	9 ± 3	–	–	–
		0.98 ± 0.29		**2734.3 ± 1.0[p]**	**0.23 ± 0.05[p]**	**2.55**
2746.29 ± 0.34	0.08 ± 0.02	3.76 ± 1.14	10 ± 3	–	–	–
		1.12 ± 0.29		**2745.0 ± 1.2[p]**	**0.26 ± 0.05[p]**	**2.92**

E_γ is the gamma-ray energy, $P_{E\gamma}(90°)/(\varepsilon_{E\gamma}\cdot f_{E\gamma})$ the net counts in the gamma-ray peak divided by the full-energy-peak efficiency and the gamma-ray self-absorption factor, I_R the relative intensity of the gamma ray and $<\sigma_{E\gamma}(90°)>$ the fission-neutron spectrum-averaged partial cross section for gamma-ray production at an angle of 90° between neutron beam and detector. R is the residual calculated by Eq. (4)

[a]Corrected for background interference.[b]confirmed by Demidov´s isotopic measurement.[c]corrected for (n,γ) interference from Dy. [d]308 and 311 keV (unresolved doublet by Demidov). [e]assigned as (n,γ) neutron capture line of Sm, as the capture contributions are approximately 100%; net counts, intensities and cross sections are calculated neglecting the capture counts and are given to support the discussion. [f]980 and 983 keV(unresolved doublet by Demidov). [g]corrected for (n,g) interference from Cl. [h]corrected for the contribution of single escape paeak of 1763 keV (31% of net counts). [i]corrected for the contribution of single escape peak of 1951 keV (4.1% of net counts). [j]1554 and 1556 keV (unresolved doublet by Demidov). [k]1582 and 1586 keV (unresolved doublet by Demidov).[l]corrected for interference from ^{37}Cl with $\langle\sigma_{E\gamma}(90^\circ)\rangle = (2.38 \pm 0.56)$ mb from the $CeCl_3$ measurement [8] (42% contribution to the net counts). [m]corrected for interference from ^{18}O with $\langle\sigma_{E\gamma}(90^\circ)\rangle = (201 \pm 28)$ mb from the $CaCO_3$ measurement [3] (53% contribution to the net counts). [n]from elemental measurement [14]. [o]from isotopic measurement [14]. [p]from isotopic measurement [18]

cases. Without any correction, the residual distribution is centered at 0.82 ± 0.05 and is shifted at 1.16 ± 0.10 after corrections. Therefore, an incomplete and inaccurate correction for neutron capture interferences was assumed. However, in contrast to Sm, it cannot be concluded that the neglection of interferences arising from neutron capture would lead to the agreement between the data. The intensities of the lines free of any (n,γ)-interferences at 167.2 keV (^{161}Dy + ^{163}Dy), 244.7 keV (^{163}Dy), 588.3 keV (^{161}Dy), 677.6 keV (^{162}Dy), 911.2 keV (^{164}Dy) and 965.6 keV (^{164}Dy) were determined relative to the 244.7 keV line. The values obtained (474 ± 35) %, (31 ± 8) %, (31 ± 4) %, (39 ± 8) % and (47 ± 5) % were found in good agreement with those derived from the elemental measurement in [14], i.e. (441 ± 141) %, (25 ± 6) %, (30 ± 8) %, (33 ± 8) % and (28 ± 7) %. This observation confirms that the deviations were due to interferences of (n,γ) reactions. The partial cross sections for gamma-ray production are given in column 4 of Table 12, 13, 14, 15, and 16.

Detection limit

The detection limit (DL), which represents the smallest amount of pure element than can be detected, was calculated by means of relation (6) given in [11] from the beam background. The DL of samarium and dysprosium were determined from their most intense gamma lines at 333.4 keV (^{150}Sm) and 184.8 keV (^{162}Dy) for a counting time of 12 h and a net count uncertainty of 50%. Due to the non-negligible contribution of radiative capture in ^{149}Sm and in ^{162}Dy and ^{164}Dy (see Table 11 and 16), elemental cross sections of $<\sigma^Z_{E\gamma}(90°)>= 967$ mb for the 333.4-keV line of ^{150}Sm and $<\sigma^Z_{E\gamma}(90°)>=285$ mb for the184.8-keV line of ^{162}Dy were determined. Considering a net counts uncertainty of 50% the smallest amounts of samarium and dysprosium that can be detected are 0.6 mg and 1.6 mg, respectively.

Conclusions

Prompt gamma rays of samarium and dysprosium induced by $(n,n'\gamma)$- and (n,γ)-reactions were measured by irradiating a $SmCl_3 \cdot 7H_2O$ and a $DyCl_3 \cdot 6H_2O$ sample with fission neutrons. For samarium, we identified 140 prompt gamma lines associated with the $(n,n'\gamma)$- reaction (2 of ^{144}Sm, 13 of ^{147}Sm, 14 of ^{148}Sm, 9 of ^{149}Sm, 20 of ^{150}Sm, 18 of ^{152}Sm, 12 of ^{154}Sm and 52 lines of more than one isotope) and 15 mainly from (n,γ) reaction (1 from ^{150}Sm and 14 from ^{152}Sm). In the case of dysprosium, 148 lines were associated with the $(n,n'\gamma)$-reaction (13 to ^{161}Dy, 48 to ^{162}Dy, 28

Table 14 Prompt gamma rays of ^{163}Dy induced by inelastic scattering of fission neutrons

This work				From Demidov Atlas [5]		
E_γ (keV)	$P_{E\gamma}(90°)/(\varepsilon_{E\gamma} \cdot f_{E\gamma}) \times 10^{-8}$ (count)	I_R(relative) (%)	$<\sigma_{E\gamma}(90°)>$ (mb)	E_γ (keV)	I_{RD}(relative) (%)	R
93.78 ± 0.06[a]	0.59 ± 0.06	29 ± 5	78 ± 8	–	–	–
		32 ± 5		**93.81 ± 0.02[e]**	**13.2 ± 0.9[e]**	**3.70**
177.39 ± 0.04[a]	0.39 ± 0.04	19.0 ± 3.5	52 ± 6	–	–	–
		21 ± 3		**177.45 ± 0.01[e]**	**10.7 ± 0.6[e]**	**3.37**
207.86 ± 0.04[a]	1.06 ± 0.05	52 ± 8	141 ± 8	208.15 ± 0.10	94 ± 20	− 1.95
		57 ± 7		**208.15 ± 0.10[d]**	**58 ± 18[d]**	**− 0.05**
				208.15 ± 0.01[e]	**41.5 ± 2.5[e]**	**2.08**
244.72 ± 0.05	0.51 ± 0.03	25 ± 4	67 ± 4	245.3 ± 0.2	34 ± 6	− 1.25
		27 ± 4		**245.3 ± 0.2[d]**	**21 ± 4[d]**	**1.06**
				245.07 ± 0.01[e]	**28.2 ± 1.5[e]**	**− 0.28**
250.52 ± 0.03[a]	1.85 ± 0.23	90 ± 18	246 ± 32	250.94 ± 0.10	161 ± 35	− 1.80
		100		**250.94 ± 0.10[d]**	**100**	
				250.90 ± 0.01[e]	**100**	
262.75 ± 0.04[a,b]	1.42 ± 0.09	69 ± 12	189 ± 14	263.20 ± 0.10	82 ± 15	− 0.68
		78 ± 11		**263.20 ± 0.10[d]**	**51 ± 14[d]**	**1.52**
				263.11 ± 0.01[e]	**62.8 ± 3.2[e]**	**1.33**
266.21 ± 0.13[a]	0.07 ± 0.02	3.18 ± 0.92	9 ± 2	–	–	–
		3.78 ± 1.18		**266.61 ± 0.05[e]**	**4.3 ± 0.4[e]**	**− 0.42**
305.71 ± 0.12[a]	0.10 ± 0.02	4.68 ± 1.22	13 ± 3	–	–	–
		5.40 ± 1.27		**306.34 ± 0.01[e]**	**6.4 ± 0.4[e]**	**− 0.75**
315.70 ± 0.06[a]	0.13 ± 0.03	6.22 ± 1.95	17 ± 4	316.2 ± 0.3	23 ± 4	–3.77
		7.03 ± 1.84		**316.2 ± 0.3[d]**	**14 ± 4[d]**	**− 1.58**
				316.33 ± 0.01[e]	**19.1 ± 1.0[e]**	**− 5.76**
350.55 ± 0.03[a,b]	0.32 ± 0.09	15.8 ± 4.8	43 ± 12	351.22 ± 0.10	84 ± 11	− 5.68
		17 ± 5		**351.22 ± 0.10[d]**	**52 ± 13[d]**	**− 2.51**
				351.19 ± 0.01[e]	**59.6 ± 3.1[e]**	**− 7.24**
353.67 ± 0.04[a]	0.67 ± 0.13	33 ± 8	90 ± 18	354.29 ± 0.10	52 ± 6	− 1.90
		36 ± 14		**354.29 ± 0.10[d]**	**32 ± 8[d]**	**0.25**
				354.24 ± 0.01[e]	**48.9 ± 2.6[e]**	**− 0.90**
385.32 ± 0.07[a]	0.24 ± 0.06	11.9 ± 3.3	33 ± 8	385.8 ± 0.3	16 ± 4	− 0.79
		13 ± 4		**385.8 ± 0.3[d]**	**10 ± 3[d]**	**0.60**
				385.63 ± 0.04[e]	**10.4 ± 0.8[e]**	**0.64**
389.06 ± 0.04[a]	0.89 ± 0.19	43 ± 12	118 ± 25	389.82 ± 0.10	72 ± 7	− 2.09
		48 ± 12		**389.82 ± 0.10[d]**	**45 ± 11[d]**	**0.18**
				389.76 ± 0.14[e]	**58.0 ± 2.9[e]**	**− 0.81**
401.31 ± 0.05[a]	0.61 ± 0.08	30 ± 6	81 ± 11	402.1 ± 0.2	31 ± 4	− 0.14
		33 ± 6		**402.1 ± 0.2[d]**	**19 ± 5[d]**	**1.73**
				401.96 ± 0.01[e]	**31.9 ± 1.6[e]**	**0.18**
406.94 ± 0.13[a]	0.16 ± 0.04	7.76 ± 2.09	21 ± 5	–	–	–
		8.65 ± 2.41		**407.62 ± 0.01[e]**	**6.8 ± 0.4[e]**	**0.75**
421.08 ± 0.05[a]	0.72 ± 0.16	35 ± 10	96 ± 22	421.90 ± 0.10	64 ± 6	− 2.49
		39 ± 10		**421.90 ± 0.10[d]**	**40 ± 9[d]**	**− 0.07**
				421.84 ± 0.01[e]	**50.3 ± 2.6[e]**	**− 1.09**
427.00 ± 0.04[a]	0.48 ± 0.08	23 ± 5	64 ± 12	427.4 ± 0.2	23 ± 2	0
		26 ± 5		**427.4 ± 0.2[d]**	**14 ± 3[d]**	**2.06**
				427.66 ± 0.01[e]	**32.2 ± 1.6[e]**	**− 1.18**
435.60 ± 0.17[a,c]	0.09 ± 0.02	4.47 ± 1.39	12 ± 3	436.8 ± 0.3	9.7 ± 0.9	− 3.16
		4.86 ± 1.23		**436.8 ± 0.3[d]**	**6.02 ± 1.42[d]**	**− 0.63**
				436.78 ± 0.06[e]	**2.41 ± 0.24[e]**	**1.30**

Table 14 (continued)

This work				From Demidov Atlas [5]		
E_γ (keV)	$P_{E\gamma}(90°)/(\varepsilon_{E\gamma}\cdot f_{E\gamma})$ $\times 10^{-8}$ (count)	I_R(relative) (%)	$<\sigma_{E\gamma}(90°)>$ (mb)	E_γ (keV)	I_{RD}(relative) (%)	R
440.45 ± 0.05[a]	0.33 ± 0.04	16 ± 3.1	44 ± 6	441.3 ± 0.3	16 ± 2	0
		18 ± 3		**441.3 ± 0.3[d]**	**9.9 ± 2.5[d]**	**2.07**
				441.11 ± 0.01[e]	**21.4 ± 1.1[e]**	**−1.06**
474.72 ± 0.03[a]	0.58 ± 0.07	28.0 ± 5.5	76 ± 11	475.5 ± 0.2	24 ± 3	0.64
		31 ± 5		**475.5 ± 0.2[d]**	**15 ± 4[d]**	**2.50**
				475.39 ± 0.02[e]	**36.3 ± 2.4[e]**	**−0.95**
478.73 ± 0.04[a]	0.22 ± 0.04	10.7 ± 2.5	29 ± 5	479.4 ± 0.2	22 ± 3	−2.89
		12 ± 3		**479.4 ± 0.2[d]**	**14 ± 4[d]**	**−0.40**
				479.38 ± 0.02[e]	**27.8 ± 1.9[e]**	**−4.45**
541.03 ± 0.17	0.20 ± 0.03	9.63 ± 2.24	26 ± 4	–	–	–
		11 ± 2		**541.55 ± 0.01[e]**	**7.9 ± 0.4[e]**	**1.52**
552.32 ± 0.13[a]	0.09 ± 0.02	4.35 ± 1.04	12 ± 3	–	–	–
		4.86 ± 1.23		**553.02 ± 0.01[e]**	**7.9 ± 0.4[e]**	**−2.35**
558.85 ± 0.10[a]	0.05 ± 0.01	2.58 ± 0.75	7 ± 1	–	–	–
		2.70 ± 0.63		**559.55 ± 0.02[e]**	**1.5 ± 0.3[e]**	**1.72**
633.30 ± 0.13[a,c]	0.24 ± 0.03	11.7 ± 2.3	32 ± 4	633.6 ± 0.2	7.5 ± 2.0	1.38
		13 ± 2		**633.6 ± 0.2[d]**	**4.66 ± 1.60[d]**	**3.26**
				633.94 ± 0.04[e]	**6.1 ± 0.4[e]**	**3.38**
637.32 ± 0.19[a]	0.08 ± 0.02	3.66 ± 1.16	10 ± 3	–	–	–
		4.32 ± 1.21		**638.02 ± 0.03[e]**	**5.8 ± 0.4[e]**	**−1.16**
710.90 ± 0.13[a]	0.12 ± 0.02	5.92 ± 1.40	16 ± 3	711.57 ± 0.10	15 ± 2	−3.72
		6.49 ± 1.35		**711.57 ± 0.10[d]**	**9.32 ± 2.38[d]**	**−1.25**
				711.46 ± 0.02[e]	**13.7 ± 0.7[e]**	**−4.74**
726.84 ± 0.19[a,b]	0.19 ± 0.03	9.31 ± 1.95	25 ± 4	–	–	–
		10 ± 2		**727.60 ± 0.02[e]**	**5.79 ± 0.18[e]**	**2.10**

E_γ is the gamma-ray energy, $P_{E\gamma}(90°)/(\varepsilon_{E\gamma}\cdot f_{E\gamma})$ the net counts in the gamma-ray peak divided by the full-energy-peak efficiency and the gamma-ray self-absorption factor, I_R the relative intensity of the gamma ray and $<\sigma_{E\gamma}(90°)>$ the fission-neutron spectrum-averaged partial cross section for gamma-ray production at an angle of 90° between neutron beam and detector. R is the residual calculated by Eq. (4)

[a]Corrected for (n,γ) interference from Sm. [b]corrected for background interference. [c]corrected for (n,γ) interference from Cl. [d]from elemental measurement [14]. [e]from isotopic measurement [19]

to ^{163}Dy, 44 to ^{164}Dy and 15 to more than one isotope) and 12 mainly to neutron capture reaction (4 from ^{161}Dy, 6 from ^{162}Dy and 2 from ^{164}Dy). Many $(n,n'\gamma)$-lines of samarium and dysprosium were found to be affected by the interferences with the (n,γ)-lines mainly produced by the capture of epithermal neutrons. Subsequently, their contributions to the net counts were corrected. Relative intensities and fission-neutron spectrum-averaged partial production cross sections of the gamma rays were presented. Compared with the measurements performed with the samples of natural abundance [14], due to the better energy resolution of our detector and a relative higher neutron beam energy, 80 and 68 additional lines were detected for samarium and dysprosium, respectively. The measured relative intensities agree with the values obtained from irradiation of samples of natural abundance [14] or isotopically enriched [14–20] with reactor fast neutrons at 1.8 σ level for samarium and 2.2σ level for dysprosium. Large discrepancies between the set of data indicates a systematic effect due to interferences of (n,γ) reactions and implies that corrections for neutron capture were inaccurate or missed in [14]. Besides the fact that detailed information on the correction process was missing in [14], there are two aspects that one should consider and critically review: (1) it is unlikely that the databases used in [14] for capture lines, i.e., [44] were complete in those days, and secondly (2) it might be that the values available in those days were inaccurate compared to those listed in existing databases [23, 24]. The discrepancies in relative intensity compared to [14–20] can also be attributed to the difference in the neutron energy spectra. Indeed, the irriadiation

Table 15 Prompt gamma rays of ^{164}Dy induced by inelastic scattering of fission neutrons

This work				From [14, 20]		
E_γ (keV)	$P_{E\gamma}(90°)/(\varepsilon_{E\gamma}.f_{E\gamma})$ $\times 10^{-8}$ (count)	I_R(relative) (%)	$<\sigma_{E\gamma}(90°)>$ (mb)	E_γ (keV)	I_{RD}(relative) (%)	R
123.26 ± 0.16	0.14 ± 0.03	6.58 ± 1.89	16 ± 3	–	–	–
		2.65 ± 0.60		**123.32 ± 0.06**[i]	**2.82 ± 0.14**[i]	**− 0.28**
148.65 ± 0.06[a]	1.06 ± 0.05	52 ± 8	141 ± 8	148.7 ± 0.3	26 ± 8	2.29
		20 ± 2		**148.7 ± 0.3**[g]	**6.50 ± 2.38**[g]	**4.34**
				148.7 ± 0.2[h]	**7.1 ± 1.7**[h]	**4.91**
				148.70 ± 0.01[i]	**6.83 ± 0.23**[i]	**6.54**
168.74 ± 0.03[a,b]	5.28 ± 0.38	257 ± 44	619 ± 50	169.0 ± 0.2	400 ± 80	− 1.57
		100		**169.0 ± 0.2**[g]	**100**	
				168.8 ± 0.2[h]	**100**	
				168.84 ± 0.01[i]	**100**	
214.89 ± 0.03[a]	1.79 ± 0.20	87 ± 17	210 ± 25	215.23 ± 0.10	140 ± 25	− 1.75
		34 ± 4		**215.23 ± 0.10**[g]	**35 ± 9**[g]	**− 0.10**
				214.9 ± 0.2[h]	**34 ± 8**[h]	**0**
				215.10 ± 0.01[i]	**41.6 ± 1.1**[i]	**− 1.83**
277.04 ± 0.04[a,b]	0.70 ± 0.09	34 ± 7	82 ± 11	277.6 ± 0.2	50 ± 10	− 1.31
		13.2 ± 1.9		**277.6 ± 0.2**[g]	**12.5 ± 3.5**[g]	**0.18**
				277.7 ± 0.2[h]	**12.5 ± 2.6**[h]	**0.22**
				277.49 ± 0.01[i]	**17.5 ± 0.4**[i]	**− 2.21**
294.21 ± 0.04[a]	0.17 ± 0.04	8.09 ± 2.49	20 ± 5	294.7 ± 0.2	51 ± 10[d]	− 3.10
		3.22 ± 0.79		**294.7 ± 0.2**[g]	**12.8 ± 3.6**[g,d]	**− 1.49**
				294.7 ± 0.2[h]	**7.8 ± 1.3**[h]	**− 3.01**
				294.55 ± 0.01[i]	**14.3 ± 0.3**[i]	**− 13.1**
308.48 ± 0.11[c]	0.26 ± 0.04	12.7 ± 2.9	31 ± 5	–	–	–
		4.92 ± 0.83		**309.3 ± 0.2**[h]	**4.1 ± 1.3**[h]	**0.53**
				309.18 ± 0.15[i]	**4.44 ± 0.11**[i]	**0.66**
461.59 ± 0.05[a]	0.19 ± 0.02	9.18 ± 1.70	22 ± 2	462.2 ± 0.4	8.3 ± 1.1	0.43
		3.60 ± 0.46		**462.2 ± 0.4**[h]	**2.08 ± 0.50**[h]	**2.24**
				461.26 ± 0.13[i]	**0.32 ± 0.03**[i]	**7.11**
464.94 ± 0.06[a]	0.08 ± 0.02	4.09 ± 1.19	10 ± 2	–	–	–
		1.51 ± 0.39		**465.37 ± 0.15**[i]	**0.60 ± 0.08**[i]	**3.05**
522.67 ± 0.13[c]	0.11 ± 0.02	5.49 ± 1.48	13 ± 2	–	–	–
		2.08 ± 0.41		**523.2 ± 1.0**[h]	**0.4 ± 0.2**[h]	**3.68**
				523.33 ± 0.02[i]	**1.54 ± 0.05**[i]	**1.31**
548.18 ± 0.09[a]	0.18 ± 0.02	8.83 ± 1.74	21 ± 2	548.5 ± 0.5	9.0 ± 2.0[e]	2.98
		3.41 ± 0.45		**548.5 ± 0.5**[g]	**2.25 ± 0.67**[g]	**4.94**
				548.5 ± 0.2[h]	**1.2 ± 0.2**[h]	**4.49**
				548.82 ± 0.03[i]	**2.51 ± 0.06**[i]	**1.98**
585.24 ± 0.05[a]	0.49 ± 0.05	24 ± 5	58 ± 6	585.63 ± 0.10	31 ± 3	− 1.20
		9.28 ± 1.16		**585.63 ± 0.10**[g]	**7.75 ± 1.72**[g]	**0.74**
				585.5 ± 0.2[h]	**6.1 ± 0.7**[h]	**2.35**
				585.98 ± 0.01[i]	**10.94 ± 0.24**[i]	**− 1.40**
610.57 ± 0.11[a,c]	0.50 ± 0.06	24 ± 5	58 ± 6	–	–	–
		9.47 ± 1.32		**611.0 ± 1.0**[h]	**1.0 ± 0.7**[h]	**5.67**
				611.17 ± 0.01[i]	**6.59 ± 0.14**[i]	**2.17**
651.77 ± 0.20	0.09 ± 0.03	4.28 ± 1.42	10 ± 3	–	–	–
		1.70 ± 0.58		**652.23 ± 0.01**[i]	**2.51 ± 0.06**[r]	**− 1.39**
673.12 ± 0.04[a]	0.78 ± 0.10	38 ± 8	92 ± 12	673.66 ± 0.10	38 ± 4	0
		15 ± 2		**673.66 ± 0.10**[g]	**9.50 ± 2.15**[g]	**1.87**
				673.7 ± 0.2[h]	**12.5 ± 2.0**[h]	**0.62**
				673.74 ± 0.01[i]	**20.7 ± 0.5**[i]	**− 2.76**
687.83 ± 0.04[a]	2.13 ± 0.29	104 ± 21	250 ± 35	688.46 ± 0.10	94 ± 10	0.43
		40 ± 6		**688.46 ± 0.10**[g]	**23.5 ± 5.3**[g]	**2.06**

Table 15 (continued)

This work				From [14, 20]		
E_γ (keV)	$P_{E\gamma}(90°)/(\varepsilon_{E\gamma}.f_{E\gamma})$ $\times 10^{-8}$ (count)	I_R(relative) (%)	$<\sigma_{E\gamma}(90°)>$ (mb)	E_γ (keV)	I_{RD}(relative) (%)	R
				688.4 ± 0.4 [h]	**51 ± 7** [h]	**− 1.24**
				688.42 ± 0.01 [i]	**62.8 ± 1.4** [i]	**− 3.70**
754.31 ± 0.04[a]	2.05 ± 0.32	100	241 ± 38	754.86 ± 0.10	100	–
		39 ± 7		**754.86 ± 0.10** [g]	**25 ± 1** [g]	**1.98**
				754.8 ± 0.2 [h]	**49 ± 7** [h]	**− 1.01**
				754.81 ± 0.01 [i]	**61.8 ± 1.4** [i]	**− 3.19**
761.34 ± 0.04[a]	1.96 ± 0.25	95 ± 19	230 ± 30	761.87 ± 0.10	75 ± 8	0.97
		37 ± 5		**761.87 ± 0.10** [g]	**19 ± 4** [g]	**2.68**
				761.7 ± 0.2 [h]	**37 ± 6** [h]	**0**
				761.81 ± 0.01 [i]	**60.4 ± 1.3** [i]	**− 4.53**
781.89 ± 0.05[a]	0.75 ± 0.04	36 ± 6	88 ± 6	782.31 ± 0.10	18 ± 2	2.85
		14 ± 1		**782.31 ± 0.10** [g]	**4.50 ± 1.0** [g]	**6.71**
				782.3 ± 0.2 [h]	**6.5 ± 1.3** [h]	**4.57**
				782.40 ± 0.01 [i]	**10.99 ± 0.24** [i]	**2.93**
911.16 ± 0.11	0.20 ± 0.02	9.93 ± 1.88	24 ± 3	911.4 ± 0.2	12 ± 2	–0.75
		3.79 ± 0.47		**911.4 ± 0.2** [g]	**3.00 ± 0.78** [g]	**0.87**
				911.1 ± 0.4 [h]	**1.1 ± 0.2** [h]	**5.27**
				911.34 ± 0.03 [i]	**1.63 ± 0.05** [i]	**4.57**
955.25 ± 0.28	0.09 ± 0.02	4.29 ± 1.24	10 ± 2	–	–	–
		1.70 ± 0.40		**954.57 ± 0.24** [i]	**0.15 ± 0.02** [i]	**3.87**
965.61 ± 0.10	0.24 ± 0.02	11.8 ± 2.2	29 ± 3	965.1	10 ± 2	0.60
		4.55 ± 0.50		**965.1** [g]	**2.50 ± 0.71** [g]	**2.36**
				966.2 ± 1.0 [h]	**1.7 ± 0.7** [h]	**3.31**
				965.91 ± 0.01 [i]	**2.93 ± 0.09** [i]	**3.19**
982.64 ± 0.20[b,c]	0.13 ± 0.02	6.24 ± 1.40	15 ± 2	–	–	–
		2.46 ± 0.42		**982.1 ± 1.0** [h]	**1.3 ± 0.3** [h]	**2.25**
				982.93 ± 0.02 [i]	**2.19 ± 0.07** [i]	**0.63**
1001.84 ± 0.21[a,c]	0.13 ± 0.03	6.38 ± 1.72	15 ± 3	–	–	–
		2.46 ± 0.42		**1000.2 ± 1.0** [h]	**0.5 ± 0.2** [h]	**4.21**
				1002.35 ± 0.04 [i]	**0.93 ± 0.04** [i]	**3.63**
1072.07 ± 0.26[a]	0.11 ± 0.02	5.30 ± 1.30	13 ± 3	–	–	–
		2.08 ± 0.41		**1072.18 ± 0.13** [i]	**0.36 ± 0.03** [i]	**4.18**
1412.18 ± 0.22[a,b]	0.05 ± 0.01	2.61 ± 0.71	6 ± 1	–	–	–
		0.95 ± 0.20		**1411.48 ± 0.09** [i]	**0.89 ± 0.07** [i]	**0.28**
1515.81 ± 0.18[b,c]	0.11 ± 0.02	5.39 ± 1.24	13 ± 2	–	–	–
		2.08 ± 0.41		**1515.6 ± 0.5** [h]	**1.2 ± 0.2** [h]	**1.93**
				1515.94 ± 0.03 [i]	**1.91 ± 0.08** [i]	**0.41**
1543.64 ± 0.46[c]	0.10 ± 0.02	4.75 ± 1.34	11 ± 3	–	–	–
		1.89 ± 0.40		**1543.2 ± 0.6** [h]	**0.4 ± 0.1** [h]	**3.61**
				1543.00 ± 0.16 [i]	**0.22 ± 0.03** [i]	**4.16**
1553.96 ± 0.34[c]	0.10 ± 0.02	4.89 ± 1.36	12 ± 2	–	–	–
		1.89 ± 0.40		**1555.5 ± 1.0** [h]	**0.5 ± 0.2** [h]	**3.11**
				1554.50 ± 0.07 [i]	**0.80 ± 0.04** [i]	**2.71**
1581.62 ± 0.28[c]	0.11 ± 0.02	5.43 ± 1.35	13 ± 3	–	–	–
		1.89 ± 0.40		**1582.0 ± 0.5** [h]	**0.6 ± 0.1** [h]	**3.13**
				1581.31 ± 0.03 [i]	**1.97 ± 0.08** [i]	**–0.20**
1600.88 ± 0.13[a,b,f]	0.27 ± 0.03	13.3 ± 2.5	32 ± 4	1599.8 ± 0.8	7.8 ± 2.3	1.62
		5.11 ± 0.67		**1599.8 ± 0.8** [g]	**1.95 ± 0.69** [g]	**3.28**
				1601.3 ± 0.2 [h]	**1.5 ± 0.3** [h]	**4.92**
				1601.53 ± 0.02 [i]	**3.63 ± 0.13** [i]	**2.17**
1641.97 ± 0.14[b,f]	0.22 ± 0.03	10.6 ± 2.1	26 ± 4	1642.8 ± 0.8	5.4 ± 1.6	1.99
		4.17 ± 0.64		**1642.8 ± 0.8** [g]	**1.35 ± 0.48** [g]	**4.77**

Table 15 (continued)

This work				From [14, 20]		
E_γ (keV)	$P_{E\gamma}(90°)/(\varepsilon_{E\gamma}.f_{E\gamma})$ $\times 10^{-8}$ (count)	I_R(relative) (%)	$<\sigma_{E\gamma}(90°)>$ (mb)	E_γ (keV)	I_{RD}(relative) (%)	R
				1642.6 ± 1.0 [h]	**2.0 ± 0.7** [h]	**2.29**
				1642.81 ± 0.08 [i]	**4.28 ± 0.16** [i]	**–0.17**
1666.41 ± 0.20[c]	0.25 ± 0.03	12.2 ± 2.3	29 ± 4	–	–	–
		4.73 ± 0.66		**1668.1 ± 1.0** [h]	**0.7 ± 0.3** [h]	**5.56**
				1667.26 ± 0.03 [i]	**1.95 ± 0.08** [i]	**4.18**
1674.35 ± 0.29[a,b]	0.10 ± 0.02	5.00 ± 1.27	12 ± 2	–	–	–
		1.89 ± 0.40		**1674.95 ± 0.03** [i]	**2.51 ± 0.10** [i]	**−1.50**
1684.63 ± 0.17	0.16 ± 0.02	7.84 ± 1.66	19 ± 2	1685.8	3.8 ± 1.1	2.03
		3.03 ± 0.43		**1685.8** [g]	**0.95 ± 0.33** [g]	**3.84**
				1683.0 ± 0.5 [h]	**0.9 ± 0.2** [h]	**3.93**
				1684.75 ± 0.03 [i]	**2.49 ± 0.10** [i]	**1.22**
1722.69 ± 0.22[a]	0.39 ± 0.04	18.9 ± 3.6	45 ± 5	1724.0 ± 0.8	5.0 ± 1.5	3.56
		7.39 ± 0.92		**1724.0 ± 0.8** [g]	**1.25 ± 0.45** [g]	**6.00**
				1723.26 ± 0.03 [i]	**3.40 ± 0.14** [i]	**4.29**
1735.98 ± 0.15[a]	0.31 ± 0.03	15.2 ± 2.9	37 ± 4	1735.4 ± 0.8	8.4 ± 1.7	2.02
		5.87 ± 0.71		**1735.4 ± 0.8** [g]	**2.10 ± 0.45** [g]	**4.48**
				1735.0 ± 0.5 [h]	**2.4 ± 0.7** [h]	**3.48**
				1736.17 ± 0.02 [i]	**4.71 ± 0.18** [i]	**1.58**
1836.16 ± 0.20[a,c]	0.11 ± 0.02	5.49 ± 1.23	13 ± 2	–	–	–
		2.08 ± 0.41		**1838.5 ± 1.0** [h]	**1.0 ± 0.3** [h]	**2.12**
				1836.18 ± 0.06 [i]	**0.64 ± 0.03** [i]	**1.94**
1840.69 ± 0.22	0.13 ± 0.02	6.11 ± 1.37	15 ± 2	–	–	–
		2.46 ± 0.42		**1840.70 ± 0.04** [i]	**1.55 ± 0.07** [i]	**2.14**
1859.35 ± 0.15[c]	0.21 ± 0.03	10.4 ± 2.2	25 ± 4	–	–	–
		3.98 ± 0.64		**1858.7 ± 0.5** [h]	**0.7 ± 0.2** [h]	**4.89**
				1859.81 ± 0.06 [i]	**2.28 ± 0.09** [i]	**2.63**
1905.09 ± 0.43[c]	0.09 ± 0.02	4.60 ± 1.27	11 ± 2	–	–	–
		1.70 ± 0.40		**1906.2 ± 1.0** [h]	**0.8 ± 0.3** [h]	**1.80**
				1905.98 ± 0.07 [i]	**0.94 ± 0.05** [i]	**1.88**
1910.13 ± 0.27	0.09 ± 0.02	4.59 ± 1.22	11 ± 2	–	–	–
		1.70 ± 0.40		**1910.17 ± 0.07** [i]	**0.72 ± 0.04** [i]	**2.44**
1980.04 ± 0.23[c]	0.15 ± 0.02	7.36 ± 1.55	18 ± 2	–	–	–
		2.84 ± 0.43		**1979.0 ± 0.5** [h]	**1.1 ± 0.3** [h]	**3.32**
				1979.86 ± 0.03 [i]	**1.73 ± 0.06** [i]	**2.56**
2509.58 ± 0.32	0.09 ± 0.02	4.16 ± 1.02	10 ± 2	–	–	–
		1.70 ± 0.40		**2509.77 ± 0.16** [i]	**0.39 ± 0.03** [i]	**3.26**

E_γ is the gamma-ray energy, $P_{E\gamma}(90°)/(\varepsilon_{E\gamma}.f_{E\gamma})$ the net counts in the gamma-ray peak divided by the full-energy-peak efficiency and the gamma-ray self-absorption factor, I_R the relative intensity of the gamma ray and $<\sigma_{E\gamma}(90°)>$ the fission-neutron spectrum-averaged partial cross section for gamma-ray production at an angle of 90° between neutron beam and detector. R is the residual calculated by Eq. (4)

[a]Corrected for (n,γ) interference from Dy. [b]corrected for background interference. [c]confirmed by Demidov´s isotopic measurements. [d]292 and 294 keV (unresolved doublet by Demidov). [e]548 and 550 keV (unresolved doublet by Demidov). [f]corrected for (n,γ) interference from Cl. [g]from elemental measurement [14]. [h]from isotopic measurement [14]. [i]from isotopic measurement [20]

at the IRT and IR-8 reactors would induce different excitation level of the nuclei than in this work. Finally, the detection limits of samarium and dysprosium were estimated as 0.6 mg and 1.6 mg for a measuring time of 12 h. This excellent sensitivity indicates that magnet samples can be rapidly characterized by means of the PGAINS technique with the FaNGaS instrument confirming the simulation results obtained in [4] in view of their sorting for an efficient recycling at industrial scale.

Table 16 Prompt gamma rays of induced by inelastic scattering of fission neutrons in multiple Dy isotopes

This work				From [14]		
E_γ (keV)	$P_{E\gamma}(90°)/(\varepsilon_{E\gamma} f_{E\gamma})$ $\times 10^{-8}$ (count)	I_R(relative) (%)	$<\sigma_{E\gamma}(90°)>$ (mb)	E_γ (keV)	I_{RD}(relative) (%)	R
^{161}Dy + ^{162}Dy						
80.60 ± 0.06[a]	7.04 ± 0.57	343 ± 60	528 ± 47	–	–	–
^{161}Dy + ^{163}Dy						
167.20 ± 0.04[a]	2.42 ± 0.11	118 ± 19	183 ± 10	167.3 ± 0.2	150 ± 40	− 0.72
285.14 ± 0.04[a]	1.22 ± 0.08	59 ± 10	92 ± 7	285.8 ± 0.2	71 ± 15	− 0.66
^{161}Dy + ^{164}Dy						
532.33 ± 0.08[a,b]	0.17 ± 0.02	8.24 ± 1.66	22 ± 3	533.7 ± 0.2	6.6 ± 1.0	0.85
^{162}Dy + ^{163}Dy						
247.31 ± 0.06[a]	0.33 ± 0.03	16.0 ± 2.8	22 ± 2	247.9 ± 0.2	23 ± 4	− 1.43
347.00 ± 0.05[a]	0.13 ± 0.03	6.40 ± 1.93	9 ± 2	347.4 ± 0.3	20 ± 4	− 3.06
572.25 ± 0.15[a]	0.11 ± 0.02	5.36 ± 1.29	7 ± 1	572.8 ± 0.3	15 ± 2	− 4.05
^{162}Dy + ^{164}Dy						
842.65 ± 0.06[a,b]	0.43 ± 0.05	21 ± 4	26 ± 3	842.7 ± 0.2	27 ± 3	− 0.60
1610.82 ± 0.22	0.16 ± 0.02	7.70 ± 1.63	19 ± 2	–	–	–
1648.06 ± 0.16[a,c]	0.24 ± 0.02	11.9 ± 2.2	15 ± 1	1649.8 ± 0.8	7.4 ± 2.2	1.45
^{163}Dy + ^{164}Dy						
211.68 ± 0.04[a]	1.71 ± 0.13	83 ± 14	106 ± 9	212.06 ± 0.10	119 ± 23	− 1.34
238.21 ± 0.10	0.14 ± 0.02	6.66 ± 1.48	8 ± 1	–	–	–
414.42 ± 0.07[a]	0.16 ± 0.04	7.73 ± 2.32	9 ± 2	–	–	–
^{162}Dy + ^{163}Dy						
259.54 ± 0.04[a]	1.96 ± 0.14	95 ± 16	83 ± 7	260.00	145 ± 30	− 1.47
646.86 ± 0.04[a,c]	0.38 ± 0.02	18.3 ± 3.0	16 ± 1	647.2 ± 0.2	6.3 ± 0.9	3.83

E_γ is the gamma-ray energy, $P_{E\gamma}(90°)/(\varepsilon_{E\gamma} f_{E\gamma})$ the net counts in the gamma-ray peak divided by the full-energy-peak efficiency and the gamma-ray self-absorption factor, I_R the relative intensity of the gamma ray and $<\sigma_{E\gamma}(90°)>$ the fission-neutron spectrum-averaged partial cross section for gamma-ray production at an angle of 90° between neutron beam and detector. R is the residual calculated by Eq. (4)

[a]Corrected for (n,γ) interference from Dy. [b]Corrected for background interference. [c]Corrected for (n,γ) interference from Cl

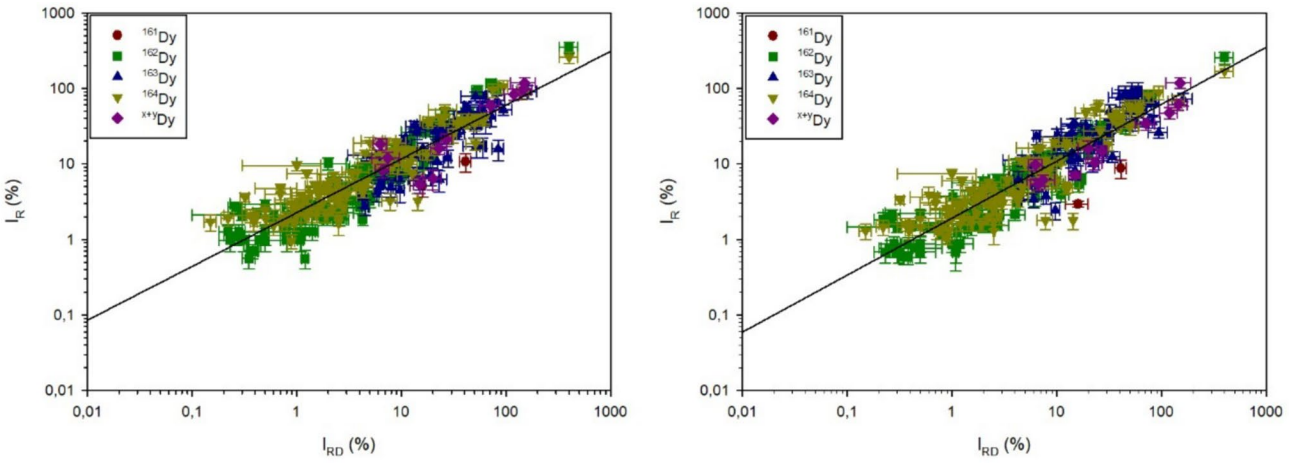

Fig. 7 Correlation between the relative intensities I_R of the prompt gamma rays from inelastic scattering $(n,n'\gamma)$ reactions on samarium measured in this work and the relative intensities I_{RD} obtained from measurement with reactor fast neutrons [14, 18–20]. Data points of $^{X+Y}$Dy indicate multi-isotope lines (see Table 9). Left: the gamma lines measured in this work are corrected for neutron capture interferences. Right: the gamma lines measured in this work are not corrected for neutron capture interferences. The fit of the data with Eq. (3) is shown by the solid line with $a = 2.26 \pm 0.10$ and $b = 0.71 \pm 0.02$ (left plot), and $a = 1.91 \pm 0.08$ and $b = 0.75 \pm 0.02$ (right plot)

Table 17 Relevant contributions of neutron capture (n,γ) reactions to gamma lines primarily identified as (n,n′γ) lines of dysprosium

This work ($n,n'\gamma$)		PGNAA database (n,γ)		$P_{E\gamma}(n,\gamma)/P_{E\gamma}$ (%)
E_γ (keV)	^{A}Z	E_γ in keV (^{A}Z)	$I_{E\gamma}$ (%)	
80.6	^{161}Dy,^{162}Dy	80.6 (^{161}Dy)	14.54 ± 0.75	7.58 ± 2.31
93.8	^{163}Dy	93.8 (^{162}Dy)	0.27 ± 0.04	4.41 ± 1.45
148.7	^{164}Dy	148.7 (^{161}Dy)	0.63 ± 0.08	5.96 ± 1.81
157.0	^{161}Dy	157.0 (^{164}Dy)	0.24 ± 0.01	2.13 ± 0.76
168.7[a]	^{164}Dy	168.7 (^{162}Dy), 168.7(^{163}Dy)	1.48 ± 0.23 (^{162}Dy), 14.8 ± 1.9 (^{163}Dy)	23.6 ± 8.9
177.3	^{163}Dy	177.4 (^{162}Dy), 177.4(^{164}Dy)	1.23 ± 0.60 (^{162}Dy), 0.24 ± 0.04 (^{163}Dy)	30 ± 9
184.8[a]	^{162}Dy	184.8 (^{161}Dy), 184.8(^{164}Dy)	34.5 ± 1.4 (^{161}Dy), 19.6 ± 2.0 (^{164}Dy)	31 ± 9
207.9	^{163}Dy	207.9 (^{162}Dy)	0.13 ± 0.04	1.31 ± 0.41
211.7	^{163}Dy, ^{164}Dy	211.7 (^{161}Dy), 211.7(^{162}Dy)	0.96 ± 0.11 (^{161}Dy), 1.78 ± 0.24 (^{162}Dy)	12.0 ± 3.2
214.9	^{164}Dy	214.9 (^{163}Dy)	9.20 ± 0.70	35 ± 11
235.7	^{162}Dy	236.6 (^{161}Dy)	0.98 ± 0.04	37 ± 11
247.3	^{162}Dy, ^{163}Dy	247.3 (^{161}Dy)	0.74 ± 0.17	21 ± 5
250.5	^{163}Dy	250.5 (^{162}Dy)	10.6 ± 1.3	37 ± 12
259.5	^{162}Dy, ^{163}Dy, ^{142}Dy,	259.5 (^{161}Dy), 259.5 (^{162}Dy)	7.31 ± 0.40 (^{161}Dy), 1.10 ± 0.13 (^{162}Dy)	22 ± 5
262.8[a]	^{163}Dy	262.7 (^{162}Dy)	0.69 ± 0.17	5.15 ± 1.97
266.2	^{163}Dy	266.2 (^{162}Dy)	1.00 ± 0.13	61 ± 21
267.4	^{163}Dy	267.4 (^{162}Dy)	1.32 ± 0.29	92 ± 34
277.0[a]	^{164}Dy	277.0 (^{163}Dy)	4.52 ± 0.53	43 ± 16
282.4	^{162}Dy	282.4 (^{161}Dy)	6.87 ± 0.39	25 ± 8
285.1	^{161}Dy,^{163}Dy,	285.1 (^{162}Dy)	1.84 ± 0.82	13.6 ± 4.3
292.0	^{161}Dy	292.0 (^{35}Cl), 292.0(^{162}Dy)	0.271 ± 0.004 (^{35}Cl), 0.10 ± 0.03 (^{162}Dy)	5.31 ± 1.65
294.2	^{164}Dy	294.2 (^{163}Dy)	8.33 ± 0.72	85 ± 26
305.7	^{163}Dy	305.7(^{162}Dy)	0.092 ± 0.024	9.03 ± 3.38
310.7	^{162}Dy	310.7 (^{161}Dy), 310.7 (^{162}Dy)	1.85 ± 0.36	85 ± 24
315.7	^{163}Dy	315.7 (^{162}Dy)	6.16 ± 0.16	83 ± 27
333.5	^{162}Dy	333.5 (^{161}Dy)	4.32 ± 0.39	27 ± 8
343.3	^{161}Dy	343.2 (^{162}Dy), 343.2 (^{164}Dy)	0.04 ± 0.01 (^{162}Dy), 0.48 ± 0.06 (^{164}Dy)	16.8 ± 6.2
347.0	^{162}Dy, ^{163}Dy,	347.0 (^{162}Dy)	4.62 ± 0.81	80 ± 25
350.6[a]	^{163}Dy	350.5 (^{162}Dy), 350.5 (^{164}Dy)	22.3 ± 2.2 (^{162}Dy), 1.97 ± 0.10 (^{164}Dy)	88 ± 33
353.7	^{163}Dy	353.7 (^{162}Dy), 353.7 (^{164}Dy)	7.25 ± 4.62 (^{162}Dy), 0.66 ± 0.15 (^{164}Dy)	54 ± 18
371.2	^{162}Dy	371.2 (^{162}Dy)	1.84 ± 0.22	50 ± 17
385.3	^{163}Dy	385.3 (^{162}Dy), 385.3 (^{164}Dy)	2.81 ± 0.58 (^{162}Dy), 4.66 ± 0.12 (^{164}Dy)	65 ± 22
389.1	^{163}Dy	389.0 (^{162}Dy)	15.7 ± 1.6	65 ± 21
401.3	^{163}Dy	401.3 (^{162}Dy)	3.31 ± 0.42	35 ± 11
406.9	^{163}Dy	406.9 (^{162}Dy)	0.67 ± 0.09	7.76 ± 1.93
414.4	^{163}Dy, ^{164}Dy	414.4 (^{162}Dy), 414.4 (^{164}Dy)	3.21 ± 0.42 (^{162}Dy), 4.14 ± 0.68 (^{164}Dy)	76 ± 25
421.1	^{163}Dy	421.0 (^{162}Dy), 421.0 (^{164}Dy)	14.5 ± 2.0 (^{162}Dy), 1.58 ± 0.04 (^{164}Dy)	68 ± 22
427.0	^{163}Dy	427.0 (^{161}Dy), 427.0 (^{162}Dy)	3.83 ± 0.49 (^{161}Dy), 1.46 ± 0.23 (^{162}Dy)	49 ± 15
435.6	^{163}Dy	435.6 (^{35}Cl), 435.6 (^{162}Dy)	0.93 ± 0.01 (^{35}Cl), 0.027 ± 0.004 (^{162}Dy)	7.51 ± 2.53
440.5	^{163}Dy	440.4 (^{161}Dy), 440.4 (^{162}Dy)	0.56 ± 10 (^{161}Dy), 1.15 ± 0.21 (^{162}Dy)	31 ± 10
461.6	^{164}Dy	461.6 (^{162}Dy)	0.39 ± 0.09	17.9 ± 5.8
464.9	^{164}Dy	464.9 (^{164}Dy)	5.09 ± 0.13	70 ± 24
474.7	^{163}Dy,	474.7 (^{161}Dy), 474.7(^{162}Dy), 474.7 (^{164}Dy)	0.27 ± 0.10 (^{161}Dy), 3.50 ± 0.46 (^{162}Dy), 1.30 ± 0.10 (^{162}Dy)	42 ± 11
478.7	^{163}Dy	478.7 (^{164}Dy)	5.06 ± 1.63	46 ± 16
528.7	^{162}Dy	528.7 (^{162}Dy), 528.7 (^{164}Dy)	0.19 ± 0.03 (^{162}Dy), 0.73 ± 0.12 (^{164}Dy)	42 ± 14
532.3[a]	^{161}Dy, ^{164}Dy	532.3 (^{162}Dy)	0.65 ± 0.09	23 ± 9
548.2	^{164}Dy	548.2 (^{164}Dy)	0.50 ± 0.05	9.50 ± 3.42

Table 17 (continued)

This work ($n,n'\gamma$)		PGNAA database (n,γ)		$P_{E\gamma}(n,\gamma)/P_{E\gamma}$ (%)
E_γ (keV)	^{A}Z	E_γ in keV (^{A}Z)	$I_{E\gamma}$ (%)	
552.3	^{163}Dy	552.3 (^{162}Dy)	0.16 ± 0.02	15.6 ± 5.6
556.1	^{162}Dy	556.1 (^{164}Dy)	0.29 ± 0.02	13.7 ± 5.6
558.9	^{163}Dy	558.8 (^{162}Dy)	0.69 ± 0.32	57 ± 20
565.3	^{162}Dy	565.3 (^{162}Dy), 565.3 (^{164}Dy)	0.029 ± 0.004 (^{162}Dy), 0.78 ± 0.94(^{164}Dy)	12.5 ± 4.1
572.3	^{162}Dy, ^{163}Dy	572.2 (^{161}Dy)	3.38 ± 1.41	62 ± 15
585.2	^{164}Dy	585.2 (^{162}Dy), 585.2 (^{164}Dy)	1.41 ± 0.35 (^{162}Dy), 3.21 ± 0.09 (^{164}Dy)	35 ± 8
607.9[a]	^{161}Dy	607.8 (^{162}Dy)	1.37 ± 0.16	39 ± 16
610.6	^{164}Dy	610.6 (^{162}Dy)	0.08 ± 0.0	
1	1.56 ± 0.52			
633.3	^{163}Dy	633.3 (^{35}Cl), 633.3 (^{161}Dy), 633.3 (^{162}Dy)	0.34 ± 0.06 (^{35}Cl), 1.05 ± 0.16 (^{161}Dy), 0.35 ± 0.05 (^{162}Dy)	27 ± 6
637.3	^{163}Dy	637.3 (^{162}Dy)	0.73 ± 0.16	51 ± 19
646.9	^{162}Dy, ^{163}Dy, ^{164}Dy	646.9 (^{161}Dy)	2.74 ± 0.21	6.07 ± 1.82
673.1	^{164}Dy	673.1 (^{162}Dy), 673.1 (^{163}Dy)	0.32 ± 0.04 (^{162}Dy), 5.10 ± 1.22 (^{164}Dy)	42 ± 16
687.8	^{164}Dy	687.8 (^{163}Dy)	14.1 ± 1.4	41 ± 13
696.6	^{162}Dy	696.6 (^{161}Dy), 696.6 (^{162}Dy)	2.91 ± 0.29 (^{161}Dy), 0.14 ± 0.02 (^{162}Dy)	25 ± 7
710.9	^{163}Dy	710.9 (^{161}Dy), 710.9 (^{162}Dy)	2.00 ± 0.21 (^{161}Dy), 1.16 ± 0.15 (^{162}Dy)	64 ± 16
726.8[a]	^{163}Dy	726.8 (^{162}Dy)	0.72 ± 0.18	28 ± 12
754.3	^{164}Dy	754.3 (^{163}Dy)	19.2 ± 1.6	50 ± 15
761.3	^{164}Dy	761.3 (^{163}Dy)	12.3 ± 1.1	40 ± 12
770.4[a]	^{162}Dy	770.4 (^{162}Dy)	0.98 ± 0.13	52 ± 22
781.9	^{164}Dy	781.9 (^{162}Dy)	0.16 ± 0.02	2.13 ± 0.67
794.9	^{162}Dy	794.8 (^{161}Dy), (^{162}Dy)	5.99 ± 0.42 (^{161}Dy), 0.86 ± 0.18 (^{162}Dy)	37 ± 9
807.1[a]	^{162}Dy	807.1 (^{161}Dy), 807.1 (^{162}Dy)	10.7 ± 0.6 (^{161}Dy), 1.79 ± 0.42 (^{162}Dy)	26 ± 9
842.7[a]	^{162}Dy, ^{164}Dy	842.6 (^{161}Dy), 842.6 (^{162}Dy)	2.71 ± 0.82 (^{161}Dy), 0.29 ± 0.04 (^{162}Dy)	28 ± 9
878.7	^{162}Dy	878.7 (^{161}Dy), 878.7 (^{162}Dy)	0.97 ± 0.27 (^{161}Dy), 0.18 ± 0.02 (^{162}Dy)	35 ± 10
881.9[a]	^{162}Dy	881.9 (^{161}Dy), 881.9 (^{162}Dy)	16.1 ± 0.9 (^{161}Dy), 0.18 ± 0.02 (^{162}Dy)	27 ± 9
887.8	^{162}Dy	887.8 (^{161}Dy)	9.17 ± 0.58	19.5 ± 5.8
916.7[a]	^{162}Dy	916.7 (^{161}Dy), 916.7 (^{162}Dy)	4.75 ± 0.48 (^{161}Dy), 0.53 ± 0.07 (^{162}Dy)	37 ± 15
944.2	^{162}Dy	944.1 (^{161}Dy)	6.34 ± 0.38	57 ± 17
980.1[a]	^{162}Dy	980.1 (^{161}Dy)	7.49 ± 0.47	58 ± 22
1001.8	^{164}Dy	1001.8 (^{162}Dy)	1.10 ± 0.13	47 ± 16
1021.8[a]	^{162}Dy	1021.8 (^{161}Dy)	0.70 ± 0.27	44 ± 21
1072.1	^{164}Dy	1072.1 (^{162}Dy)	0.20 ± 0.02	16.2 ± 5.9
1092.0	^{162}Dy	1091.9 (^{161}Dy)	2.38 ± 0.37	24 ± 7
1124.6[a]	^{162}Dy	1124.6 (^{161}Dy)	3.52 ± 0.30	58 ± 25
1129.2[a]	^{162}Dy	1129.2 (^{35}Cl), 1129.2 (^{161}Dy)	1.90 ± 0.02 (^{35}Cl), 5.02 ± 0.41 (^{161}Dy)	30 ± 11
1187.6	^{162}Dy	1187.6 (^{161}Dy), 1187.6 (^{162}Dy)	1.41 ± 0.37 (^{161}Dy), 0.12 ± 0.02 (^{162}Dy)	40 ± 11
1195.2	^{162}Dy	1195.2 (^{161}Dy), 1195.2(^{162}Dy)	3.17 ± 0.38 (^{161}Dy), 0.41 ± 0.09 (^{162}Dy)	24 ± 6
1252.6[b]	^{162}Dy	1252.6 (^{162}Dy)	0.11 ± 0.02	7.76 ± 1.93
1276.5	^{162}Dy	1276.5 (^{161}Dy), 1276.5 (^{162}Dy)	7.23 ± 1.72 (^{161}Dy), 0.13 ± 0.03 (^{162}Dy)	28 ± 7
1308.6	^{162}Dy	1308.6 (^{161}Dy)	1.50 ± 0.36	28 ± 9
1372.4	^{162}Dy	1372.3 (^{161}Dy)	2.11 ± 0.36	23 ± 7
1412.2[a]	^{164}Dy	1412.2 (^{164}Dy)	0.61 ± 0.07	30 ± 15
1528.9	^{164}Dy	1528.9 (^{162}Dy)	0.51 ± 0.09	42 ± 15
1600.9[a]	^{164}Dy	1600.9 (^{35}Cl), 1600.9 (^{162}Dy)	3.67 ± 0.21 (^{35}Cl), 0.15 ± 0.03 (^{164}Dy)	11.2 ± 3.7
1648.1	^{162}Dy, ^{164}Dy	1648.0 (^{35}Cl), 1648.1 (^{164}Dy)	0.53 ± 0.02 (^{35}Cl), 0.29 ± 0.04 (^{164}Dy)	5.38 ± 1.59
1674.4[a]	^{164}Dy	1674.3 (^{164}Dy)	0.48 ± 0.07	15.3 ± 6.9

Table 17 (continued)

This work ($n,n'\gamma$)		PGNAA database (n,γ)		$P_{E\gamma}(n,\gamma)/P_{E\gamma}$ (%)
E_γ (keV)	^{A}Z	E_γ in keV (^{A}Z)	$I_{E\gamma}$ (%)	
1722.7	^{164}Dy	1722.7 (^{164}Dy)	0.42 ± 0.05	4.08 ± 1.46
1736.0	^{164}Dy	1735.9 (^{164}Dy)	0.51 ± 0.05	5.89 ± 2.11
1836.2	^{164}Dy	1836.1 (^{164}Dy)	0.43 ± 0.08	12.7 ± 4.8
2020.9	^{162}Dy	2020.8 (^{35}Cl), (^{164}Dy)	0.49 ± 0.02 (^{35}Cl), 0.33 ± 0.07 (^{164}Dy)	23 ± 9
2241.5	^{162}Dy	2241.5 (^{164}Dy)	0.44 ± 0.07	29 ± 13

E_γ is the gamma-ray energy, ^{A}Z denotes the considered isotopes, $I_{E\gamma}$ is the absolute gamma-ray intensity and $P_{E\gamma}(n,\gamma)/P_{E\gamma}$ is thefraction of calculated neutron capture counts to the net counts in the gamma-ray peak

[a]Corrected for background interference. [b]corrected for the contribution of the single escape peak of 1763 keV

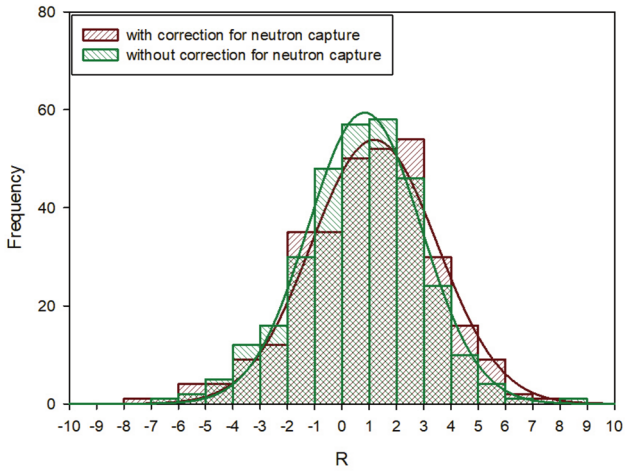

Fig. 8 Histogram of the residuals R in units of standard deviation [σ] calculated with Eq. (4) showing the level of agreement between the relative intensities of prompt gamma rays produced by inelastic scattering on samarium derived in this work (corrected and uncorrected for neutron capture interferences) with the data listed in [15-19-21]. The data was fitted with a Gaussian, which is shown by the solid lines

Author contribution Z.I., C.S., Z.R. performed the measurement N.O., I.M., T.R. and E.M. performed data analysis, N.O. and E.M. wrote the main manuscript text and prepared Figs. 1, 2, 3, 4, 5, 6, 7 and 8. All authors reviewed the manuscript.

Funding Open Access funding enabled and organized by Projekt DEAL. This research did not receive funding.

Data availability Data sets generated during the current study are available from the corresponding author on reasonable request.

Declarations

Competing interests The authors have no competing interests to declare that are relevant to the content of this article. The authors have no affiliations with or involvement in any organization or entity with any financial interest or non-financial interest in the subject matter or materials discussed in this manuscript. The 5th author, Zsolt Révay is a member of the Editorial Board of the journal. Therefore, he did not take part in the review process in any capacity and the submission was handled by a different member of the editorial board.

References

1. Randriamalala TH, Rossbach M, Mauerhofer E, Révay Z, Söllradl S, Wagner FM (2016) FaNGaS: a new instrument for ($n,n'\gamma$) reaction measurements at FRM II. Nucl Instrum Methods A 806:370–377
2. Ilic Z, Mauerhofer E, Stieghorst C, Révay Z, Rossbach M, Randriamalala TH, Brückel T (2020) Prompt gamma rays induced by inelastic scattering of fission neutrons on iron. J Radioanal Nucl Chem 325:641–645
3. Ophoven N, Ilic Z, Mauerhofer E, Randriamalala TH, Vezhlev E, Stieghorst C, Révay Z, Brückel T, Jolie J, Strub E (2022) Fast neutron induced gamma rays from (n,n'), (n,p) and (n,α) reactions on CaCO3. J Radioanal Nucl Chem 331:5729–5740
4. Meleshenkovskii I, Mauerhofer E (2024) Numerical study on the characterization of NdFeB permanent magnets with fast-neutrons induced ($n,n'\gamma$) reactions. J Radioanal Nucl Chem 333:2487–2494
5. Bouat S, Pinier L, Sebastian X, Losko A, Schütz R, Schulz M, Revay Z, Ilic Z, Mauerhofer E, Brückel T, Gilles R (2022) Detection of hydrate plugs inside submarine pipelines using neutrons. Nondestr Test Eval 37:245–257
6. Mauerhofer E, Ilic Z, Stieghorst C, Révay Z, Rossbach M, Li J, Randriamalala TH, Brückel T (2021) Prompt and delayed gamma rays induced by epithermal and fast neutrons with indium. J Radioanal Nucl Chem 331:535–546
7. Mauerhofer E, Ilic Z, Stieghorst C, Révay Z, Vezhlev E, Ophoven N, Randriamalala TH, Brückel T (2022) Prompt gamma rays from

fast neutron inelastic scattering on aluminum, titanium and copper. J Radioanal Nucl Chem 331:3987–4000
8. Ophoven N, Ilic Z, Mauerhofer E, Randriamalala TH, Vezhlev E, Stieghorst C, Révay Z, Brückel T, Jolie J, Strub E (2023) Prompt gamma rays from fast neutron induced reactions on cerium and chlorine. J Radioanal Nucl Chem 332:3133–3145
9. Ophoven N, Ilic Z, Mauerhofer E, Randriamalala TH, Vezhlev E, Stieghorst C, Révay Z, Brückel T, Jolie J, Strub E (2023) Prompt gamma rays of terbium induced by inelastic scattering of fission neutrons. J Radioanal Nucl Chem 333:1287–1300
10. Mauerhofer E, Ophoven N, Ilic Z, Stieghorst C, Révay Z, Meleshenkovskii I, Randriamalala TH (2024) Gamma emission from interaction of fission neutrons on nickel and zirconium. J Radioanal Nucl Chem 333:4333–4352
11. Ophoven N, Mauerhofer E, Ilic Z, Stieghorst C, Révay Z, Meleshenkovskii I, Randriamalala TH (2025) Prompt gamma rays of lanthanum and praseodymium produced by inelastic scattering of fission neutrons. J Radioanal Nucl Chem 334:953–967
12. Mauerhofer E, Ophoven N, Ilic Z, Stieghorst C, Révay Z, Meleshenkovskii I, Randriamalala TH (2025) Prompt gamma rays induced by fission neutrons on sodium, silicon, sulfur and potassium. J Radioanal Nucl Chem 334:3227–3240
13. Ophoven N, Mauerhofer E, Ilic Z, Stieghorst C, Révay Z, Meleshenkovskii I, Randriamalala TH (2025) Prompt gamma rays of neodymium from the $(n,n'\gamma)$- reaction with fission neutrons. J Radioanal Nucl Chem. https://doi.org/10.1007/s10967-025-10361-2
14. Demidov A, Govor L, Cherepantsev M, Ahmed S, Al-Najjar M, Al-Amili N, Al-Assafi N, Rammo N (1978) Atlas of gamma-ray spectra from the inelastic scattering of reactor fast neutrons. Atomizdat, Moscow
15. Avchukhov VD, Baskova KA, Bondarenko VA, Vovk AV, Gerus TM, Govor LI, Demidov AM (1983) Investigation of the level scheme of ^{147}Sm. Izv Akad Nauk SSSR Ser Fiz 47:851
16. Berzin YaYa, Vinogradov VM, Grigor´ev EP, Guseva TV, Tamberg YuYa, Arado Lopez O (1986) Excitation of ^{152}Sm levels by $(n,n'\gamma)$ reaction. Izv Akad Nauk, Ser Fiz 50(1):58–64
17. Demidov AM, Govor LI, Kurkin VA, Mikhailo IV (2006) Mulipole mixtures in γ transitions from the reaction ^{154}Sm$(n,n'\gamma)$. Phys At Nucl 69(4):555–561
18. Govor LI, Demidov AM, Kurkin VA (2002) Mulipole mixtures in γ transitions accompanying the $(n,n'\gamma)$ reaction on ^{16}2Dy. Phys At Nucl 65(5):785–794
19. Schmidt HH, Hungerford P, Von Egidy T, Scheerer HJ, Börner HG, Kerr SA, Schreckenbach K, Hoyler F, Colvin GG, Bruce AM, Casten RF, Warner DD, Kugava IL, Bondarenko VA, Kramer ND, Prokofjev PT (1989) Nuclear structure of ^{163}Dy studied with (n,γ), $(n,n'\gamma)(d,p)$ and (d,t) reactions. Nucl Phys A 504:1–35
20. Govor LI, Demidov AM, Kurkin VA, Mikhailo IV (2017) Level structure of ^{164} Dy from the $(n,n'\gamma)$ reaction. Phys At Nucl 80(1):1–24
21. Révay Z, Belgya T, Molnár GL (2005) Application of hypermet-PC in PGAA. J Radioanal Nucl Chem 265:261–265
22. NuDat 3.0 National Nuclear Data Center, Brookhaven National Laboratory https://www.nndc.bnl.gov/nudat3/
23. Zs R, Firestone RB, Belgya T, Molnár (2004) Prompt gamma-ray spectrum 480. In: Molnár GL (ed) Handbook of prompt gamma activation analysis with neutron 481 beams. Kluwer Academic Publishers, New York, pp 173–364
24. International Atomic Energy Agency (IAEA). PGAA-IAEA database viewer https://www-nds.iaea.org/pgaa/pgaa7/index.html
25. Sonzogni AA (2001) Nuclear data sheets for $A=144$. Nucl Data Sheets 93:599–762
26. Nica N, Singh B (2022) Nuclear data sheets for $A=147$. Nucl Data Sheets 181:1–74
27. Nica N (2014) Nuclear data sheets for $A=148$. Nucl Data Sheets 117:1–229
28. Singh B, Chen J (2022) Nuclear structure and decay data for A149 isobars. Nucl Data Sheets 185:2–559
29. Basu SK (2013) Nuclear data sheets for $A=150$. Nucl Data Sheets 114:435–660
30. Martin MJ (2013) Nuclear data sheets for $A=152$. Nucl Data Sheets 114:1497–1848
31. Nica N (2025) Nuclear data sheets for $A=154$. Nucl Data Sheets 200:2–524
32. Reich CW (2011) Nuclear data sheets for $A=161$. Nucl Data Sheets 112:2497–2713
33. Nica N (2024) Nuclear data sheets for $A=162$. Nucl Data Sheets 195:1–367
34. Reich CW, Singh B (2011) Nuclear data sheets $A=163$. Nucl Data Sheets 111:1211–1469
35. Singh B, Chen J (2018) Nuclear data sheets for $A=164$. Nucl Data Sheets 147:1–381
36. NIST XCOM: Photons cross sections database, National Institute of Standards and Technology https://physics.nist.gov/PhysRefData/Xcom/html/xcom1.html
37. Berger MJ, Hubbell JH, Seltzer S, Chang J, Coursey JS, Sukumar R, Zucker DS (2009) XCOM: photon cross sections database. NIST Stand Ref Data 8:87–3597
38. Brown DA et al (2018) ENDF/B-VIII.0: The 8th major release of the nuclear reaction data library with CIELO-project cross sections, new standards and thermal scattering data. Nucl Data Sheets 148:1–142
39. MacFarlane RE, Kahler AC (2010) Methods for processing ENDF/B-VII with NJOY. Nucl Data Sheets 111:2739–2890
40. MacFarlane R, Muir DW, Boicourt RM, Kahler AC, Conlin JL (2017) The NJOY nuclear data processing system, version 2016. https://doi.org/10.2172/1338791
41. OECD NEA Data Bank (2020) JANIS Book of neutron-induced cross-sections https://www.oecd-nea.org/janis/book/book-neutron-2020-09.pdf
42. Initial MCNP6 release overview MCNP6 Version 1.0, Los Alamos National Laboratory report LA-UR-13–22934
43. Goorley T et al (2017) Initial MCNP6 release overview. Nucl Technol 180:298–315
44. Groshev L, Demidov AM, Pelekhov VI, Sokolovskii BGA, Doveika A, Eastwood KM, Monaro S (1968) Compendium of thermal-neutron-capture γ-ray measurements part II $Z=41$ to $Z=67$ (Ag to Ho). Nucl Data Sheets A5:1–242. https://doi.org/10.1016/S0550-306X(68)80008-4